A Numerical and Experimental Investigation of Enhanced Open-Loop Air-Based Building-integrated Photovoltaic/Thermal (BIPV/T) Systems

Tingting Yang

A Thesis

In the Department

of

Building, Civil and Environmental Engineering

Presented in Partial Fulfillment of the Requirements

for the Degree of Doctor of Philosophy (Building Engineering) at

Concordia University

Montreal, Quebec, Canada

March 2015

CONCORDIA UNIVERSITY
SCHOOL OF GRADUATE STUDIES

This is to certify that the thesis prepared

By: Tingting Yang

Entitled: A Numerical and Experimental Investigation of Enhanced Open-Loop Air-Based

Building-integrated Photovoltaic/Thermal (BIPV/T) Systems

and submitted in partial fulfillment of the requirements for the degree of

DOCTOR OF PHILOSOPHY (Building Engineering)

complies with the regulations of the University and meets the accepted standards with respect to originality and quality.

Signed by the final examining committee:

Dr. S. Bergler   Chair

Dr. C. Menezo   External Examiner

Dr. G. Vatistas   External to Program

Dr. L. Wang   Examiner

Dr. R. Zmeureanu   Examiner

Dr. A. Athienitis   Thesis Supervisor

Approved by

_____
Chair of Department or Graduate Program Director

_____   _____
                          Dean of Faculty

Abstract

A Numerical and Experimental Investigation of Enhanced Open-Loop Air-Based Building-Integrated Photovoltaic/Thermal (BIPV/T) Systems

Tingting Yang, Ph.D.

Concordia University, 2015

This thesis investigates air-based building integrated photovoltaic/thermal (BIPV/T) systems. A building-integrated photovoltaic/thermal (BIPV/T) system converts solar energy into electricity and useful heat, while also serving as the functional exterior layer of the building envelope and thereby achieving the design of net-zero energy buildings.

A comprehensive literature survey of a variety of BIPV/T systems points out the need to develop enhanced air-based BIPV/T systems with aesthetical and mechanical requirements taken into account. This thesis examines improved designs of open-loop air-based BIPV/T systems both numerically and experimentally. A BIPV/T design with two inlets was proposed and a prototype using custom-made frameless PV modules was constructed for feasibility validation. The experiments were performed using a solar irradiance simulator and included testing under varying irradiance levels, flow rates and wind speeds. Experimental results validated that the two-inlet BIPV/T concept improved thermal efficiency by 5% compared to a conventional single-inlet system. Detailed BIPV/T channel air temperature measurements showed that the mixing of the warm outlet air from the first section and the cool ambient air drawn in from the

second inlet contributes to the improved performance of the two-inlet system. The heat transfer characteristics in the BIPV/T channel between air and PV panel was studied through the development of Nusselt number correlations. Comparative tests were also conducted on a prototype using opaque mono-crystalline PV modules and a prototype using semi-transparent mono-crystalline PV modules. Results showed that applying semi-transparent PV modules (with 80% module area covered by solar cells) in BIPV/T systems increased thermal efficiency (ratio between the thermal energy recovered by the channel air and solar energy incident on the upper surface of PV) by up to 7.6% compared to opaque ones, particularly when combined with multiple inlets.

A variation of this two-inlet BIPV/T design that includes a vertical solar air heater embedded with a packing material (wire mesh) was presented and analyzed. The additional solar air heater receives high amount of solar energy during the winter period when solar altitude is low, enabling the outlet air to be heated to a higher temperature. A lumped parameter thermal network model of this BIPV/T system was verified using experimental data obtained for a single-inlet BIPV/T prototype. Simulation results indicate that the application of two inlets on a BIPV/T collector increases thermal efficiency by about 5% and increases electrical efficiency marginally. An added vertical glazed solar air collector improves the thermal efficiency by about 8%, and the improvement is more significant with wire mesh packing in the collector by an increase of about 10%. A case study is performed using this lumped thermal model and showed that the thermal efficiency of a BIPV/T roof of an existing solar house is improved by 7% with four air inlets. In conclusion, this thesis presents validated models for the design of open-loop BIPV/T air systems with multiple inlets and possibly semi-transparent PV covers.

Acknowledgements

Table of Contents

List of Figures

xiv

List of Tables

Nomenclature

English

A	Heat transfer area, m^2
A_f	Frontal area, m^2
c_p	Specific heat of air, J/(kg K)
D	Depth of collector bed, m
D_h	Hydraulic diameter, m
d_w	Wire diameter of the wire matrices, m
dx	Length of a control volume, m
F	View factor
f_p	Average friction factor for packed bed
f_c	Average friction factor for conventional duct
G	Solar radiation, W/m^2
h	Heat transfer coefficient, $W/(m^2 K)$
J_h	Colburn factor
k	Conductivity, W/(m K)
L	Length of collector, m

m	Mass flow rate of air, kg/s
n	Number of wire mesh layers
Nu	Nusselt number
P	Porosity of the wire mesh matrix
P_{elec}	Electricity generation, W
PF	Packing factor
Pr	Prandtl number
P_t	Pitch of wire mesh, m
Q_{air}	Heat absorbed by air, W
R	Thermal resistance, $(m^2K)/W$
Re	Reynolds number
Re_p	Packed bed Reynolds number
r_h	Hydraulic radius for the packed bed, m
St_p	Stanton number for packed bed
T	Temperature, °C
V_{wind}	Wind velocity, m/s
W	Width of the collector, m

Greek

α	absorptivity
β	Packing factor
ε	emissivity
τ	transmissivity
μ	Dynamic viscosity of air, $(N\ s)/m^2$
ρ	Density of air, kg/m^3
σ	Stefan-Boltzmann constant, $5.67 \times 10^{-8} W/(m^2 K^4)$

Subscripts

a	Ambient air
e	EVA
f	Air flow
g	Glass of the PV module; glazing of the solar air heater
insu	insulation
pv	Of the PV covered portion of the system
mix	the layers of backing substrate, Tefzel, adhesive and steel sheet in the PV module
plate	back surface of the PV module

r	Radiative heat transfer
ref	Reference
top	heat transfer between air and the PV module
bot	heat transfer between air and the insulation

Acronym

a-Si	Amorphous silicon
BAPV	Building added photovoltaic
BIPV	Building integrated photovoltaic
BIPV/T	Building integrated photovoltaic/thermal
CHTC	Convective heat transfer coefficient
c-Si	Crystalline silicon
EVA	Ethylene vinyl acetate
IEC	International Electrotechnical Commission
JMSB	John Molson School of Business
PCM	Phase change material
PET	Polyester
PV	Photovoltaic
PVC	Polyvinyl chloride

PVF   Polyvinyl fluoride

UL   Underwritters Laboratories

UTC   Unglazed transpired collector

1. Introduction

1.1 Background

According to the International Energy Agency, buildings account for 32% of the world's energy consumption (Roaf, 2015), and this significantly motivates the development of near net-zero energy buildings. A BIPV/T system makes use of the building envelope for solar energy collection to produce both electrical and thermal energy, providing an efficient way of reducing building energy consumption. Establishing BIPV/T systems both as a standard architectural concept and as a functional building component replacing conventional claddings and roofing materials, would aid in the widespread use of BIPV/T systems. In contrast, building-added photovoltaic/thermal (BAPV/T) systems are fixed onto the outer surface of the building structure without necessarily being part of the functional building envelope itself. Regardless, both BIPV/T and BAPV/T systems supply on-site electrical and thermal energy to buildings, and can be integrated with other energy systems such as a heat pump or a heat recovery ventilator. Building-integrated photovoltaic (BIPV) and building-added photovoltaic (BAPV) systems have no tangible thermal component included in the design. Examples of these are PV window overhangs and BIPV shingles on the roof. Nevertheless, the energy performance of a building may also be enhanced by the use of BIPV or BAPV systems. All of the systems mentioned here share some common characteristics, can contribute to achieving net-zero energy buildings and are therefore included in the scope of this work. Generally, a BIPV/T system possesses the following features:

- The system is physically attached with buildings

- The system generates electricity

- The system generates thermal energy ready to be collected and utilized by the building, or the thermal behaviour of the system has a positive effect on the energy performance of the building.

Although the research and development of the photovoltaic/thermal (PV/T) technology began in the 1970s (Wolf, 1976; Florschuetz, 1979), the concept of the BIPV/T appeared much later. It started emerging in the 1990s (Clarke et al., 1996), and at this time a demonstrative BIPV/T system was installed on the roof of a restaurant for electricity and hot water production in North Carolina, USA as part of the PV Bonus initiative (Hayter and Martin, 1998). An office building of the Aerni Fenster factory in Switzerland was among the first in Europe to have a façade-integrated BIPV/T air system (Eiffert, 2000). Similar installations in Europe include the Scheidegger façade-integrated BIPV/T air system, the Brig roof-integrated BIPV/T air system and the Rigi roof-integrated BIPV/T air system (Posnansky et al., 1994). The BIPV/T technology has attracted increasing attention since 2000 due to its potential to promote net-zero energy buildings through enhanced solar energy utilisation. It has been shown that BIPV/T design is a promising technology for generating electricity and useful heat. Fujisawa and Tani (1997) compared the performance of a hybrid PV/T system and a unit of separate PV and thermal system covering the same area on the basis of exergy efficiency. They found that the hybrid design achieved higher exergy output. Each of the studies of roof-integrated BIPV/T systems by Dupeyrat et al. (2014), Fraisse et al. (2007), and Kazanci et al. (2014) arrived at similar conclusions.

2

The integration of a PV/T system with a building is not equivalent to a simple addition to a building. In terms of building energy savings, the BIPV/T system not only works as an energy provider, but it also interacts with the building itself in terms of various loads (heating, cooling and lighting). For example, there can be an air gap between the PV module and the building envelope, acting as an insulation layer of the building, adding an additional energy conservation benefit. On the other hand, the building structure can affect BIPV/T performance. A stand-alone PV/T system may be installed at optimised orientations and tilting angles according to local surroundings and latitudes, whereas the placement of the BIPV/T collector is largely dictated by the building design and requirements.

Considering the near-south-facing surface, working media and installation location, a BIPV/T system can be categorised as shown in Figure 1.1. A BIPV/T system receives solar radiation using either a flat surface (Guiavarch and Peuportier, 2006; Assoa et al., 2007; Vats et al., 2012), or a refractive/reflective concentrating device (Mittelman et al., 2007; Davidsson et al., 2010; Chemisana et al., 2011). A number of media can be used to cool the PV, including air, water and refrigerants. A variety of innovative BIPV/T systems and products have been developed and many approaches have been used in BIPV/T system studies.
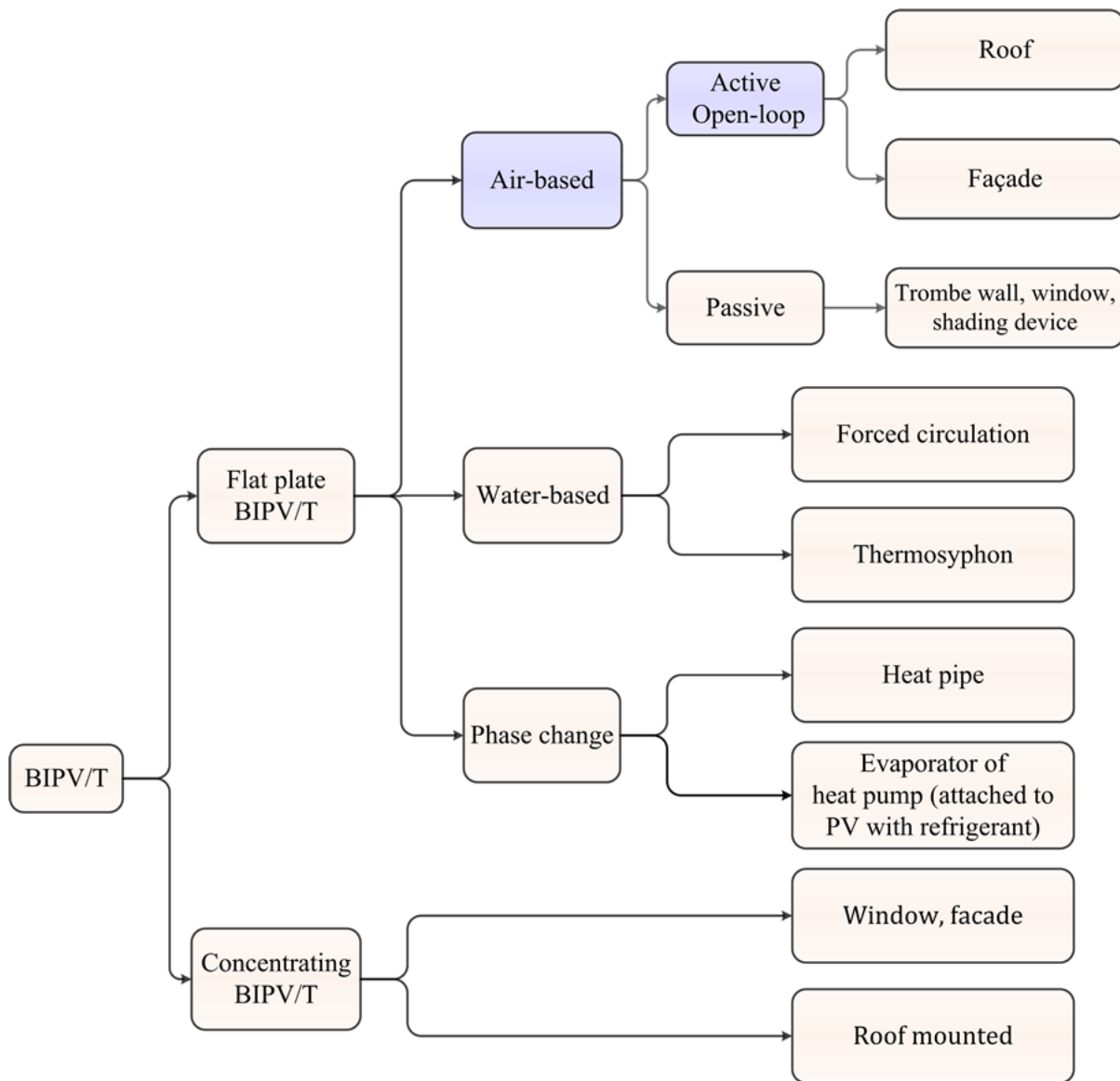
Figure 1.1. Categorization of BIPV/T systems

Among the variations of BIPV/T systems, the active open-loop air-based BIPV/T system has lower installation costs, reduced risk of leakage and freezing, and ease of maintenance compared to other liquid-based BIPV/T systems. The air gap of a BIPV/T system is situated between the upper PV modules and the lower insulation layer, allowing fan-driven ambient air to cool the modules, resulting in improved PV electrical efficiency. The hot air may have the potential to

assist space heating, domestic hot water heating and even solar cooling. Generally, BIPV/T air system performance is low due to the inherent physical properties of the air such as low density, low heat capacity and low heat conductivity, resulting in a need to enhance the performance of air-based BIPV/T system. With improved BIPV/T system designs, the outlet air temperature may be raised while the module temperature is lowered resulting in higher electrical efficiencies. A major objective of the thesis is to study the design and performance of open-loop air-based BIPV/T system designs that facilitate more effective air heating and PV electrical production.

1.2 Variations of Open-Loop Air-Based Solar Collectors

This section will briefly describe the various open-loop solar air heating systems including glazed solar heaters, photovoltaic/thermal (PV/T) collectors and BIPV/T collectors. Generally, system performance is enhanced through increased convective heat transfer coefficient and/or heat exchange area.

Table 1.1. Variations of open-loop air-based solar collectors

System Design	Key Facts
1. Solar air collectors with re-organized channels	
(1) (2) (3) (4)	The Model 1 PV/T collector has the lowest overall performance. The Model 3 PV/T collector has the highest overall performance for high air mass flow rates (Hegazy, 2000)
  TMS sheet: Thin Metal (aluminum) Sheet	Air is passed through both the upper and lower channels. The thin metal sheet suspended at the middle of the air channel increases the heat exchange surface and improves heat extraction from PV panels (Shahsavar and Ameri, 2010).
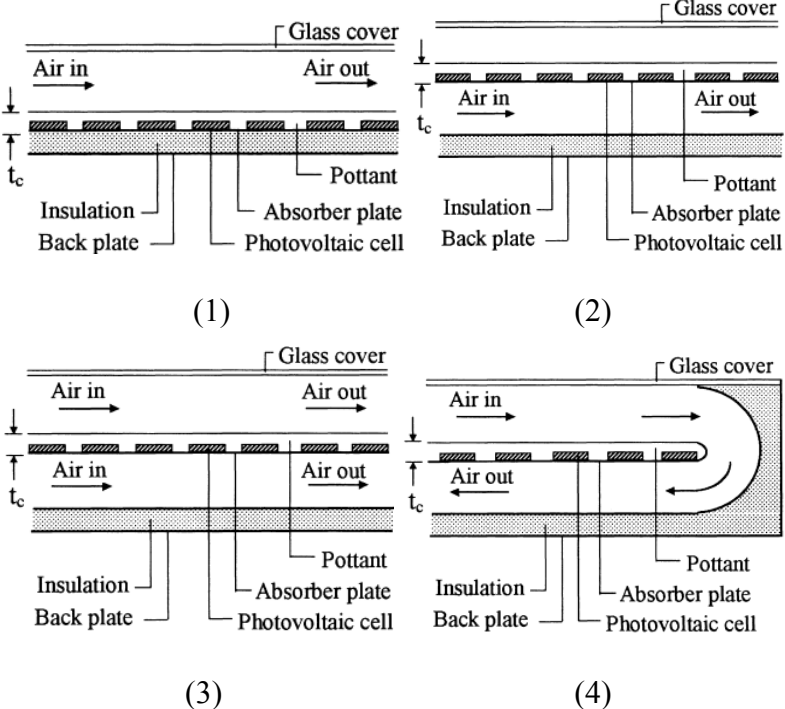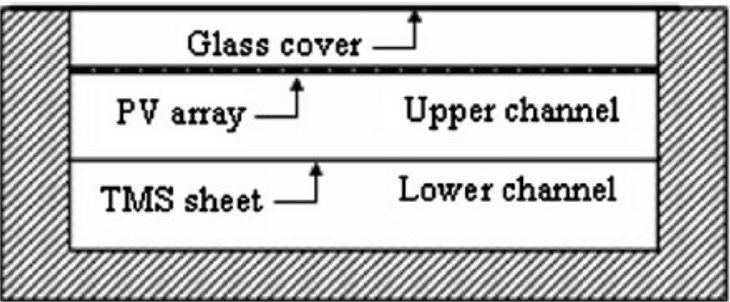
The air channel rows of the BIPV/T installation may be connected in series or in parallel. Simulation results show that the serial connection may result in the highest energy and exergy generations (Agrawal and Tiwari, 2010b).
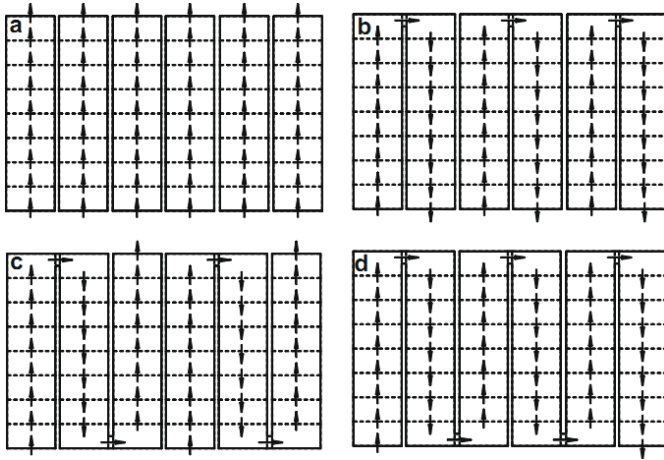
2. Solar air collectors with fins
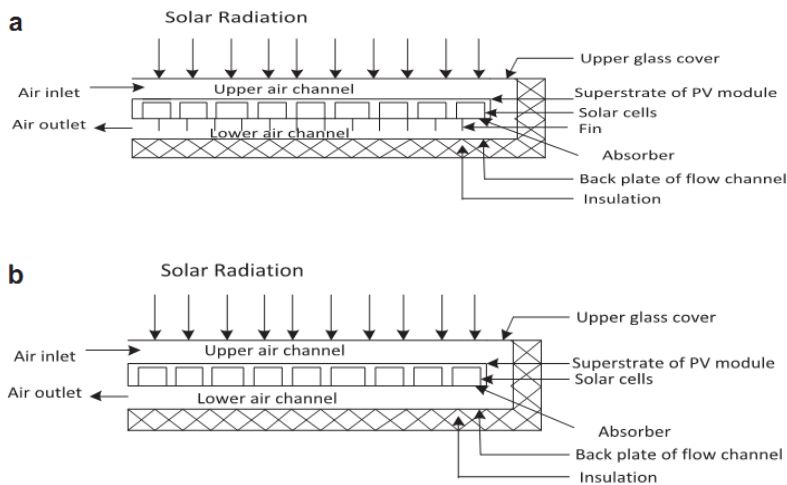
The extended fin area reduces the solar cell temperature from 82 ºC to 66 ºC (Kumar and Rosen, 2011b)
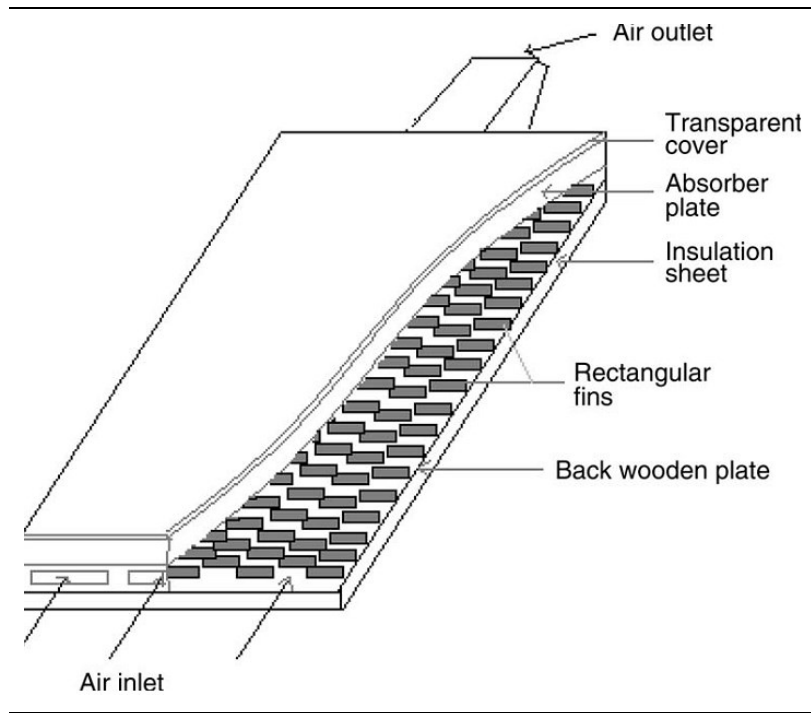
Thermal efficiency of the collector is increased from 45% to 80% with added fins for a volume flow rate of 60 m^3/h m^2. (Moummi et al., 2004)

3. Solar air collector with slat
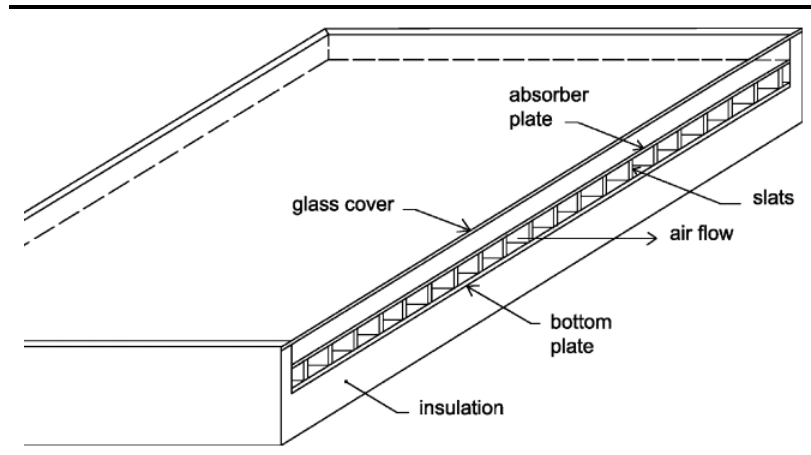
Air channels are formed by providing metal slats running along the air passage. Numerical simulation results show that higher thermal efficiency may be obtained with the slats (Ammari, 2003)

4. Solar air collector with porous packing materials
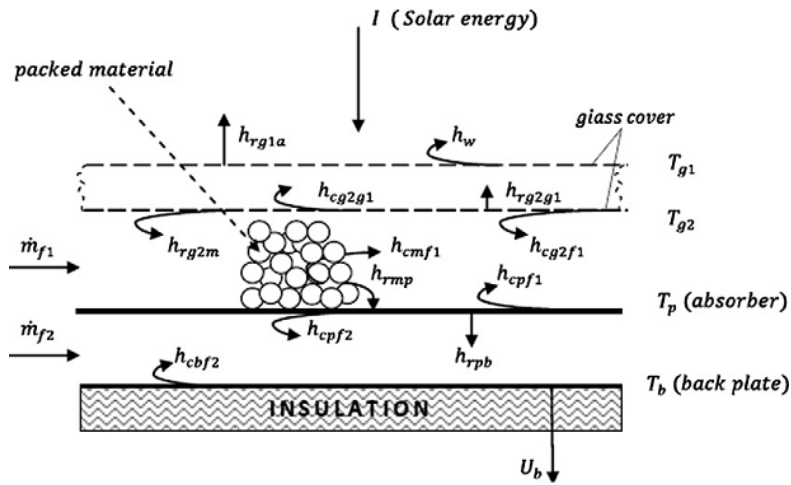
I (Solar energy) *packed material* *glass cover* h_{rg1a} h_w T_{g1} h_{cg2g1} h_{rg2g1} T_{g2} $\dot{m}_{f1}$ h_{rg2m} h_{cmf1} h_{cg2f1} h_{rmp} h_{cpf1} T_p *(absorber)* $\dot{m}_{f2}$ h_{cpf2} h_{cbf2} h_{rpb} T_b *(back plate)* INSULATION U_b	The parallel flow solar air heater is packed with porous material in its upper channel. The packed material may increase the thermal efficiency by 10-20% compared to the conventional non-porous double flow heater (Dhiman et al., 2011)
single glazing inlet unit with wire screens and flow straightener outlet unit with wire screens and perforated plates *warm air flow* adjustable double layered matrix with exchangeable frame and black wire screens adjustable collector bottom	The absorber in the middle of the air channel is fine-meshed wire screens made of copper. The metal matrix may yield an improved thermal performance of the collector (Kolb et al., 1999).
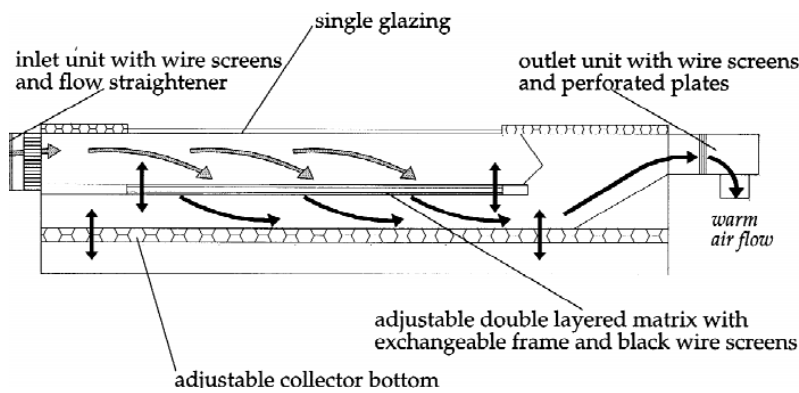
5. Solar air collector with corrugated surface
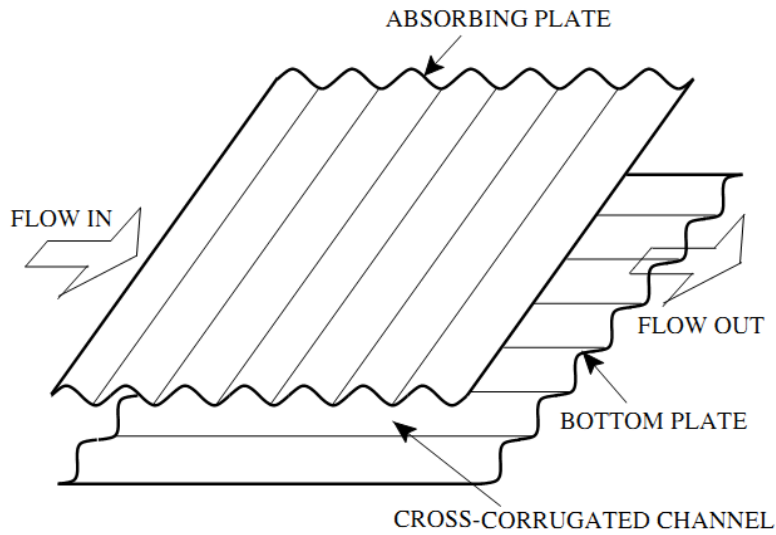
The solar air collector consists of crosswise wavelike top absorbing plate and bottom plate. Both experimental and analytical results show that the thermal efficiencies of the flat-plate and cross-corrugated solar air heaters are about 49% and 60% (Gao et al., 2007).

6. Solar air heaters with ribs
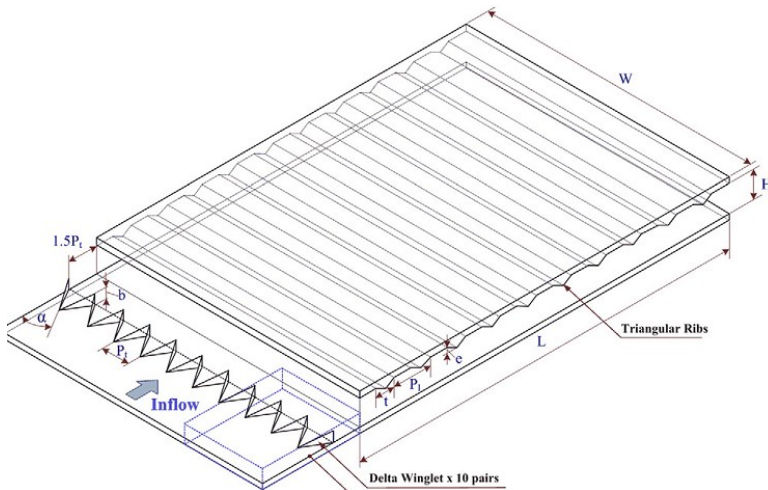
Ribs combined with delta-winglet type vortex generators are used to enhance the thermal behaviour of the solar air heater. Experimental results show that the Nusselt number for combined rib and vortex generator are much higher than the rib/vortex generator alone (Promvonge et al., 2011)

1.3 Problem Statement

The above Table 1.1 summarizes the heat transfer enhancement measures in the literature for solar air heating systems including glazed solar air heaters, PV/T collectors and BIPV/T collectors. These proposed systems result in an increase in outlet air temperature, and this may result in an increased system applications. Also electrical efficiency may be improved due to lowered solar cell temperature for PV/T and BIPV/T systems. However, some of these designs need modifications to be suitable for BIPV/T installations. For example, due to the constraint of the PV panel's flat configuration, the cross-corrugated solar air heater design is not readily transferrable to the BIPV/T system. Installing vortex generators in front of the air inlet of the BIPV/T system can be challenging due to aesthetic concerns and the difficulty to release rain water blocked by the generator. Therefore there is a need to improve BIPV/T system performance while fully considers the aesthetical and envelope requirements of the building.

Since a BIPV/T installation usually covers a large area, Agrawal and Tiwari (2010b) considered connecting the air channels under each row of PV panels both in series and parallel in order to maximize outlet air temperature, energy gains and exergy gains. Pantic et al. (2010) explored the feasibility of connecting a 1.5 m vertical glazed solar air collector in series with the outlet of the conventional BIPV/T system. This system expanded the usable roof area and enabled the vertical section to receive high amounts of solar radiation during the winter when the solar altitude is low. Numerical simulation results showed a significant outlet air temperature increase was obtained for the improved system. However, research, specifically targeted at improved energy performance of open-loop air-based BIPV/T systems, is lacking.

1.4 Main Objectives

This thesis aims at proposing enhanced BIPV/T system designs and investigating their performances through experimentation in a solar simulator and numerical modelling. The specific objectives of this thesis are:

- To propose improved designs of open-loop air-based BIPV/T systems that may be conveniently adopted in future BIPV/T installations.

- To carry out experiments on the BIPV/T prototypes and evaluate their performances under varied operating conditions including irradiance level, wind speed and air flow rate.

- To study the heat transfer mechanism in the BIPV/T air channel through accurate temperature measurement. Nusselt number correlations are developed to characterise the convective heat transfer in the BIPV/T system, and these correlations are also used as important inputs in the lumped-parameter thermal network models to quantitatively evaluate system performance.

- To develop a lumped-parameter thermal network model for the design of open-loop BIPV/T air systems.

1.5 Scope

This thesis mainly deals with the performance evaluation and modelling of the proposed BIPV/T system designs. Experimental prototypes of the BIPV/T systems are built and tested.

This work does not elaborate on the integrated energy performance of the BIPV/T system and the

building. A variety of software such as EnergyPlus, ESP-r and TRNSYS has been adopted for this purpose. However, the Nusselt number correlations developed in this work may be used in the above-mentioned computer codes to assist the energy modeling of buildings installed with BIPV/T systems.

1.6 Overview

Chapter 1, the introductory chapter, includes a description of the background, a summary of existing solar air heating devices with enhanced performance, the problem statement, the main objectives of this work, and the scope of investigation.

Chapter 2 presents an extensive literature review on BIPV/T systems. These systems are discussed based on the categorisation shown in Figure 1.1. The following topics – the building-integration issue, the research and development advancement, the numerical and experimental investigation approaches and the system's thermal effect on energy performance of buildings, are thoroughly addressed in this chapter. The commonly adopted lumped parameter thermal network model is also taken into account in this thesis. This chapter also establish some suggestions for future research on BIPV/T systems, including but not limited to the open-loop air-based type.

Chapter 3 proposes an open-loop air-based BIPV/T system enhanced with an additional vertical glazed solar air heater whose channel is packed with wire mesh (a metallic matrix). Also the effect of applying multiple air inlets in the PV covered section is examined. To demonstrate the performance of a typical BIPV/T system and obtain data for model verification, experimental study is conducted in a full-scale solar simulator. A lumped parameter thermal network model is developed for the tested BIPV/T system and later used to assess the performance of the proposed

system.

Chapter 4 presents the experimental investigation on a BIPV/T prototype enhanced with two air inlets. Comparative tests are carried out on BIPV/T system with one and two inlets, under a variety of conditions with different wind speeds and channel air flow rates. Detailed temperature profile is measured to examine the temperature development and potentially the air mixing process. Nusselt number correlations are developed to further understand the heat transfer process with the added inlet and to assist further analysis of BIPV/T systems.

Chapter 5 summarises the main research findings and propose potential future work based on the findings of this investigation.

2. Literature Review [1]

2.1 Chapter Overview

This chapter provides an extensive review on a variety of BIPV/T systems. Section 2.2 discusses the integration of the BIPV/T system into the building envelope, addressing aesthetical and mechanical considerations and integration of PV modules used in the built environment. Sections 2.3, 2.4 and 2.5 review BIPV/T systems of an extensive variety that include air-based, water-based, phase change process based and concentrated sub-systems. Section 2.6 introduces the numerical and experimental approaches that are usually adopted in the investigation of BIPV/T systems. Section 2.7 presents a summary of the review, followed by section 2.8 identifying opportunities worthy of attention for future study and improvement of BIPV/T systems.

2.2 Integration with the Building Envelope

A BIPV/T system may be either fully integrated into or simply mounted onto a building. Examples of these two installation techniques are:

- Roofing elements directly replacing traditional roofing tiles or installed on flat or low-sloped roofs (Chen et al., 2010; Bakker et al., 2005; Ban-Weiss et al., 2013; Bucker et al., 2014);

- Ventilated facades with PV as the external cladding element (Athienitis et al. 2011;

---

[1] The study presented in this chapter is submitted to a peer-reviewed journal as:
Tingting Yang, Andreas K. Athienitis. A review of research and developments of building-integrated photovoltaic/thermal (BIPV/T) systems. Sustainable and Renewable Energy Reviews.

Peng et al., 2013a);

- Window elements (Davidsson et al., 2010; Han et al., 2010; Chae et al., 2014)

- Rainscreen cladding and curtain walling (SolarPV.co.uk, 2014)

The best integration results may be achieved when BIPV/T system design is taken into consideration in the building design stage. The optimal aesthetic effect of photovoltaic panels integrated into buildings should satisfy the following criteria, as summarized by Reijenga (2000) in an IEA-PVPS report:

- Natural integration that is architecturally pleasing;

- Good composition between materials, colors and dimensions;

- Consistency with the building concept and framework;

- Well-engineered and innovative integration.

It is possible to achieve a visually pleasant architectural design using photovoltaic modules. Figure 2.1 shows the skylight installed for the Bejar market retrofit project in Spain, utilising three types of PV glasses with different colours and transparencies to create an aesthetical mosaic inspired by Piet Mondrian Neoplasticism (OnyxSolar, 2014). The solar manufacturing industry is developing photovoltaic modules to enable more aesthetical building integration opportunities. A BIPV solution was provided that included colored PV glasses in different thickness, sizes, transparencies and colours for them to be integrated as an artistic building element. SwissINSO and the Ecole Polytechnique Federale de Lausanne developed colour treated glass with an opaque finish (Kromatix glass) to be integrated with PV modules. The developer (SwissINSO, 2013) states that Kromatix glass shields the inner workings of the PV

module from being seen, while negligibly reducing the module efficiency. CSEM in Switzerland recently developed white solar modules which convert infrared solar light into electricity while scattering the complete visible light spectrum. This may broaden building design choices and increase interests in the integration of solar modules into buildings (CSEM, 2014).
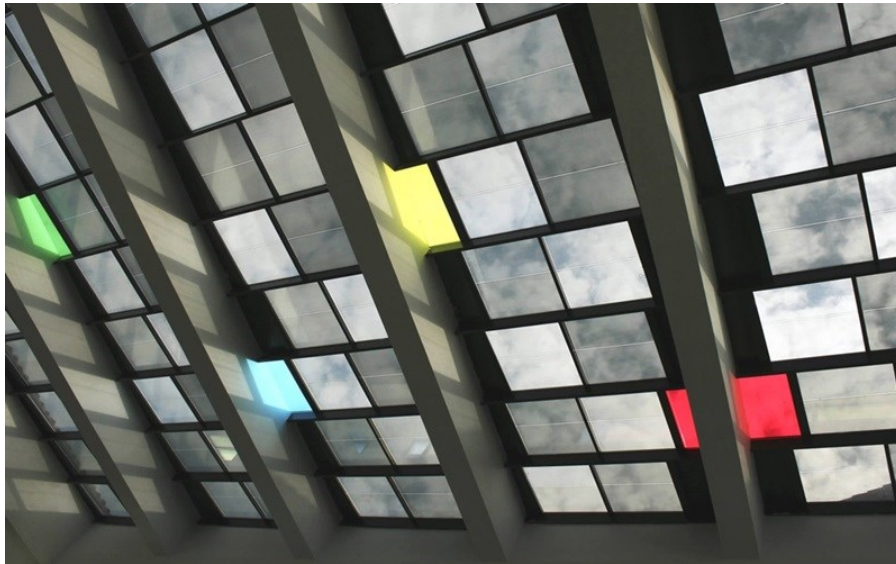
Figure 2.1. Photo of the BIPV skylight installed for the Bejar market retrofit project in Spain inspired by Piet Mondrian Neoplasticism (OnyxSolar, 2014)

A well designed BIPV/T system should blend in with the building seamlessly to achieve an integral appearance. The John Molson School of Business (JMSB) building at Concordia University, Canada houses a fully integrated open-loop air BIPV/T facade installed on its top floors. The size of the PV modules was custom designed to match the dimensions of the curtain wall system that covers the rest of the façade area and to achieve a pleasant visual effect (Figure 2.2). The aluminum frames and the backsheets of the PV modules are black to allow a homogenous appearance of the BIPV/T system consisting of PV modules mounted onto the black transpired collector and also to increase solar absorption and thermal efficiency of the

BIPV/T system (Athienitis et al., 2011). Anderson et al. (2009) proposed integrating PV modules onto troughed sheet roofs with the latter providing structural strength while forming passageways for the thermal cooling medium. This roof-integrated BIPV/T water system did not add significant visual obstruction to the original roof and provided a protective layer to the original roofing material.

Figure 2.2. The BIPV/T system of the JMSB building

A BIPV/T system can reflect the design concept and framework of a building and this can have novel effects. For example, solar cells have been used to power satellite and space stations since the 1950s and therefore, PV modules were integrated with the facades, skylight, roof and canopies of a new facility of the National Air and Space Museum of the Smithsonian Institution to exhibit technologies derived from space exploration (Eiffert and Kiss, 2000). Xuan and Zheng (2009) point out that PV panels may reflect the architectural character better for a high-tech construction such as a modern research institute. Other examples include train stations, airports

18

(Ruther and Braun, 2009), schools (James et al., 2009) and office buildings to further increase public awareness of the BIPV/T technology. It should be noted that when PV systems occupy multiple facades of the building or when a massive façade is installed with several PV strings, multiple inverters may be used to account for the differing electrical characteristics of the PV clusters (Hao et al., 2009; Eiffert and Kiss, 2000).

Jelle and Breivik (2012) stated that when used in the building environment, PV modules had to account for various building physical issues such as heat and moisture transfer. Jelle (2012) further elaborated on the influence of climate exposure factors leading to the ageing of PV modules. These factors include solar radiation, high and low temperatures, temperature changes (and associated freezing/thawing processes) and physical strains such as due to snow loads and wind force. Presented examples show how BIPV/T technology can cope with various building envelope performance challenges. The Eco-Terra near net-zero solar demonstration house was constructed in Quebec, Canada and included an open-loop BIPV/T air system (Chen et al. 2010). A schematic of the BIPV/T collector composition is shown in Figure 2.3. The amorphous PV modules were glued onto the metal roofing using a thermally conductive paste and further affixed to the roofing under the roof cap using a screw on the top side to reinforce the structural stability. No other screws were used since constraining more than one side of the PV module can result in delamination between PV and roofing metal, each have different thermal expansion and shrinkage rates. This issue is especially important for cities like Montreal with a large temperature range throughout the year, with summer temperatures reaching 35 °C and winter temperatures dropping to -30 °C. Similar considerations were made for the JMSB BIPV/T system design (Athienitis et al., 2011). Custom-manufactured c-Si PV modules were mounted

onto the transpired collector using specially designed clamps. Space was left between the modules and clamps to adequately release the thermal stress of different components. A BAPV system was designed to be installed on the roof of a building in downtown Boston, which is among the windiest cities in the USA. To withstand the wind force, a PV system was especially selected for its cost-effectiveness taking into account that extreme roof penetration was required. A low-energy solar house with a fully roof-integrated BIPV/T air system similar to that of Eco-Terra was presented (Athienitis, 2007). It was stated that the metal roofing underneath the PV modules could cause noise in windy weather. These examples illustrate the necessity of proper structural engineering in the design of BIPV/T systems as a functional building envelope.
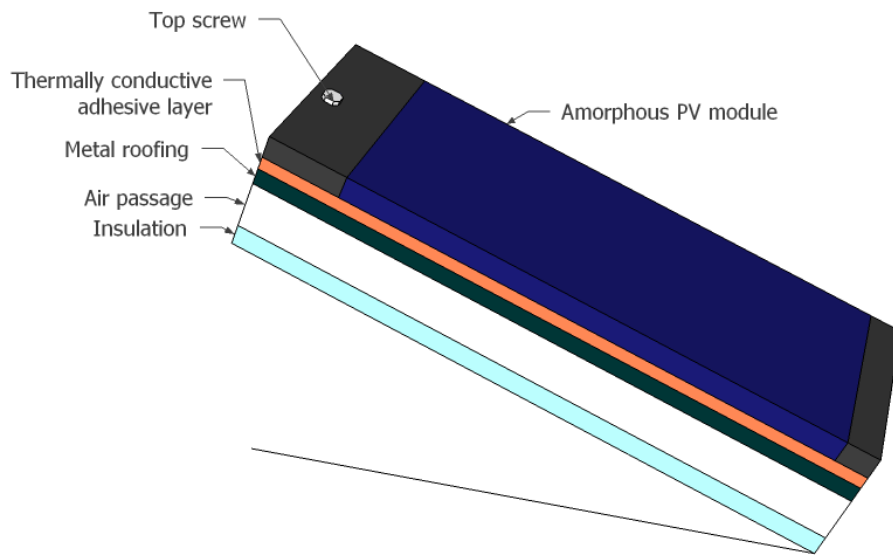
Figure 2.3. Schematic of the composition of the BIPV/T air system installed in Eco-Terra low-energy solar demonstration house (not to scale)

It is therefore essential to develop standards and codes for BIPV (BIPV/T) technology that impose safety and performance requirements on this technology, both as a PV system and as a building construction material. Table 2.1 lists some key Underwritters Laboratories (UL) and

International Electrotechnical Commission (IEC) standards for a stand-alone PV module and associated components. In addition Table 2.2 shows some relevant standards for PV modules to be used in building-integrated applications (UL, 2007).

Table 2.1. Key UL and IEC standards for photovoltaic parts and components (UL, 2007)

Solar Modules & Panels	
Standards	Description
UL 1703	Flat-Plate Photovoltaic Modules and Panels
IEC 61215	Crystalline Silicon Terrestrial Photovoltaic Modules – Design Qualification and Type Approval
IEC 61646	Thin-film Terrestrial Photovoltaic Modules – Design Qualification and Type Approval
IEC 61730	Photovoltaic Module Safety Qualification
Other Major Parts and Components of Photovoltaic Systems	
Standards	Description
UL 1741	Inverters, Converters, Controllers and Interconnection System Equipment for Use with Distributed Energy Resources
UL 4703	Outline for Photovoltaic Wire

Table 2.2. Additional assessments/standards for BIPV products

BIPV Products	Additional Assessments/Standards
Replacing roofing materials	UL 790
Used as facades or building glass	ANSIZ97.1-1984
Used in locations traditionally employed glazing materials, such as building facades, skylights and solarium roof	Mounting and wiring methods must be evaluated with the PV modules for impact resistance and must comply with Part IV of Article 690 in the NEC.
IEC 61730	Photovoltaic Module Safety Qualification

BIPV systems are subject to the safety standard UL 1703 for flat-plate photovoltaic modules and panels, which contains a specific subset of UL 790 for fire tests of roof coverings used for determining the fire rating for each PV module (Rosenthal et al., 2010). Some time later concerns were raised whether and how PV modules with lower fire ratings may affect the performance of higher rated roofing systems. To address these concerns, tests on various combinations of PV designs and roof coverings were jointly conducted by UL and the Solar America Board for Codes and Standards. The test results demonstrated that the fire classification rating of the PV module alone, determined by the standard UL 1703, may not predict the fire performance of the PV module, mounting system, and roof assembly as a whole system. As a result, an updated UL 1703 standard was published in October 2013, treating the PV modules and the roofing materials as an integrated building element (Sherwood et al., 2013). This change is expected to be included in newer versions of the International Building Code (Sherwood, 2012). The adaptation of PV and building standards to BIPV system fire rating codes, illustrated

the effort being made to update building standards to reflect the increasingly widespread BIPV technology. However, as Scott and Zielnik (2009) pointed out, BIPV products conform separately to both PV and building standards but there are essentially no integrated standards specifically for BIPV products. Also, current standards primarily address specific safety and electrical issues but do not address long term performance requirements as either a PV panel or building material. Bloem (2008) suggested that less than optimal tilt angles of BIPV systems and the lack of convection at the back of the PV for some thermally insulated BIPV installations may result in significant BIPV performance impairments that do not exist for standalone PV under standard test conditions. Bloem et al. (2012) recommended that the complete BIPV/T system be tested using a comprehensive assessment procedure covering: electrical performance, thermal performance and its seasonal variation, ventilation performance, visual effect, maintenance and other performance criteria. Furthermore, building codes impose requirements for PV as a construction material such as: wind resistance, wind-driven rain and accelerated weathering. For example, in regions with heavy precipitation and strong wind, this weather presents severe challenges to the mechanical stability of PV modules, while in coastal regions, salted moisture may inflict harsh stress on the PV modules (PV-lab,2012). Therefore the future standardization of the BIPV technology should also involve the efforts of local building code councils.

2.3 BIPV/T Air System

Air is lightweight and easy to transfer, giving a BIPV/T air system the flexibility for integration with various building elements such as: roofs, facades, windows and skylights. A BIPV/T air systems can be categorized as active open-loop and passive based on the buoyancy force. Also

small leaks in air systems do not adversely affect performance and air systems are less costly.

An active BIPV/T system is commonly installed in an open-loop configuration in which outdoor air is driven by a fan and passes through the channel behind the PV panels. Since an open-loop air system normally runs at a lower temperature than the close-loop air system, higher thermal efficiency and better PV performance and durability can be achieved. In addition, open-loop systems have the potential for supplying pre-heated fresh air to a building.

In a passive system, extra ducting or moving parts are not usually required since the heated air is either fed into the indoor space or exhausted into the ambient. This type of installation is often called a BIPV or a BAPV (building added photovoltaic) system, although significant consideration is made of the thermal aspects during the design process. A passive system usually interacts with the building environment in regard to heating, cooling, lighting loads, and electricity production.

2.3.1 Active BIPV/T Air System

The schematic of a typical open-loop BIPV/T air system is shown in Figure 2.4 (Athienitis, 2008). Depending on the solar cell type, about 6-16% of the incoming solar radiation is converted into electricity, with the rest either reflected (about 10%) or transferred into heat. This means that approximately 70% of the incident solar energy has to dissipate in the form of thermal energy. The heat accumulated in the PV is dissipated via four heat transfer paths: radiative exchange with the sky, convection with the outdoor air, radiative exchange with the solid surrounding surfaces in the BIPV/T channel, and convection with the fan-induced air flow in the channel. With much heat recovered from the PV, the electrical performance of PV is

enhanced and useful heat is obtained. The fully incorporated BIPV/T system may also replaces shingles on the roof, or expensive materials such as natural stone, marble, ceramic and granite on the façade (Zogou & Stapountzis, 2011a).
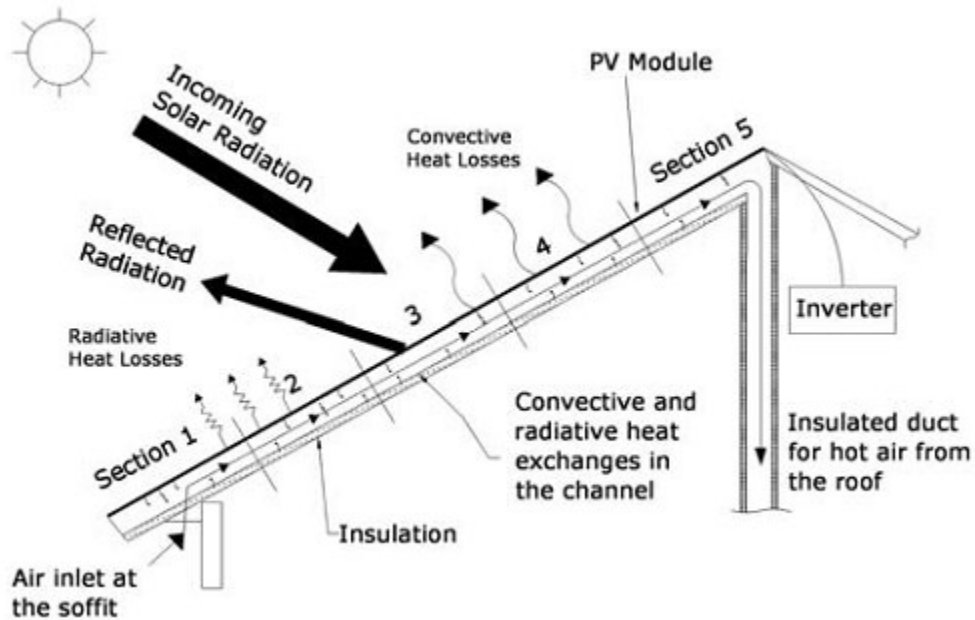
Figure 2.4. Schematic of a typical active air-based BIPV/T system (Athienitis, 2008)

In Canada, an open-loop BIPV/T air system (Figure 2.5) was installed as the upper roof of the EcoTerra low energy solar demonstration house (Chen et al., 2010). Thermographic image taken during a warm summer day showed PV temperatures between 50-60 °C, while temperatures were higher than 70 °C for the metal roofing without PV coverage and air ventilation. This temperature difference illustrates the effective air cooling of the PV panels. It was demonstrated that the BIPV/T system together with other passive solar designs such as large south-facing windows and distributed thermal mass in the direct solar gain zone, reduced the annual space

heating energy consumption to about 5% of the national average. Pre-fabrication of the BIPV/T roof ensured high-quality construction in terms of air tightness, thermal insulation and pressure drop balance. Also, pre-fabrication enabled work to take place during the winter when it was not possible to perform outdoor site work in the cold climate.

Figure 2.5. EcoTerra low energy solar demonstration house in Quebec, Canada (Chen et al., 2010)

The advantages of modularization were also experienced by Nagano et al. (2003) who developed a BIPV/T system integrated with vertical exterior wallboards that allowed for modular assembly in the cold climate. The authors proposed a wallboard integrated BIPV/T system tilted at 80° instead of 90° as a compromise between reduction of snow coverage, architectural constraints and annual electrical generation. Six variants of the system were tested outdoors for two winter months. It was found that the PV protective material being either glass or Teflon did not considerably affect the electricity generation. The addition of the cover glass in front of the whole wallboard increased the thermal efficiency from approximately 22% to more than 29%,

which echoed the work of Tripanagnostopoulos et al. (2002) on PV/T systems. The electrical efficiency was reduced by the cover glass due to condensation on the inner surface of the glass.

It is advantageous to integrate the BIPV/T system with an existent building energy system, such as the unglazed transpired collector (UTC). A UTC is a perforated, dark-colored and corrugated metal panel that is usually fixed onto the equator-facing façade of a building. With a typical thermal efficiency of 65%-75% (NREL, 1998), this system is able to collect suitable energy for fresh air pre-heating (Fleck et al., 2002) or crop drying (Leon & Kumar, 2007). Naveed et al. (2006) showed that the PV module mounted on a UTC is cooled by 3-9 °C on a typical day in February compared to a PV module attached to the wall.

Athienitis et al. (2011) investigated the performance of a BIPV/T prototype integrated with UTCs (Figure 2.6a). The authors selected black PV module backsheet as well as black aluminum frame to maximise solar energy absorption and to create a uniform appearance of the whole system. Figures 2.6b, 2.6c and 2.6d shows the layers of the BIPV/T system, namely the transpired collector and the PV modules, were integrated as the façade of the mechanical room. It can be seen that the BIPV/T system was not applied to an existing building facade, but rather constitute itself alone as a functional building wall. Furthermore, the corrugations of the UTC ran horizontally instead of vertically in order to form sealed air gaps with the PV to induce turbulent flow in the air gaps. Comparative experiments between a bare UTC and a BIPV/T prototype with 70% PV coverage indicated that the BIPV/T system was 7-17% higher in efficiency than the UTC, with the assumption that electricity is four times more valuable than heat. This integration concept was further applied on a newly constructed office building – the John Molson School of Business (JMSB) at Concordia University in Montreal, Canada. The BIPV/T installation

provided a peak power generation of 24.5 kW electrical and 75 kW thermal for the building. The authors pointed out that this BIPV/T demonstration project could provide a model for retrofit applications where a new BIPV/T façade could be built over the existing façade.

(a)   (b)

(c)   (d)
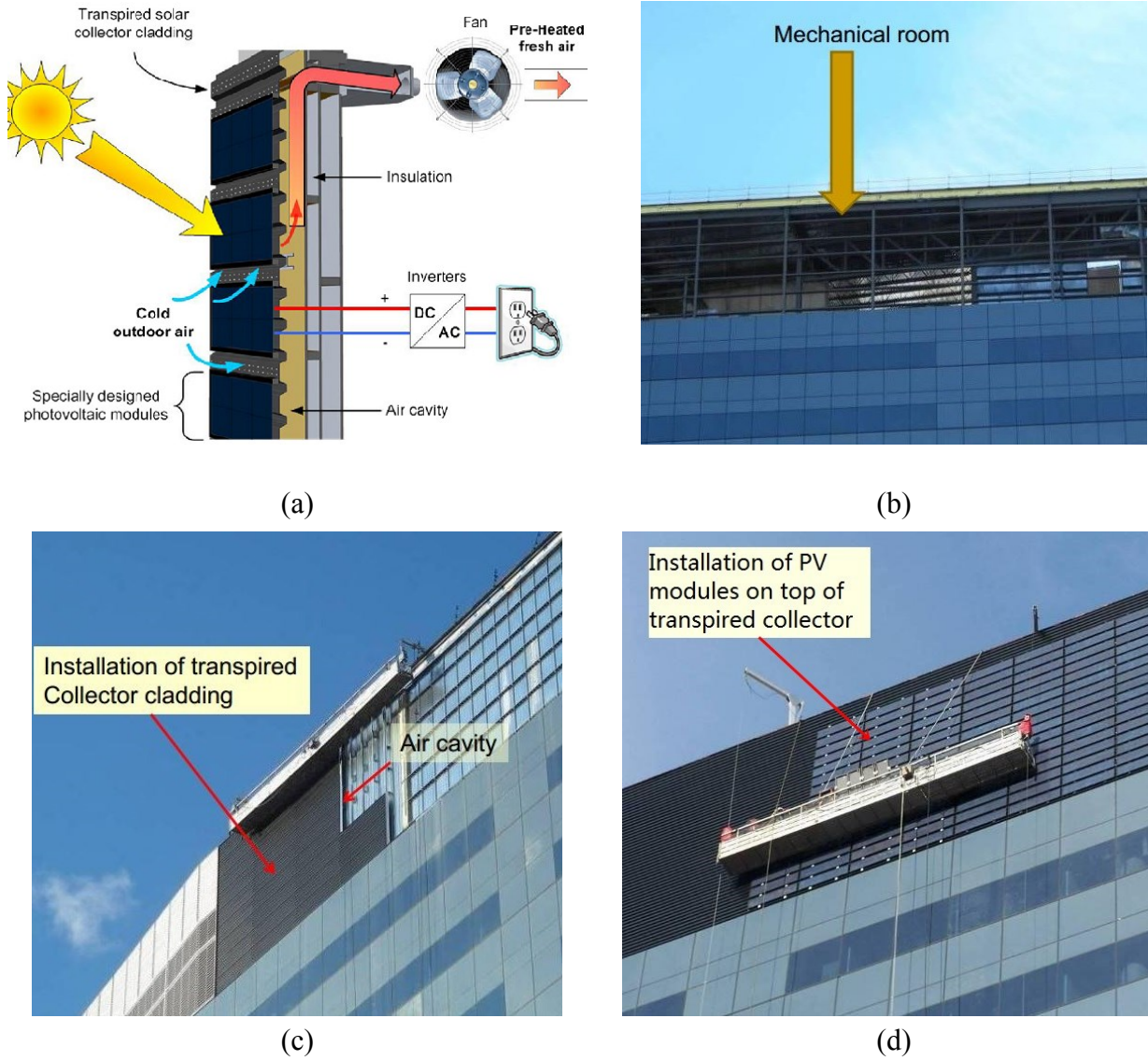
Figure 2.6. (a) Schematic illustration of a BIPV/T system integrated with UTC (Athienitis et. al, 2011); (b) Mechanical room of the JMSB building before BIPV/T system installation; (c) Transpired collector installed as part of the mechanical room facade; (d) PV modules mounted on

top of the transpired collector as the outermost layer of the mechanical room facade

Using an experimentally calibrated model, Pantic et al. (2010) predicted that a significant outlet air temperature increase would be achieved by connecting a 1.5 m vertical glazed solar air collector in series with the outlet of the conventional BIPV/T system. The air temperature rise enables coupling with a rockbed heat storage. The added vertical solar air collector expands usable roof area and receives high amounts of solar radiation in winter when the solar altitude was low. Further simulation showed that more thermal energy was collected by adding a glazing above the PV, while electricity generation was greatly reduced due to diminished solar input through the glazing and higher PV temperature.

Assoa et al. (2007) developed a BIPV/T system with co-generation of hot air and water, which applied adjacent hybrid bi-fluid thermal collectors and PV panels above the rib structures. The combined thermal efficiency reached approximately 80% under favorable operating conditions. Assoa et al. (2014) extended this design with a variant roof-integrated BIPV/T system using a ribbed sheet steel absorber and using natural ventilation air as the working fluid (Figure 2.7). The system was integrated into the roof of a manufacturing company building and monitored for two years. A numerical model showed that although forced ventilation achieved higher thermal production than natural ventilation, the difference between the calculated electrical yields of the two operating modes was marginal.
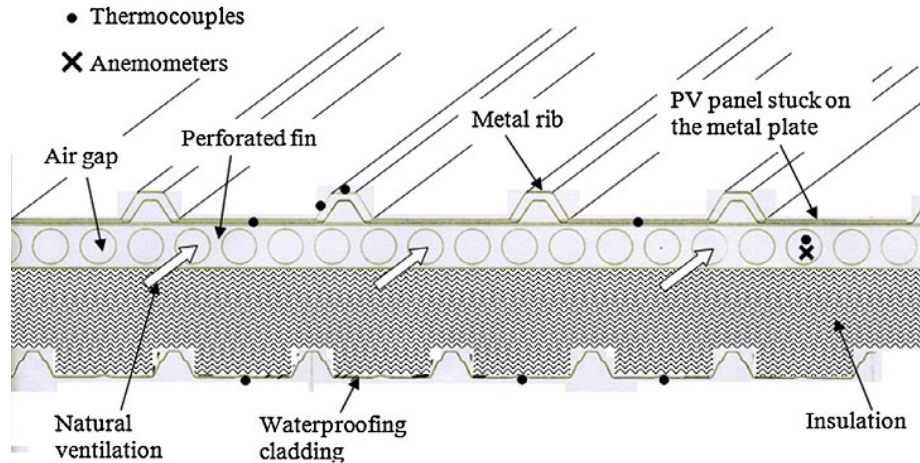
Figure 2.7. Schematic of a roof-integrated BIPV/T air collector (Assoa and Menezo, 2014)

Lin et al. (2014) combined phase change materials (PCM) in a roof-integrated BIPV/T air system. This system allowed for not only electricity generation, solar heating during winter daytime and sky radiative cooling during summer nighttime, but also increased insulation plus thermal energy storage with the PCM component. TRYNSYS simulations showed that the BIPV/T air system maintained indoor air temperatures consistently above 18.9 °C on typical winter days in Sydney.

Using a building simulation tool, Guiavarch and Peuportier (2006) found that the thermal efficiency of the BIPV/T system depended on which zones the heated air would be directed to. The simulation results also suggested the advantage of using semi-transparent PV modules instead of opaque PV modules because less heat was lost at non-packing areas with low emissivity and because the transmitted solar radiation was absorbed at the back of the system. Vats et al. (2012) analytically showed that a decrease in semi-transparent PV module packing factor (percentage of the total PV module area covered by solar cells) resulted in decreased module temperature and increased system thermal output. Bloem (2008) drew the same

conclusion through experiments performed using a test environment box. It was pointed out that convective and radiative heat exchanges on the rear side of the PV module in the building-integrated application were different from those for the open rack mounted PV. This was addressed by the test environment box that facilitated changing materials (e.g. metal, brick, wood) at the surface facing the rear of the PV. Aste et al. (2008) developed a BIPV/T component using semi-transparent PV modules and implemented this design concept for the Fiat Research Center at Orbassano, Italy. The installed system has a power of 20 kW_p and the hot air was used for preheating air in winter and desiccant cooling in summer.

Charron and Athienitis (2006) carried out an optimization study of the performance of ventilated double-facades integrated with PV panels and motorized blinds. Installing PV modules in the middle of the glazed cavity was found to enhance the heat recovery at the cost of reduced electricity generation. Integrating fins to the back of the PV resulted in a similar increase in thermal efficiency without compromising electrical output. It was concluded that optimization strategies depended on the intended use of the façade incorporating both a BIPV/T system and motorized blinds.

Kaiser et al. (2014) developed semi-empirical correlations for PV module temperature and resulting electrical efficiency in relation to depth-to-length channel aspect ratio, channel air velocity, ambient temperature and incident solar radiation. For systems with forced convection, lower aspect ratios were suggested to enhance PV cooling. For naturally ventilated systems, a critical channel aspect ratio of 0.11 was suggested to reduce the overheating of PV modules.

Zogou and Stapountzis (2011b) assessed typical transient behaviour of a BIPV/T air system in outdoor conditions in Greece. The authors further performed indoor tests to study the air flow

field in the BIPV/T setup, using flow visualization instruments as well as a hot wire anemometry system (Zogou and Stapountzis, 2012). A significant flow entrance effect was observed in the cases studied of their work. It was found that the flow rate and the heat transfer coefficient between the back of PV module and air are critical to the system performance. Candanedo et al. (2011) performed an experimental study to develop convective heat transfer coefficient correlations for an open-loop air-based BIPV/T system for Reynolds numbers ranging between 250 and 7500. The ever-changing ambient temperature, wind speed and sky cloudiness conditions in outdoor tests can result in large measurement uncertainties, therefore experiments need to be done under controlled conditions, such as in a solar simulator lab.

Sohel et al. (2014) developed a dynamic model capable of simulating the performance of BIPV/T air systems under real operation conditions. The numerical model showed that thermal efficiency increases with increasing ambient temperature in an approximate linear manner, while electrical and exergy efficiencies decrease with an increase in ambient temperature. Higher air flow rates were found to benefit electrical and exergy efficiencies until the flow rate exceeded 300 L/s at which point the efficiencies were not sensitive to the changes in flow rate.

Agrawal and Tiwari (2010b) designed BIPV/T air channels that can be connected in series or parallel for use in the cold climate. Numerical simulations suggested that the series configuration was more suitable for a constant air mass flow rate in terms of energy and exergy production, whereas the parallel configuration was better in the case of constant air velocity. Overall, the series configuration with constant mass flow rate was found to generate the most annual energy and exergy including thermal and electrical gains.

An unglazed BIPV/T system with PV directly exposed to the ambient air could result in a peak

PV temperature of about 60 °C on a warm sunny day (Chen et al. 2010). Yang and Athienitis (2014) proposed using multiple air inlets instead of one inlet for the BIPV/T system that usually involves large-scale installation. Based on experiments carried out on a conventional one-inlet BIPV/T system in an indoor solar simulator, a lumped parameter thermal network model was developed and verified with experimental data. Simulation results of a BIPV/T system with two inlets showed that the thermal efficiency was increased by 5% and the peak PV temperature was reduced by about 1.5 °C compared to a one-inlet system assuming equal total flow rates were used for each system. The authors pointed out that the local heat transfer coefficients were higher near the added inlet because the boundary layer had been broken, and that the air drawn into the second inlet has already been pre-heated by the PV top surface. It was suggested that for actual roofs of 5-6 meters long, the reduction of maximum PV temperature would be at least 5-10 °C depending on flow rate and wind conditions.

Karava et al. (2011) pointed out that the Nusselt number correlations previously developed for plates subjected to uniform approach flow should not be used directly for roof surfaces because of the complex wind flow field around buildings. In the context of BIPV/T application, a correlation for Nusselt number was developed that included the effects of free stream turbulence intensity and average Reynolds number. The importance of using actual distributed wind velocities as opposed to an assumed uniform velocity in the simulation of building-integrated solar systems was further discussed by Vasan and Stathopoulos (2014). They experimentally measured the wind velocity distribution on the BIPV/T façade using a physical model of the JMSB building of Concordia University (Athienitis et al, 2012) in an open circuit wind tunnel. It was observed that the velocity near building edges could be 50% higher than those above the

33

roof. The surrounding structures were found to increase the local wind velocities by 20-30% compared with the case when they were removed from the vicinity of the JMSB building. Full-scale measurements of wind-induced convective heat transfer coefficients for a flat plate solar collector mounted on a pitched roof was conducted by Sharples and Charlesworth (1998).

2.3.2 Passive BIPV/T Air System

Gaillard et al. (2014) conducted an experimental evaluation of a naturally ventilated two-storey BIPV system under real operating conditions. Monitored data suggested that the system may contribute to the heating and ventilation needs of the building in addition to electrical power generation, especially during the spring and autumn. With sheltered air inlets, the air movement behind the PV modules was found to be dominated by buoyancy effect, whereas no clear correlation was observed between the magnitude of channel air and outdoor wind speed. Using parametric analysis of the measured data, the authors developed linear models composed of a few independent variables to characterise the electrical and thermal performance of the BIPV façade, suggesting that simplified physical models should be appropriate to predict system performance despite the complexity of real operating conditions and unconventional geometries.

Analytical models are useful to predict the thermal behaviour of a passive BIPV system. Brinkworth et al. (2000) developed an analytical model to predict the thermal behaviour of a BIPV system with buoyancy driven laminar flow. The model is straightforward to use either as an Excel spreadsheet or coupled to a building simulation package. Also using analytical expressins of a passive BIPV system, Sandberg and Moshfegh (2002) found that the maximum flow rate was obtained by increasing the height of the air channel until a balance between friction

and buoyancy was achieved for a given heat input.

Wong et al. (2008) found that semi-transparent PV modules used as tilted residential skylights reduce the annual building heating load but cause overheating issues in regions with a cooling season in Japan. It was proposed to use transparent insulation for cold regions and opaque movable insulation for moderate regions to optimize the building energy performance. Varying the module packing factor was also found essential to achieve maximum energy savings in different climate conditions. Xu et al. (2014) concluded that implementing the optimal semi-transparent PV module packing factor achieved an average energy saving of 13% compared to the least favourable PV packing factor. Yun et al. (2007) discussed the optimum transparent window to opaque PV ratio for different climates, building characteristics and façade configurations. In addition, they suggested that locating the air outlet in a region of wind-induced negative pressure was essential to enhancing the natural ventilation in the BIPV system.

The open-joint ventilated façade employs discontinuous external cladding on ventilated facades, resulting in localized discontinuities of the air flow at the joints (Figure 2.8). Sanjuan et al. (2011) showed that open-joint ventilated facades may achieve significant energy savings in climates with hot summers and mild winters. There is a possibility of integrating PV as a building material into this type of ventilated façade.
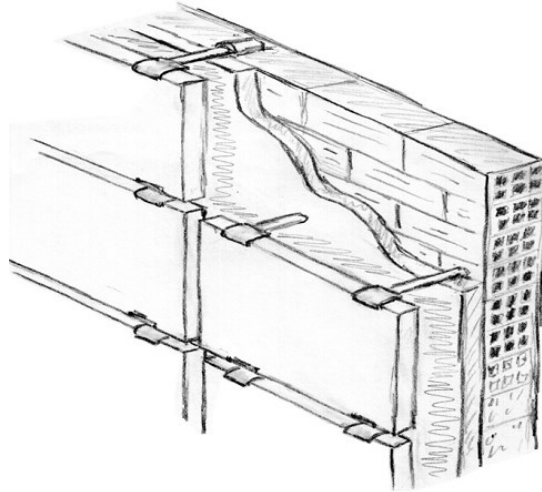
Figure 2.8. Schematic of an open-joint ventilated façade (Sanjuan et al., 2011)

In a BIPV/T Trombe wall system, the outer glazing of the traditional Trombe wall is replaced with the semi-transparent photovoltaic module, a-Si or c-Si type. While maintaining the advantages of Trombe walls such as simple configuration, no moving parts and zero running cost, the BIPV/T Trombe wall system generates electrical energy and reduces solar energy gain in summer. Furthermore, the front PV panel adds to the aesthetical appearance of the building, as compared to the black wall underneath the clear glass.

A Trombe wall consists of two solid layers – a glazing pane on the exterior and a massive thermal wall on the interior with an air cavity in between the layers. Usually there are vents at the top and the bottom of the wall to allow natural air circulation between the indoor space and the wall cavity. Driven by buoyancy force, heated air enters the room through the top openings and cool air returns to the Trombe wall through the bottom vents. Research on Trombe wall first appeared in the 1970s (Balcomb et al., 1977), and it was focused on the heat transfer and thermal modeling of the energy system (Warrington and Ameel, 1995; Chen et al., 1994; Smolec and Thomas, 1991; Utzinger et al., 1980).

Ji et al. (2007a) proposed a BIPV/T Trombe wall system and assessed the temperatures of the PV and indoor environment through numerical modeling. This BIPV/T Trombe wall system was shown to increase room temperature by a maximum value of 12.3 °C compared to the conventional wall in the winter of Hefei, China. Later, Ji et al. (2007b) found that installing a BIPV/T Trombe wall system in a fenestrated room with heat storage increased the room temperature by a maximum of 7.7 °C. Sun et al. (2011) showed that a south façade having both a BIPV/T Trombe wall and a window (Figure 2.9) achieved higher indoor temperatures than a façade with a conventional Trombe wall of the same size. Jiang et al. (2008) concluded that the indoor air temperature was increased by 6.8 °C when the PV packing factor was reduced from 0.873 to 0.207.

Koyunbaba and Yilmaz (2012) found that the BIPV/T Trombe wall system may lead to a significant room temperature increase. They suggested using an automation system for opening and closing the vents to maintain comfortable conditions in the room. In order to regulate the indoor temperature, Ji et al. (2007c) proposed a BIPV/T Trombe wall system having extra vents to exhaust the heated cavity air to the outdoor environment in summer. In addition, it was suggested to add thermal insulation, advantageous for both summer and winter conditions, and append a shading curtain in the summer to improve system performance. Aelenei et al. (2014) studied a BIPV/T Trombe wall system with the massive wall replaced with a gypsum board incorporating PCM. The PCM absorbed excessive heat during the day when solar radiation was abundant, thereby reducing the overheating of the indoor environment.
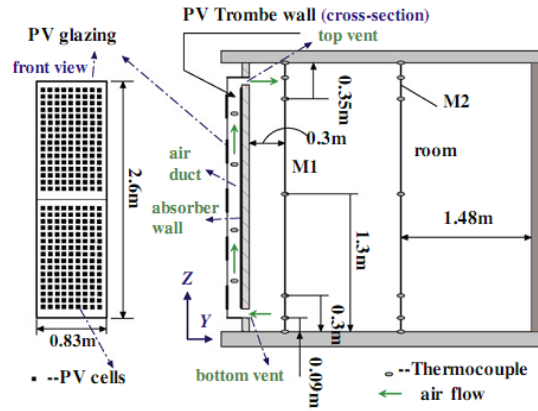
Figure 2.9. BIPV/T Trombe wall system utilizing semi-transparent c-Si PV modules (Sun et al., 2011)

Semi-transparent PV modules may replace window glazing owing to the light transmission and electricity generation capability. The interaction between the BIPV window and the building involves PV electricity generation, thermal loads, lighting consumption and visual comfort of the building. There are generally three forms of BIPV windows in current research: single pane, double-pane with enclosed air cavity, and ventilated double-pane with open air cavity.

Li et al. (2009) showed that visual discomfort, solar heat gain, lighting energy consumption and HVAC equipment size can be reduced by replacing southwest-facing tinted glass windows with semi-transparent a-Si PV panels and applying lighting controls in a typical office building in Hong Kong. Lu and Law (2013) also pointed out that using semi-transparent c-Si BIPV windows may enhance building energy performance. They suggested the following optimal office orientations for annual electricity savings in order for Hong Kong: south-east, south, east, south-west and west. Olivieri et al. (2014) concluded that for intermediate and large openings covering more than 33% of the façade area, BIPV windows account for 18-59% energy savings compared to glass when applied to a typical middle-size office building in Spain.

Figure 2.10a shows a typical double-pane BIPV window consisting of a semi-transparent PV panel at the outside and a glass pane at the inside with an enclosed air cavity in between. Miyazaki et al. (2005) showed that building primary energy consumption can be reduced by installing this type of BIPV window and adopting lighting controls. They suggested optimal transmittances of the PV module in accordance with different window to wall ratios of the building. A low emissivity coating was further shown to reduce radiative heat transfer and the U-value of this BIPV window configuration (Han et al., 2010). Chae et al. (2014) showed that up to 30% of the annual HVAC energy consumption can be saved by installing double-pane semi-transparent BIPV windows as opposed to double-pane clear glass windows, in the low and medium latitude US cities. Semi-transparent PVs of different optical properties were recommended for maximum utility cost savings for these cities.

(a)   (b)
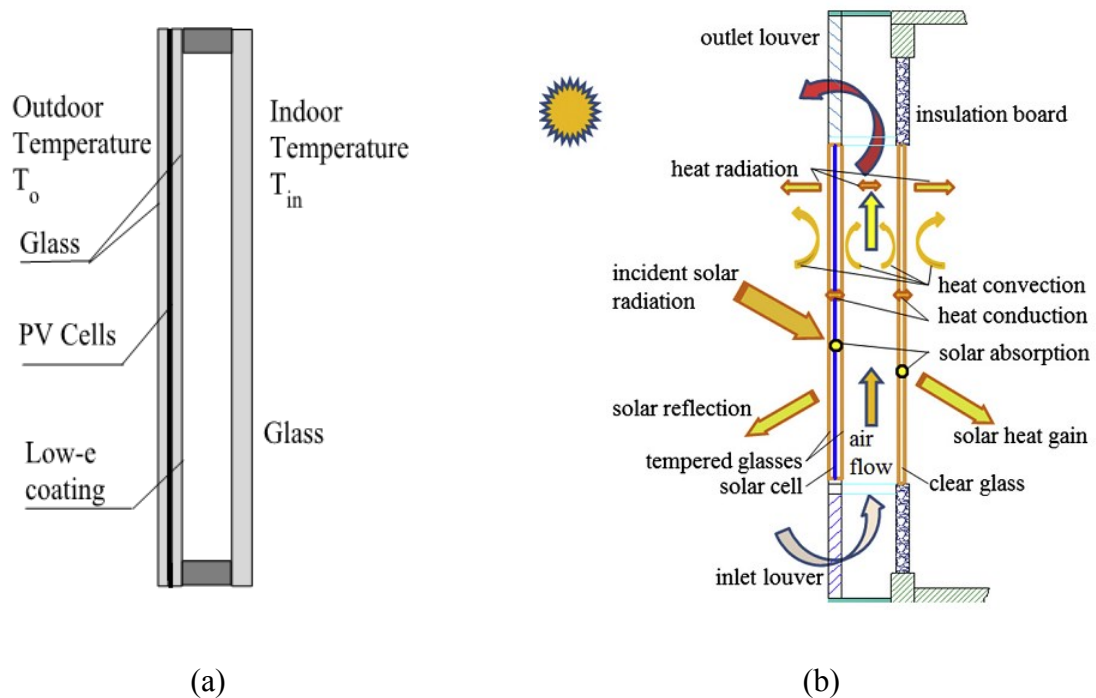
Figure 2.10. Double-pane BIPV/T windows (a) Double-pane semi-transparent photovoltaic

window with enclosed air cavity (Han et al., 2010); (b) Ventilated double-pane semi-transparent photovoltaic window with open air cavity (Peng et al., 2013a).

Figure 2.10b shows a schematic of a typical ventilated double-pane BIPV window with top and bottom vents on the exterior surface allowing heat removal from PV by naturally ventilated air. Experiments conducted by He et al. (2011) indicated that the indoor heat gain of the ventilated double-pane BIPV window was reduced to less than half of that of the single pane BIPV window. The thermal comfort level of the work space was also improved due to the lower inner surface temperature of the ventilated double-pane BIPV window. Chow et al. (2007a) showed that a PV transmittance of 0.45-0.55 in the ventilated BIPV window resulted in the most electricity saving when taking into account air-conditioning load, artificial light consumption and PV electrical generation. Annually the BIPV window can cut down the air-conditioning power consumption by 28% for a typical Hong Kong office, compared to the conventional single absorptive glass window (Chow et al., 2009a). The authors also stated that high-efficiency thin-film solar cells could facilitate the uptake of PV double-pane windows. From a monetary point of view, Ng and Mithraratne (2014) showed that with government subsidies certain PV modules with high efficiencies are cheaper to install than conventional double-glazed windows. It was also indicated that the energy payback offsetting the primary energy used to manufacture and transport the PV modules could be less than two years.

2.4 BIPV/T Water System

2.4.1 PV/T Water Collector

A typical PV/T water collector is constructed by attaching PV to the thermal absorber using

thermal paste with high conductivity (Ji et al., 2007; Zondag et al., 2003; Bakar et al., 2014), welding (Kalogirou and Tripanagnostopoulos, 2006), or mechanical force (Tripanagnostopoulos et al., 2002; Fraisse et al., 2007). Depending on the local climate and temperature conditions, an optional glazing can be added on top of the PV to form an extra stagnant air layer to increase thermal gains. The thermal performance of a PV/T water collector is affected by the following factors:

- Transmission losses through the upper glazing. The transmissivity can be increased by applying anti-reflective coatings on the two sides of the low-iron glass.

- Absorptivity of solar cells. Solar radiation absorption is optimised in the wavelength range of 300-1100 nm for silicon solar cells (Zeng et al., 2014). Ideally, the thermal performance is enhanced using a selective coating that ensures maximum solar absorption while maintains low emissivity in the infrared region. Santbergen et al. (2010) showed that anti-reflective coatings on the cover glass and the top surface of the PV improved both thermal and electrical efficiencies, while low-emissivity coating on the PV surface increased the thermal output at a cost of reduced electrical performance.

- Absorptivity of the PV module area not covered by solar cells. A common c-Si PV module is partially covered by photovoltaic cells, leaving the rest 10-15% area exposed as a sandwiched composition of glass/EVA/PVF (polyvinyl fluoride). The white PVF backsheet is highly reflective (70-80%) in order to reduce PV operating temperature. However, this leads to a reduction of available thermal energy in the PV/T system. Improvements can be achieved by using a solar absorbing or transparent backsheet.

- Thermal conductivity between the PV and thermal absorber. Good thermal contact

41

encourages more heat transfer from the solar cells to the working medium. The conductivity can be improved by using square instead of round ducts (Sobhnamayan et al., 2014), by laminating the PV with absorber using a vacuum laminator (Dupeyrat et al., 2011) or by replacing TPT (Tedlar/PET/Tedlar) backsheet of the PV module by aluminum alloy (Shan et al., 2013). Tripanagnostopoulos et al. (2002) pointed out the importance of promoting better thermal contact using a proper manufacturing procedure at the industrial scale.

- Withdrawal of electrical energy. Santbergen et al. (2010) demonstrated for the case when a low-e coating is applied on the PV surface, the PV electricity generation mainly accounted for the annual thermal energy reduction for a PV/T system than a solar heater.

The annual performance of a roof-mounted single-glazed PV/T water system was simulated to match the electricity and hot water consumption profiles of a typical UK house (Herrando et al., 2014). Simulation results identified that PV packing factor significantly influences electrical output, and that water flow rate affected hot water production to a greater extent. A packing factor of 0.8-1 and a low flow rate in the range of 20-80 L/h was suggested to increase system performance and reduce CO_2 emissions.

Bakar et al. (2014) designed an unglazed PV/T collector with co-generation of hot water and air. This system can obtain high water outlet temperatures while reducing penalty in electrical performance, if low water flow rate and proper air flow rate were maintained. With a total thermal efficiency of about 76% under favourable operating conditions, this system may potentially be used for agriculture drying, fresh air pre-heating and domestic hot water heating.

Although polymer materials have a lower thermal conductivity than copper, stainless steel and aluminum, the light weight of polymer allows a simple mounting at a lower price (Arcuri et al., 2014). Sandnes and Rekstad (2002) constructed a PV/T water collector by pasting solar cells onto the polymer absorber plate of a solar collector. Experimental results showed that the inlet water temperature should not exceed 40 °C for unglazed system and 30 °C for single-glazed system so that the solar cell temperature can be maintained below 45 °C. Fraisse et al. (2007) also examined using PV/T systems in the low-temperature application of direct floor heating. The low operating temperature of the PV/T system (below 35 °C) not only avoided overheating of the room, but also enhanced PV performance due to better cooling effect. However, PV module temperatures of above 100 °C were observed for the glazed system in summer when there were no heating needs, leading to a risk of EVA degradation and yellowing. The solutions included using amorphous modules which contained no EVA and employing non-glazed PV/T collector.

2.4.2 Investigation of BIPV/T Water System

Figure 2.11 shows examples of thermal absorbers used in BIPV/T water systems. The sheet-and-tube PV/T configuration (Figure 2.11a) can achieve satisfactory efficiencies, while being easy to manufacture by integrating a PV panel with a standard water collector with no significant modifications (Zondag et al., 2002; Zondag et al., 2003). The rectangular channels (Figure 2.11b) and flat-box absorber (Figure 2.11c) are used to enhance heat transfer in the BIPV/T system.
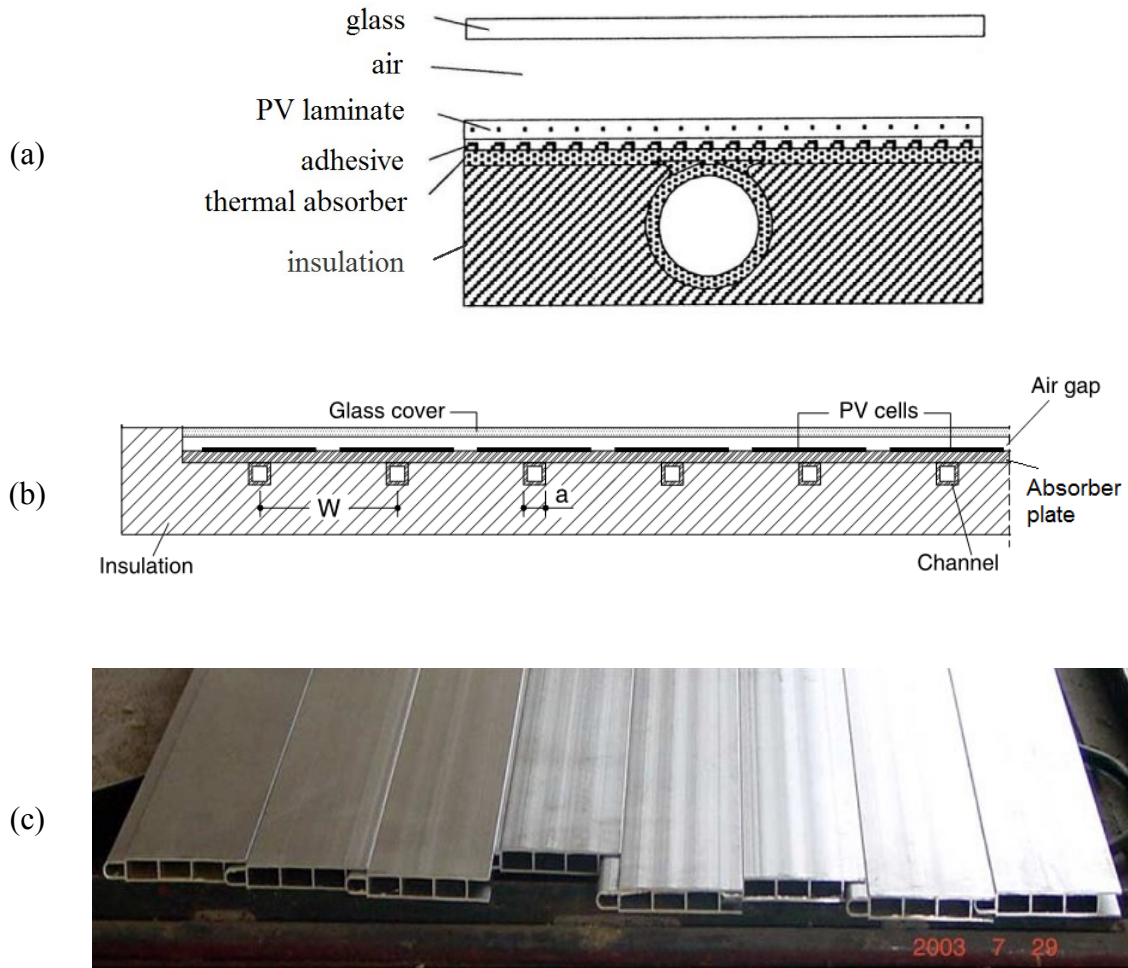
Figure 2.11. Examples of thermal absorbers of a BIPV/T water system: (a) Sheet-and tube

configuration (Zondag et al., 2002); (b) rectangular water channel (Evola and Marletta, 2014);

(c) Aluminum-alloy flat-box configuration(Chow et al., 2006)

Bakker et al. (2005) developed a manufacturing process where solar cells and a sheet-and-tube

copper absorber are laminated into a single PV/T panel. The performance of a 25 m^2 roof-size

PV/T installation coupled with ground-source heat pump was analysed using TRNSYS. The

system was found to meet the total hot water and spacing heating demand and nearly all

electricity demand for a typical Dutch single-family dwelling. Dupeyrat et al. (2011) used a

vacuum laminator to combine a PV panel and a rollbond aluminum absorber into a single PV/T component. In addition, anti-reflective coating was applied on the low-iron glass cover and mono-crystalline silicon cells with a higher absorptivity were used. This single-glazed PV/T system was shown to achieve thermal efficiency comparable to that of a thermal collector without selective coating. Moreover, Dupeyrat et al. (2014) demonstrated that a laminated BIPV/T collector achieved higher electricity and exergy outputs plus higher primary energy savings than side-by-side PV and thermal collector installations covering the same area. Also to improve the thermal contact between PV and thermal absorber, Zakharchenko et al. (2004) proposed a PV module design using a metallic substrate. A PV/T prototype using this type of PV module showed a 10% increase of power generation.

Ghani et al. (2012a) addressed the uneven flow distribution issue in sheet-and-tube BIPV/T water collectors and concluded that a manifold to riser pipe ratio of 4:1 and an array aspect ratio greater than 0.44 resulted in more uniform flow distributions. The study recommended a mass flow rate of 0.015 kg/(s·m^2) for aspect ratios less than 1.78; while for values greater than 1.78, higher mass flow rates was found to increase the net electric generation. Ghani et al. (2012b) further developed an artificial neural network to quickly evaluate the performance of BIPV/T systems according to the specific roofing conditions and energy requirements of the customer. It was demonstrated that electrical output was not always improved by increasing the number of risers, since inferior flow distribution uniformity was resulted.

Buker et al. (2014) considered using polyethylene pipes as the thermal absorber by adhering them to the rear surface of PV modules (Figure 2.12). An experimentally validated thermal model showed that the overall energy and exergy performances of this BIPV/T system were

45

better compared to the bare PV system. It was stated that the polyethylene tubes are an economical, easy-to-maintain and flexible cooling solution for existing PV systems and do not disturb the original PV system structure. In regard to affordable, easily-manufactured and easily-installed BIPV/T designs, Timmerman et al. (2009) proposed a plug-and-play liquid BIPV/T panel with the solar cells glued onto a plastic channel absorber. The authors suggested the use of labels, multiple connection points and different connectors for inlets and outlets to ensure fast and flexible connection of the BIPV/T panels.
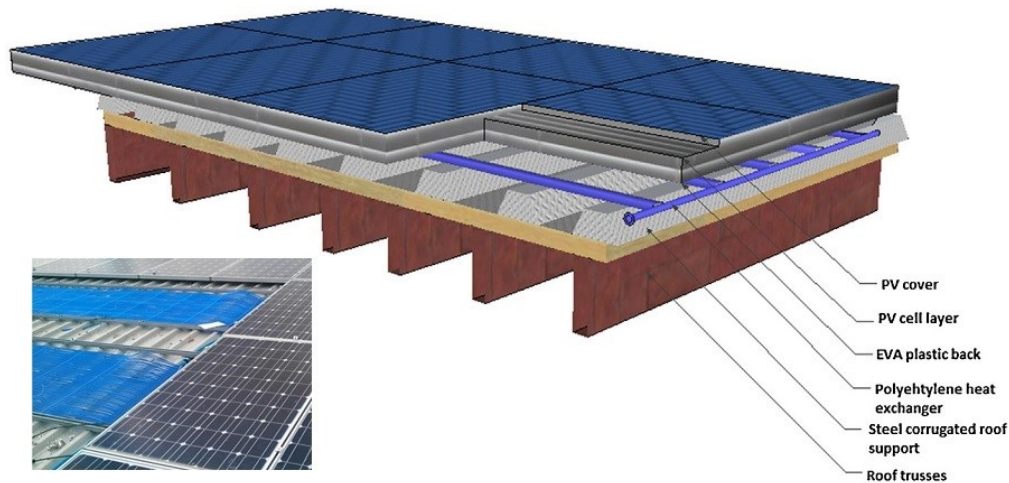
Figure 2.12. Schematic illustration and photo of the roof integrated BIPV/T water system using polyethylene pipes tested in Nottingham, UK (Buker et al., 2004)

Yin et al. (2013) designed a BIPV/T water system that incorporated a layer of mixed aluminum and insulating high density polyethylene with embedded water tubes (Figure 2.13). Experimental results showed a small temperature difference between the PV and the outlet water, suggesting that the aluminum enabled effective heat transfer to the tubes from all directions. This system can be installed as the roofing panel onto traditional roof framing, with the bottom structural substrate able to be integrated into the building skin and to provide thermal insulation. Yang et

al. (2012) implemented the numerical heat transfer simulation of this BIPV/T system using ABAQUS.
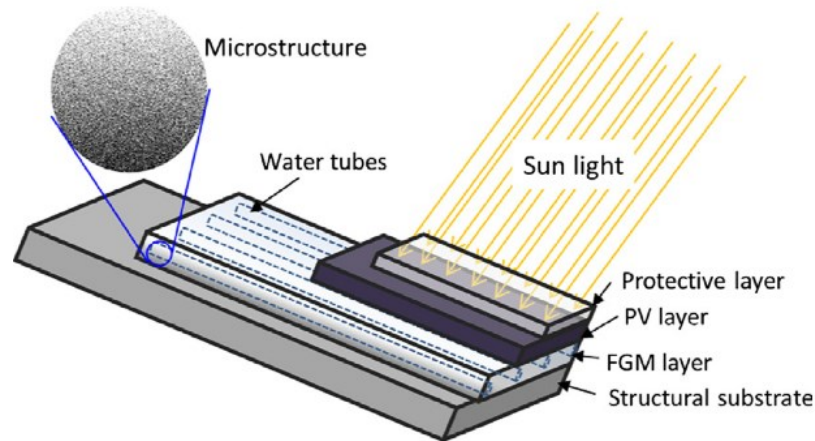
Figure 2.13. Schematic of the BIPV/T water-type roofing panel (Yin et al., 2013)

Evola and Marletta (2014) proposed a BIPV/T water collector using rectangular stainless steel ducts to enhance heat transfer between the thermal absorber and the water passage (Figure 2.11b). Thermal modeling demonstrated that there existed an optimum water inlet temperature that maximized the overall exergy efficiency of the BIPV/T collector. The optimal water supply temperature, which is a function of water mass flow rate, solar radiation and ambient air temperature could be regulated by a command-control system. Also from the point of exergy gain, Chow et al. (2009b) evaluated the performance of a thermosyphone-type PV/T water system using six parameters: PV packing factor, cell efficiency, water mass in the tank, solar radiation, ambient air temperature and wind velocity. They found that a change of any parameter affected the electric and thermal exergy efficiencies in opposite directions.

Fudholi et al. (2014) proposed three PV/T thermal absorber designs, one of which using spiral rectangular stainless steel tubes was adopted in the development of a BIPV/T water system

(Ibrahim et al., 2014). The collector was tested for energy and exergy performances in the hot and humid equatorial climate of Malaysia. The combined thermal and electrical efficiency was found to be 55-62%, while the exergy efficiency was found to be between 12% and 14%.

Chow et al. (2006) proposed a PV/T water collector with aluminum-alloy flat-box absorber underneath the PV (Figure 2.11c). With natural circulation of water, this system was shown to adapt well to 'hot summer and cold winter' climate zones of China. The flat-box-type water channel design was later implemented in a façade-integrated BIPV/T system (Chow et al., 2007b). Operated with a pre-set water consumption pattern, thermal efficiencies of the BIPV/T system under natural and forced water circulation modes were similar, and so were electrical efficiencies. The natural circulation mode was found more favourable for Hong Kong since the forced circulation mode incurred extra fan power consumption. Annual simulation of the thermosyphonic BIPV/T system showed thermal and electrical efficiencies of 37.5% and 9.39%, respectively (Chow et al., 2009c).

A BIPV/T water system with PV panels suspended 0.1 m above an array of black tube-fin absorbers was developed by the University of Colorado Solar Decathlon Team for the 2007 U.S. Solar Decathlon competition (Corbin and Zhai, 2010). A numerical model found that the thermal efficiency was lower than the results from the referenced literature owing to the ineffectiveness of heat transfer from the PV to the absorber by means of convection and radiation as opposed to conduction. An electrical efficiency correlation was developed as a function of water inlet temperature, ambient air temperature and solar insolation. Kazanci et al. (2014) also presented a BIPV/T roof panel for integration with the Solar Decathlon competition house of Technical University of Denmark. The BIPV/T installation was found to fulfill the electrical demand of the

building in addition to contributing to a significant portion of domestic hot water demand.

BIPV/T water systems have the potential of enhancing PV electrical performance in low-temperature applications, such as pool heating and direct floor heating (Tripanagnostopoulos et al., 2002), Fraisse et al., 2007; Sandnes and Rekstad, 2002). For moderate and high temperature systems (above 50 °C), it is necessary to compromise between the thermal requirement and the PV favorable operating temperature (low temperature). Malvi et al. (2011) suggested establishing thermal gain targets before PV performance is optimized by varying system parameters.

2.5 Other Systems

2.5.1 BIPV/T Systems Involving Phase Change Process

Materials have a large thermal capacity when experiencing the phase change process. They possess great potential for cooling PV modules. Huang et al. (2004) demonstrated that PV module temperatures can be maintained below 35 °C on typical June days in Southeast England by incorporating a solid-liquid phase change material (PCM) cavity at the back of the PV. The temperature regulation of PV may further be enhanced using internally finned PCM cavities (Huang et al., 2011), two PCMs with different melting temperatures (Huang, 2011), or a metal-embedded matrix (Maiti et al., 2011). Ho et al. (2012) showed that for a BIPV system cooled by a microencapsulated PCM layer, the electrical and thermal properties of the system relied on the melting temperature and width-to-height aspect ratio of the PCM layer.

To date, heat pipes and heat pump refrigerant evaporators, with a liquid-vapor phase change process, are incorporated in the BIPV/T system.

2.5.1.1 BIPV/T Heat Pipe System

Heat pipes have high thermal conductivity; they may enhance thermal performance and achieve more uniform PV module temperatures of BIPV/T systems. The independent heat pipe tubes may also avoid the problem of uneven flow distribution across multiple ducts that may be encountered in BIPV/T water systems. By selecting proper working fluids, heat pipes can maintain the operating temperature of photovoltaic modules in a suitable range. For example, Moradgholi et al. (2014) used methanol and acetone in a heat pipe PV/T system for spring and summer working conditions, respectively.

Figure 2.14 shows the schematic of a typical PV/T heat pipe system (Pei et al., 2011). The heat pipe evaporator adhered to the back of the PV module absorbs and transfers heat to the working medium. The vaporized medium then travels to the condenser section where it releases the heat and goes through a phase change to a liquid state. The liquid returns to the evaporator through a wick structure often using capillary force, beginning another heat transfer cycle.
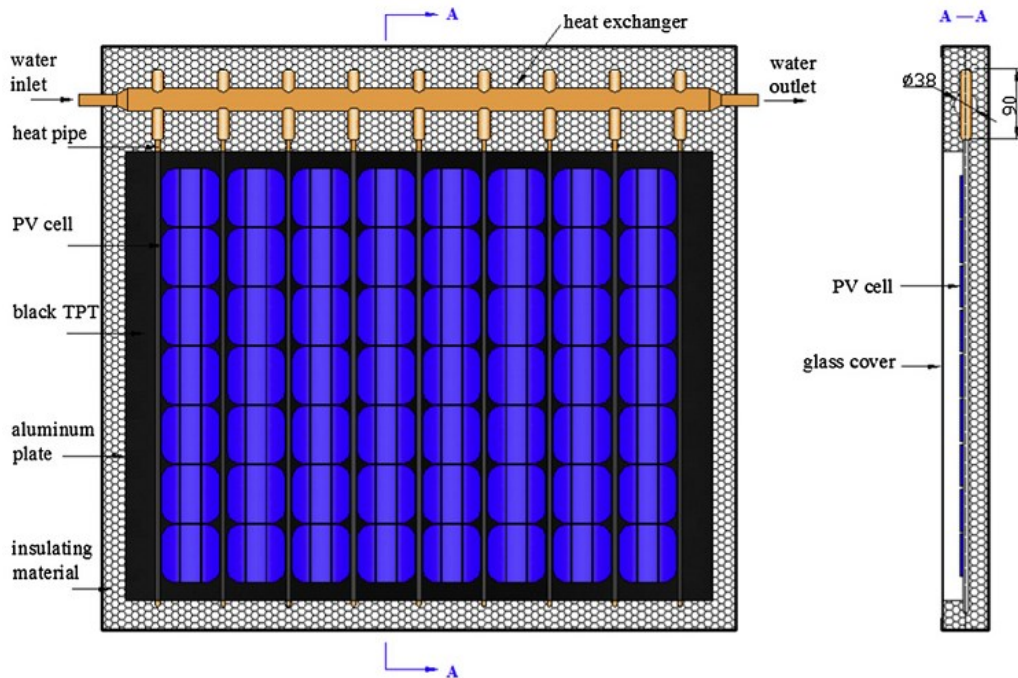
Figure 2.14. Schematic of a typical tube heat pipe PV/T system (Pei et al., 2011)

Pei et al. (2011) developed a heat pipe PV/T system with experimental thermal and electrical efficiencies of 41.9% and 9.4%, respectively. A dynamic model indicated a maximum temperature difference of 3°C between the evaporator and condenser sections of the heat pipe, showing the level of thermal conductance of the heat pipes. Further numerical study of the heat pipe PV/T system suggested that water-copper heat pipes were reliable for the operating conditions in Hong Kong, while ammonia-aluminum heat pipes were suitable for coping with the freezing problem in the cold winters of Lhasa and Beijing (Pei, et al., 2012a). A variety of parameters including water flow rate, PV packing factor, heat pipe spacing and solar absorption coefficient were discussed in terms of their influence on the system performance (Pei, et al., 2012b). Pei et al. (2010) also noted that the system performance could be improved by optimizing the refrigerant and enhancing the heat exchange between heat pipe and water tank.

Wu et al. (2011) proposed incorporating radial fins on the condenser section of the heat pipe to improve heat transfer from the heat pipe to the water flow. The system was found to achieve thermal and electrical efficiencies of 63.65% and 8.45%, respectively. PV temperatures were found within a deviation of 2.5°C, indicating the isothermal property of heat pipes.

Other types of heat pipe – the flat plate heat pipe and the loop heat pipe (LHP) are also used in BIPV/T systems. Quan et al. (2011) addressed that less thermal contact resistance was introduced with flat plate heat pipes compared to round heat pipes. On a typical March day in Beijing, a BIPV/T system using a flat plate pipe and ten 90 W PV modules was found to raise a 15 m^2 room to 26.3 °C through a floor radiative heating system. Zhao et al. (2010) stated that the LHP based water heating system can eliminate the need to transport water for a long distance since the solar receiving surface is covered by heat pipes rather than water ducts. Zhang et al. (2013) designed and fabricated a LHP with a vapour-liquid separation structure to overcome the 'dry-out' issue of conventional gravitational LHPs. Outdoor tests on such a combined PV/LHP and heat pump system showed a maximum daily temperature in the water tank to be around 54 °C in November, Shanghai. Experimental results also showed that the PV module was cooled by 5.2 °C using a coated aluminium-alloy sheet versus a conventional TPT sheet at the back of the PV module. The PV was found to generate more electricity than needed to drive the compressor in this system.

2.5.1.2 BIPV/T Evaporator System

Using a roof as the heat source (winter) and heat sink (summer) of the heat pump was proposed in the 1980s (Lazzarin and Schibuola, 1986). This concept has recently been applied to a BIPV/T evaporator system, constructed by attaching the direct-expansion evaporation coils of the heat

pump to the rear surface of building-integrated PV modules. The evaporative temperature of the refrigerant allows the PV operating temperature to be maintained at a low level (typically 0-30 °C). In comparison, Tiwari and Sodha (2006) pointed out that the PV cell temperature could reach over 55 °C in a PV/T water system.

Figure 2.15 shows a typical BIPV/T evaporator roof configuration, which incorporates the functions of roof element, electricity generator and heat pump evaporator (Zhao et al., 2011). Numerical simulation results indicated that an evaporation temperature of 0 to 10 °C and a condensation temperature of 50 to 70 °C are suitable for running this system coupled with a heat pump in UK. The system could achieve 55% of thermal efficiency and 19% of electrical efficiency under a typical Nottingham operating condition.
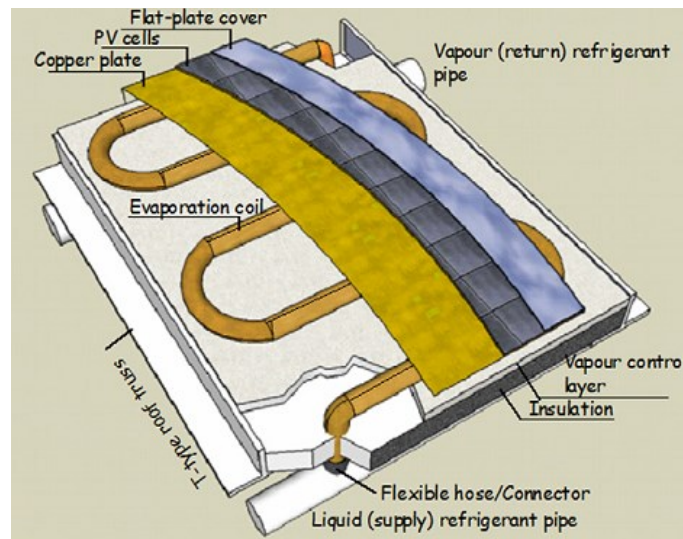
Figure 2.15. Schematic drawing of the BIPV/T evaporator roof (Zhao et al., 2011)

Xu et al. (2009) used multi-port flat aluminium extruded evaporator in a PV/T heat pump system to reduce heat transfer resistance between the PV and the evaporator. Simulation results showed that this system can heat 150 L water to 50 °C all year round in Nanjing and Hong Kong, China.

On a yearly scale, the overall performance of the PV/T heat pump system was shown to improve with varying compressor speed in different seasons. This conclusion is consistent with the result of a case study investigating the performance of a glazed PV/T heat pump system in Tibet, China (Liu et al., 2009). The refrigerant mass flow rate was matched to the ever-changing solar radiation and outdoor temperature using a variable-frequency compressor. The examined system was found to generate more electrical power than the compressor power consumption, with an average COP of 6.01 on a typical day in January. Xu et al. (2011) also used flat extruded aluminium tubes in a low-concentrating PV/T heat pump water heating system for experimental investigation in Nanjing, China. During the test period the refrigerant-cooled PV cell temperature varied between 20 °C and 30 °C, whereas the non-refrigerant-cooled PV cell temperature increased to 85 °C. PV electrical efficiency was found to be 1.36 times higher due to refrigerant cooling. Ji et al. (2008) further showed that a glazed PV/T heat pump system could achieve higher COP than the air-sourced heat pump. An average PV electrical efficiency of over 12% and an average heat pump COP of 5.4 of the PV/T heat pump system was predicted (Ji et al., 2009).

By attaching the evaporator coil of a heat pump directly under the PV modules, the heat pump is 'directly-assisted' by a BIPV/T system. Correspondingly, a BIPV/T system can 'indirectly-assist' a heat pump by providing heated medium as a heat source. Karagiorgas et al. (2010) investigated the energy potential of supplying the outlet hot air of a 23.5 m^2 façade integrated solar air heater to the evaporator of an air-source heat pump. Experimental results showed that the COP of the heat pump was increased from 3.33 to 4.94 with added solar input for ambient temperature of about 10 ºC. Hazi and Hazi (2014) compared two PV/T indirectly-assisted heat pump systems (a steam ejector heat pump and a mechanical compression heat pump) for hot water production in a

54

paper mill. Numerical simulation results showed that the system using a mechanical compression heat pump is more energy efficient. From the exergy point of view, the PV/T assisted steam ejector heat pump is more efficient for generating hot water at 70 ºC.

2.5.2 BIPV/T Concentrating System

For a BIPV/T concentrating system, a high density of luminous flux is cast on a relatively small PV surface with the use of reflective/refractive devices, resulting in a significantly high solar cell temperature. A thermal collector may be added to lower cell temperatures while producing high-temperature fluid that may effectively be used for solar heating or cooling. Generally, low concentration systems are considered promising for building integration due to the static states of concentrating device.

Chemisana et al. (2013) designed a facade-integrated concentrating BIPV/T system using Fresnel reflectors that also acted as vertical lattices for illumination control of the building. A solar cooling system consisting of such a concentrating BIPV/T collector covering an aperture area of 540 m^2 and a double-effect absorption chiller was shown to cover 39% of the cooling demand of a three-storey building on a typical summer day in Barcelona. Al-Alili et al. (2011) proposed a solar cooling unit consisting of a desiccant wheel driven by the thermal output of a concentrating PV/T system and a conventional vapor compression cycle driven by the electrical output. TRNSYS simulations results showed that the proposed system achieved a COP of 0.68, which was higher than that of either a solar absorption chiller or a standalone vapor compression cycle. Mittelman et al. (2007) addressed that the cost of a concentrating PV/T cooling system might be comparable to a conventional cooling system.

Davidsson et al. (2010) developed a concentrating BIPV/T window that incorporated multiple functions including glazing, electricity generation, hot water generation and shading. Figure 2.16 shows that the reflectors allow passive room heating at a horizontal position and enabled concentrating apparatus functioning at a vertical position. Diffuse radiation was found to account for about 40% of the electrical energy production. Annual simulation showed that the auxiliary energy need of the building with a BIPV/T window was 600 kWh less than that without a BIPV/T component (Davidsson et al., 2012).
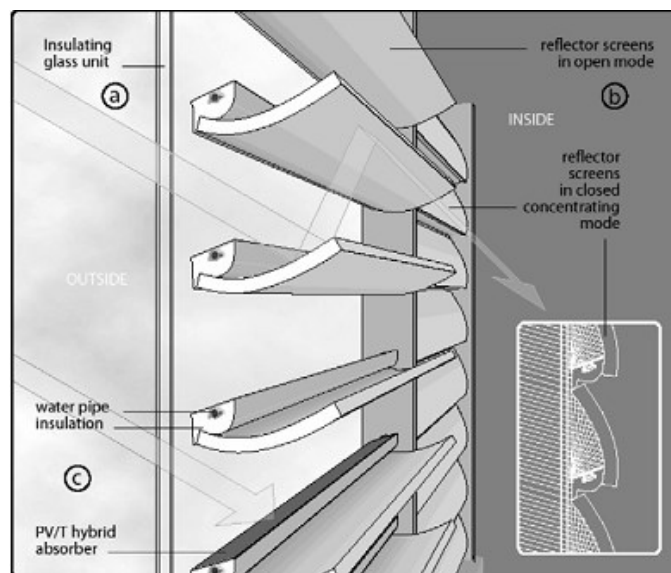
Figure 2.16. Schematic of a window-integrated concentrating BIPV/T system (Davidsson et al., 2010)

Wennerberg et al. (2000) pointed out that c-Si PV modules were more sensitive than thin-film modules to the non-uniform illumination resulted from the compound parabolic concentrator. Brogren et al. (2003) chose thin-film modules and parabolic reflectors to assemble a modular ready-to-use wall element. Measurements showed that the maximum electric power in the

concentrating system was 1.9 times that of the non-concentrating system. Gajbert et al. (2007) further optimised the geometry of the concentrating BIPV setup and identified some geometric variables allowing an annual electricity yield of 120 kWh/m^2 per cell area in Stockholm.

In addition, research has been conducted on rooftop installed concentrating BIPV/T systems that involve tracking mechanism. Parabolic trough BIPV/T prototypes with one-axis tracking systems were experimentally investigated in Sweden (Bernardo et al., 2011), Australia (Coventry, 2005) and China (Li et al., 2011). Fresnel BIPV/T system using two-axes tracking system with a higher concentration ratio was also developed in Spain (Rosell, et al., 2005).

2.6 Research Method

The following two sections will focus on the numerical and experimental approaches commonly used to evaluate the energy performance of BIPV/T systems.

2.6.1 Numerical Approach

(1) The BIPV/T collector may commonly be represented by one-dimensional thermal network models that are discretized by a finite-difference scheme. The models consist of coupled energy balance equations for each system element. Models can be applied for air systems (Wang et al., 2006; Charron and Athienitis, 2006; Sohel et al., 2014; Yang and Athienitis, 2014;), water systems (Chow et al., 2006; Herrando et al., 2014) and heat pipe systems (Ji et al., 2007a; Chow et al., 2008; Dehra, 2009; Gang et al., 2012). Nonetheless, two-dimensional heat conduction modeling of solid surfaces such as the PV module and the absorber in the BIPV/T system may be established. The sandwiched PV module may be

treated as multiple layers when writing energy balance equations. However, due to the low thickness and moderately high thermal conductivity of the PV module, a single temperature node to represent the PV may be sufficient (Infield et al., 2006). To increase the precision of electrical modeling, a five-parameter photovoltaic model may be utilised to access the electrical performance (Sarhaddi et al., 2010; De Soto et al., 2006).

On the other hand, the governing thermal model may be solved by working out the differential equations which result in analytical expressions for the unknown parameters. Such work may be found in Sandnes and Redkstad (2002), Infield et al. (2006), Dubey et al. (2009), Shahsavar and Ameri (2010), Tiwari and Sodha (2006), and Kumar and Rosen (2011).

(2) The performance of the BIPV/T system may be analysed through the use of a modified Hottel-Whillier model (Bergene and Lovvik, 1995; Vokas et al., 2006; Anderson et al., 2009).

(3) The integrated energy performance of BIPV/T systems and other energy systems can be evaluated by using software such as TRNSYS (Kalogirou and Tripanagnostopoulos, 2006; Fraisse et al., 2007; Zogou and Stapountzis, 2011a; Davidsson et al., 2012; Arcuri et al., 2014; Kamel and Fung, 2014; Dupeyrat et al., 2014), EnergyPlus (Miyazaki, et al., 2005; Olivieri et al., 2014), ESP-r (Chow et al., 2009a; DeBlois et al., 2013) and Energy-10 (King et al., 2004; Radhi, 2010). Typical building construction and local weather data may be available for use in simulations.

(4) Computational Fluid Dynamics (CFD) techniques have also been found to be useful when

assessing the BIPV/T system performance.

For all of the above methods of numerically investigating a BIPV/T system, the convective heat transfer coefficients (CHTC) needs to be available from previously validated correlations. Therefore, the degree of accuracy of the numerical models greatly depends on the adaptation of the correlations. In the case of CFD modeling, the velocity and temperature field of the working fluid of a specific system layout can be obtained by solving a set of conservation equations without using readily available CHTC correlations. On the other hand, the CHTC can be calculated based on the temperature profile generated by a CFD simulation.

The CFD model can be developed and solved either by custom written codes (Han et al., 2010; Li et al., 2014a &2014b) or by commercially available software such as FLUENT (Gan, 2009b; Karava et al., 2011; He et al., 2011; Wilson and Paul, 2011), CFX (Mittelman et al., 2009; Koyunbaba et al., 2012; Kumar et al., 2012), CHAM (Corbin and Zhai, 2010) and ALYA (Cipriano et al., 2013).

2.6.2 Experimental Approach

Well conducted experimental investigations could accurately investigate the performance of BIPV/T systems, and also be used to verify the mathematical models and simulation results. Three main experimental approaches are reported: indoor tests in built environment, outdoor tests in specially designed test cells, and building size experiments and demonstrations.

2.6.2.1 Indoor Test in Built Environment

Indoor testing in a built environment is especially useful for the development of mathematical models and the assessment of BIPV/T modules and systems. In order to perform indoor BIPV/T tests, a solar simulator is required. With the stable and controllable operating conditions of a solar simulator and the indoor environment, experiments can be performed in an accurate and repeatable manner.

Yang and Athienitis (2014) reported an indoor experimental facility with a solar simulator at Concordia University, Canada. As Figure 2.17 shows, solar radiation is simulated using eight special metal halid lamps that produce a spectrum similar to the sunlight. However, the considerably high temperature solar simulating lamps cannot adequately represent the blackbody temperature of the outdoor sky that a BIPV/T system 'sees' in the real world (Mei et al., 2009). To address this issue, an artificial sky was constructed by passing cold air between two low-iron anti-reflection glass panes to block the infrared radiation emitted by the lamps. The BIPV/T system is mounted onto the collector support that can be configured to have an angle of 0-90° simulating corresponding building envelope slopes. The air collector stand enables the cooling of PV modules with air convection at regulated flow rates. Using this solar simulator, a BIPV/T prototype was studied through a comprehensive series of experiments, based on which a numerical thermal network model was developed and verified.
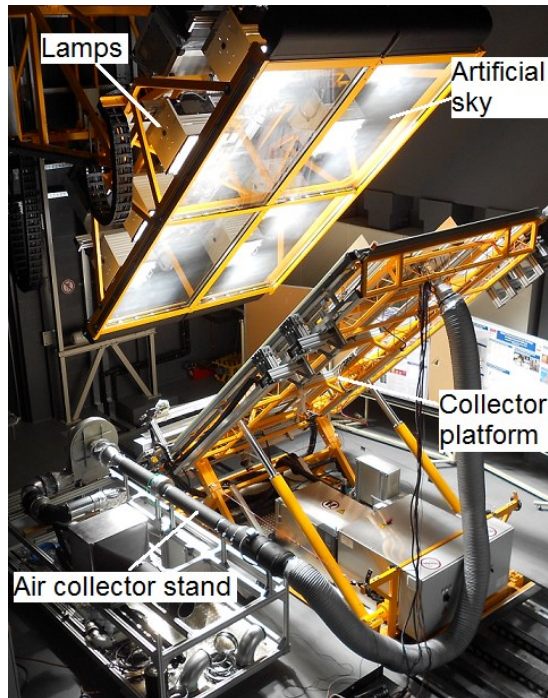
Figure 2.17. A photo of the solar simulator at Concordia University, Canada (Yang and

Athienitis, 2014)

Mei et al. (2009) examined the overheating problem of roof-integrated BIPV system in a solar

simulator at Loughborough University, UK. A simple energy exchange model was developed to

compensate for the excessive temperature elevation resulted from the hot lamps without artificial

sky. Chen et al. (2012) investigated experimentally a thin-film semi-transparent BIPV glazing

with a low solar heat gain coefficient (SHGC) by the use of an indoor calorimetric hot box. The

climate was simulated with a solar simulator and an external air curtain. Solanki et al. (2009)

experimentally studied the thermal and electrical performance of PV/T air collectors connected

in series using a solar simulator. Dupeyrat et al. (2014) obtained energy efficiency curves of

glazed and unglazed PV/T water prototypes using the indoor solar simulator of Fraunhofer ISE.

Krauter et al. (1999) studied the electrical and thermal performance as well as the thermal

insulating property of a façade-integrated BIPV/T system through the use of a solar simulator. Yin et al. (2013) also used a solar simulator to test a water-based BIPV/T roofing panel.

2.6.2.2 Outdoor Test in the Test Chamber

An indoor test facility has many advantages and high accuracy due to the built environment. However, construction of such a testing environment is costly, primarily due to the solar simulator requirement. Another option is constructing outdoor test chambers to house the BIPV/T system and at the same time simulate a building environment.

Figure 2.18 shows a BIPV/T water system integrated with the façade of an outdoor environmental chamber. Using this test chamber, Chow et al. (2007b) showed that natural convection of water was adequate for the Hong Kong climate, and that space thermal loads of the chamber was reduced through BIPV/T system integration.

Figure 2.18. A BIPV/T water system integrated with the façade of a environmental chamber

(Chow et al., 2007b)

An outdoor Test Reference Environment (TRE) was proposed to experimentally evaluate the performance of BIPV/T systems integrated as double skin in the building envelope (Bloem, 2008; Bloem et al., 2012). The TRE made it possible to study the impact of different materials for PV modules and construction design of building envelopes through electrical and thermal energy analysis. The experimental data and TRE have been used for validation of the modeling work of several research groups (Friling et al., 2009; Lodi et al., 2011).

Bigot et al. (2009) built four outdoor test cells to examine the thermal effect of naturally ventilated BIPV roofs on the building under tropical climate conditions. Measured temperatures of the roof, indoor air and inside wall surfaces for the test cells were compared with each other to find the insulating properties of each roof configuration. Experimental results were also used to validate a thermal model of the energy performance of the whole building.

Corbin and Zhai (2010) monitored the performance of a full-scale prototype of a BIPV/T water collector installed on the roof of a residential dwelling. Measured operating conditions and performance served as the basis to develop and calibrate a CFD model of the system. A correlation was developed relating electrical efficiency to operating and ambient conditions that allowed for direct calculation of the system performance.

2.6.2.3 Building Size Experiments and Demonstrations

Chen et al. (2010) conducted modeling, design, and performance assessment based on monitored data of a BIPV/T system in the EcoTerra near net-zero energy solar house. The full-scale monitored data were used to determine the performance of the BIPV/T system and judge its applicability for use in a cold climate. The measured data was also used to develop a

mathematical model for simulating the thermal performance of the BIPV/T system. The results were useful in preliminary design and for control of the air flow in the BIPV/T system and can be applied to other BIPV/T systems with similar configurations.

An open-loop active BIPV/T air system was installed as the building envelope of the near south-facing façade of the top floors of the John Molson School of Business (JMSB) building at Concordia University in Montreal (Athienitis et al., 2011). In winter the system generates a peak power output of 24.5 kW and a thermal output of 75 kW in the form of preheated fresh air. The BIPV/T system installation may also provide a model for retrofit projects where a new BIPV/T façade can be constructed over the existing building structure, thereby reducing installation costs.

Gaillard et al. (2014) conducted an experimental evaluation of a naturally-ventilated two-storey PV double-façade prototype installed on the West-North-West wall of an occupied office building in southern France. The experimental results showed that simple experimental techniques, including a database approach to filtering typical days, visualisation of data using carpet plots, estimation of global thermal performance measures, and the parametric analysis using correlation plots and empirical models, were adequate for evaluating the overall performance of PV systems installed in complex environments.

2.7 Influence on Building Energy Performance

Whether fully integrated with or superimposed on an existing building envelope, a BIPV/T (BIPV) system can influence building energy performance owing to the following factors:

- Part of the incident solar energy is directly converted into electricity by the PV module before transmitting through the envelope.

- Part of the absorbed solar energy is removed in the form of heat when a cooling medium is used.

- A BIPV/T component changes the U-value of the building envelope, thus the heat flow between the ambient and the indoor environment is adjusted.

- A PV module obstructs the solar radiation on the original wall in BAPV installations.

- The solar absorptivity of a building envelope is changed when replacing/covering conventional building structures, the reflective roof for instance, with PV modules.

- The use of semi-transparent PV modules changes the visible transmittance of light and subsequently the artificial lighting energy consumption profile.

It is difficult to arrive at general conclusions about the effect of BIPV/T systems on the thermal performance of buildings, because a broad range of factors may influence building energy performance. This topic is discussed in the context of two BIPV system types: opaque and semi-transparent.

(a)
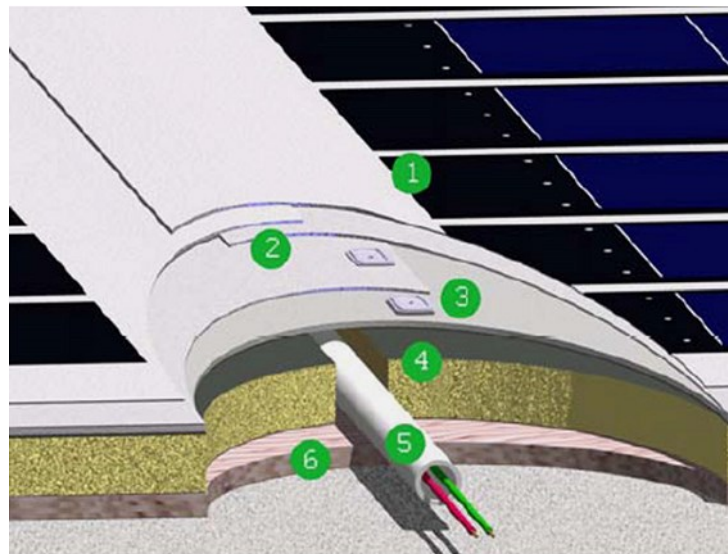
(b)

Figure 2.19. Roof BIPV systems. (a) Illustration of the installed BIPV system including (1) thin film PV; (2) white PVC membrane; (3) roof board; (4) rigid insulation; (5) electrical wire conduit; (6) the existing roof (Ban-Weiss et al., 2013); (b) Photo of a BIPV installation of thin film PV modules laminated with polyolefin membranes (Pola et al., 2007).

Applying an additional layer of BIPV system to an existing building roof/façade may generally reduce cooling load for three reasons. Firstly, solar energy input is reduced owing to the electricity conversion and the obstructed solar energy transmission into the room due to the PV. Secondly, the added BIPV component increases the thermal insulation level of the building envelope. Thirdly, a portion of the heat is removed when a cooling medium is used. Through field monitoring and modeling of real buildings, Dominguez et al. (2011) and Ban-Weiss et al. (2013) reported that heat flux through the roof may be reduced by installing a BIPV system. For such thermally insulated BIPV systems on flat roofs, Pola et al. (2007) stated that a-Si PV modules are more suitable than c-Si PV modules due to the lower temperature coefficient and the annealing mechanism of these modules can partially compensate for the low irradiation and the

high reflection due to the horizontal integration (Figure 2.19b).

In addition, leaving an air gap behind the PV was generally shown to further reduce cooling load while boosting PV electrical production (Wang et al., 2006; Chow et al., 2003; Bigot et al., 2009). Modeling of a whole residential house (Figure 2.20) showed cooling load reductions of 49-92% due to the free cooling and natural ventilation of the opaque BIPV roof solar chimney for four US climates (DeBlois et al., 2013). The ventilated BIPV chimney was found to be an energy efficient option in moderate climate cities. Similarly, PV shading devices can enable efficient energy use in buildings. Mandalaki et al. (2012) assessed a large range of window shading designs in Greece and proposed effective designs for reducing heating, cooling and lighting energy loads. A BIPV/T Trombe wall is generally found to reduce the cooling load but increase the heating load of the building (Ji et al., 2007a; Sun et al, 2011). The less efficient heating effect incurred by the PV modules may be compensated by applying thermal insulation on the massive wall (Ji et al., 2007c).
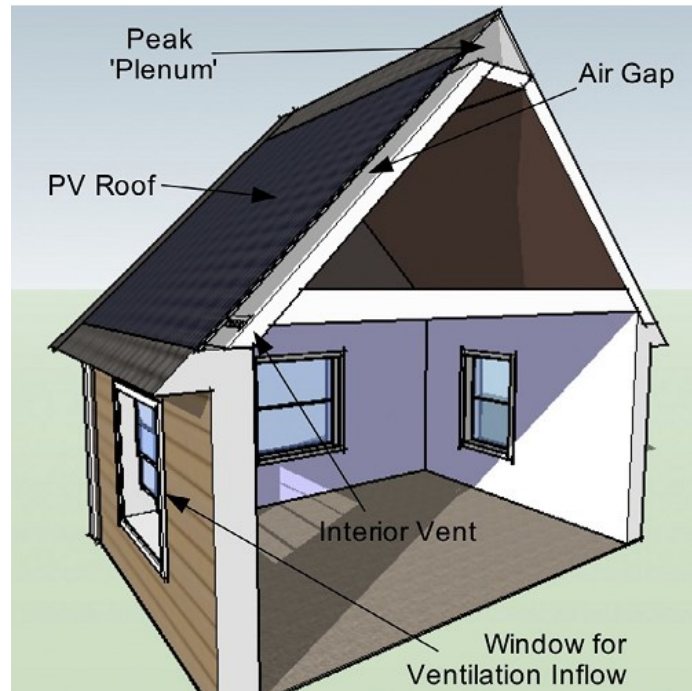
Figure 2.20. Section plane of a residential house installed with an opaque BIPV roof solar chimney (DeBlois et al., 2013)

The introduction of semi-transparent PV modules in BIPV/T designs complicates the analysis of building energy performance, which affects heating load, cooling load, artificial lighting consumption, and shade control. The optimisation of building energy conservation should usually take a holistic view, considering parameters including installation area, a-Si PV transparency (c-Si PV packing factor), room depth, ventilation mode, orientation and climate. It is generally demonstrated through numerical modeling and experimentation that using semi-transparent BIPV windows as opposed to glazed windows can provide energy saving opportunities in warm climates (Chow et al., 2007a; Li et al., 2009; Han, et al., 2013; Lu and Law, 2013; Olivieri et al., 2014; Xu et al., 2014). This is mainly due to the low solar transmittance and U-value of semi-transparent BIPV windows reducing heating loads

significantly in cooling-dominated locations. Investigation of a BIPV window system was also conducted for the cold climate such as Japan (Miyazaki et al., 2005; Wong et al., 2008). Wong recommended using transparent insulation material to increase heat gain magnitude and duration while limiting the night-time heat loss. The annual energy saving potential of integrating the a-Si PV modules into the window system of a medium-sized office building in 6 typical US climates from dry tropical to humid continental was evaluated (Chae et al., 2014). It was found that building heating energy demand was found to depend highly on the local climate and thermal-optical properties of the PV. The use of BIPV window may reduce the heating load in low latitude sites including Miami, Phoenix and Los Angeles, yet increase the heating load in Duluth at 46°47'N. It was concluded that BIPV windows may be a good candidate for reducing annual HVAC energy consumption for low and medium latitude locations.

2.8 Discussion and Conclusions

2.8.1 Summary of BIPV/T Systems

The omnipresence and light weight of air makes BIPV/T air systems available for integration with multiple building elements including roof, façade, window and skylight. Open-loop active systems are often found equipping the opaque building envelope such as the roof and façade, and the active heat recovery system may be used to provide fresh preheated air or operated in connection with other energy systems of the building. Open-loop active BIPV/T air systems may contribute to achieving net-zero energy buildings enormously where space heating load dominates the annual energy consumption of the building. Existing building materials or energy components such as ribbed metal roofing sheet, photovoltaic shingles, Trombe wall and unglazed

transpired collector may be exploited for use to develop innovative BIPV/T systems. In addition, the open-joint ventilated façade may help to achieve energy savings in climates with hot summers and mild winters. It is promising to use PV modules as the outmost cladding in this type of façade. On the other hand, the transparent surfaces of the building envelope such as window and skylight provide integration locations for passive BIPV/T system often utilising semi-transparent PV modules. The BIPV/T window has the potential of reducing cooling load, visual discomfort and artificial lighting consumption in the warm climate than conventional glass windows. However, the convective heat transfer coefficient of air was relatively low due to its low density and heat capacity, resulting in less efficient cooling of PV panels. It is therefore important to enhance the heat transfer between air and the PV.

Increasing the thermal contact between the PV module and the water channels has been a research topic for BIPV/T water heating systems. The conventional round copper tubes may be replaced by rectangular stainless steel ducts or aluminum-alloy extruded flat-box absorber so that the contact surface between PV and tubes are increased, which in turn reduces the thermal resistance. The substrate material of the PV may also be considered using a metallic layer to increase the heat dissipation rate. Although having a much lower thermal conductivity than metal, polymer is also utilised in BIPV/T water systems because the light weight allows a simple mounting and lower price reduces initial system cost. These properties are important for building application because less weight reduces the load on the building's physical structure and a significant amount of investment may be saved for a large installation on a building scale. When taking the advantages of both material options into account, it may be interesting to develop a mix of polymer material and metallic particles for BIPV/T water systems. In addition, BIPV/T

water systems have been extensively investigated in regard to the number of glazing, glazing material, anti-reflective/low-emissivity coating, as well as operating mode between natural and forced convection.

The constraints of air-based and water-based BIPV/T systems are: (1) limited heat transfer rate; (2) reduced heat absorbing ability with increased fluid temperature which results in significant temperature variations of the PV; (3) conflict between maintaining favourable low operating temperature of the PV and obtaining high-grade thermal energy. BIPV/T systems may make use of the phase change process which has considerable heat absorbing potential at a constant temperature to address the above-mentioned issues to some extent. So far, BIPV/T systems integrated with PCMs, heat pipes, and the evaporators of heat pumps have been developed and studied.

A heat pipe BIPV/T system often works with another fluid circuit that transports the thermal energy away from the condenser section of the heat pipe. The sealed heat pipes may reduce the risk of leakage and avoid uneven fluid distribution from manifold to riser pipes encountered in water and heat pump BIPV/T systems. The working medium and fill ratio of the heat pipe are yet to be explored to optimise system performance in different climates and for different serving purposes. The heat exchanger that removes thermal energy from the hot end of the heat pipe should be carefully designed to allow efficient heat transportation.

For the BIPV/T system integrated with the evaporator of a heat pump, not only can the PV temperature be maintained at favorable levels, but also the COP of the heat pump is elevated owing to the solar energy input. Selecting the refrigerant, determining the evaporation and condensation temperatures, and regulating the compressor speed with different seasons are

crucial to enhancing system performance.

The PCM in the BIPV/T cavity may cool down the PV module during the daytime through a phase change process from solid to liquid, and release the stored heat at night. Selecting adequate type and quantity of PCM according to the temperature requirements and thermal load is important to ensure sufficient cooling of the PV.

The additional reflective/refractive devices of concentrating rather than flat BIPV/T systems make it necessary to develop innovative integration designs into the building. Nonetheless, the concentrated solar energy could produce high-temperature liquids to assist solar cooling despite the system complexity. The potential of integrating more types of concentrating devices in an innovative way into buildings may be further investigated.

To further assist the understanding of the BIPV/T technology, main international research activities on BIPV/T systems are listed in Table 2.3.

Table 2.3. Main international research activities on BIPV/T systems

Country	References	Integration	PV	Approach	Findings	Highlights
Open-loop active BIPV/T air systems						
Canada	Athienitis et al. (2011)	Façade	c-Si	Experimental	• Combined electrical and thermal energy generation of the BIPV/T system integrated with UTC is 7-17% more valuable than a UTC. • The ratio of the PV area coverage of the UTC may be varied based on the fresh air heating needs and electricity needs.	• The BIPV/T concept is applied to a full scale office building demonstration project of 288 m2, providing a peak energy generation of 25 kW electrical and 75 kW thermal. • Custom-manufactured PV modules use black frames and backsheet to enhance thermal performance. • UTC corrugations are horizontally placed to facilitate air flow into the plenum.
Australia	Sohel et al. (2014)	Roof	Thin-film	Numerical	• Electrical and exergy efficiencies are less sensitive to air flow rate when it exceeds 300 L/s for the system investigated. • Thermal and overall efficiencies decrease while electrical and exergy efficiencies increase with increase of solar irradiance.	• Dynamic performance assessment under real operating conditions is performed. • BIPV/T system is installed on two buildings, one being a Solar Decathlon China 2013 house and the other being the Sustainable Building Research Centre building in Australia.
Canada	Chen et al. (2010); Candanedo et al. (2011); Yang and Athienitis (2014)	Roof	a-Si	Numerical experimental	• Significant cooling effect of the PV module is achieved with the air flow. • A typical thermal efficiency of 20% was achieved by the BIPV/T system. • Heat transfer coefficients between air and the PV panel are developed. • The thermal efficiency of the BIPV/T system may be increased by 7% with four multiple inlets.	• The BIPV/T system is installed in a low-energy solar demonstration house in Canada. • Outdoor experiments are performed. • Indoor experiments on the BIPV/T system are carried out in a full-scale solar simulator.

Country	References	Integration	PV	Approach	Findings	Highlights
UK, Germany	Infield et al. (2006); Mei et al. (2003)	Façade	c-Si (ST)	Numerical	• Outlet air temperature of the system is around 50 °C in summer and 40 °C in winter. • U-value of the façade is fairly constant over the heating season. • Twelve percent of heating energy can be saved using the ventilations air of the BIPV/T system for the Mataro Library building in Spain.	• U-values and g-values (SHGCs) are used to characterise the thermal performance of the semi-transparent BIPV/T façade and facilitate the energy modeling of the building. • Heat gains to the ventilation air may offer the potential for solar cooling in summer. • The BIPV/T system equips the Mataro Library building in Spain.
Italy, Spain	Bloem (2008); Bloem et al. (2012)	Façade	c-Si	Experimental	• Modification to the air inlet may allow air flow to enter the BIPV/T cavity homogeneously without disturbance. • Electrical and thermal performances are studied for BIPV/T systems with different PV module configurations.	• The Test Reference Environment enables the testing of BIPV/T systems using different materials under outdoor conditions. • The experimental results contribute to an improved knowledge of heat transfer and are used to validate numerical modeling by several research groups in Europe
India	Agrawal and Tiwari (2010)	Roof	c-Si	Numerical	• For a constant air mass flow rate of 1.2 kg/s, the series connection of the air channels is suitable for the BIPV/T system at Srinagar, India. • The annual electrical and thermal exergies are 16,209 kWh and 1532 kWh. The thermal efficiency is 53.7%.	• A 65 m2 BIPV/T system is installed on the roof of a building at the Centre for Sustainable Technology in India. • Parallel and serial connections of the air channels are evaluated to select an appropriate system for the local climate.
Japan	Nagano et al. (2003)	Façade	c-Si	Experimental	• Using glass or Teflon as the cover material for the PV module does not affect electrical performance significantly. • Thermal efficiencies for glazed and unglazed BIPV/T systems are 20.2-22.3% and 29.2-36.9%.	• The BIPV/T system suitable for operation in snowy regions is developed and tested. • The design facilitate modular assembly

Country	References	Integration	PV	Approach	Findings	Highlights
Greece	Zogou and Stapountzis (2011b), (2012)	Façade	c-Si	Numerical experimental	• Significant flow entrance effect is observed for the BIPV/T system. • The selection of air flow rate and the heat transfer coefficient between the PV backsheet and the air are critical to adequately characterise system performance.	• The transient performance of the BIPV/T system is studied by experiments under outdoor operating conditions. • Flow visualization techniques are used to study the air flow and turbulence field in the BIPV/T cavity under indoor steady-state conditions.
Passive BIPV/T air systems						
France	Assoa and Menezo (2014)	Roof	c-Si	Numerical experimental	• Natural air ventilation is sufficient for the cooling of PV modules in the studied configuration.	• The BIPV/T system is developed using ribbed steel sheet absorber.
USA	Mittelman et al. (2009)	Roof	c-Si	Numerical	• Inclusion of naturally ventilated air channel behind the PV modules can decrease their temperatures by 10-20 K	• A correlation is developed for the combined convection-radiation heat transfer coefficient
France	Gaillard et al. (2014)	Façade	c-Si	Experimental	• Simplified physical models are demonstrated to be able to predict system performance as a function of environmental conditions. • A variety of data-processing techniques are suitable to study the BIPV system performance in complex environments.	• Full-scale two-storey double skin BIPV/T system is installed and operated under real conditions.

75

Country	References	Integration	PV	Approach	Findings	Highlights
China	Ji et al. (2007a)(2007b), Jiang et al. (2008), Sun et al. (2011)	Façade	c-Si	Numerical experimental	• Installing the BIPV Trombe wall in a fenestrated room with heat storage might provide an energy solution to buildings with high heating demands and good solar resources. • PV packing factor may be varied to address different electrical and heating needs.	• The potential of integrating PV into the Trombe wall system is exploited.
UK	Yun et al. (2007)	Façade	c-Si	Numerical	• Optimal area ratios of PV façade to fenestration are given for London, Madrid and Stockholm. • The air outlet should be placed in a region of win-induced negative pressure to enhance the natural ventilation.	• The ventilated PV façade may provide pre-heated air in winter and reduce PV temperature using room exhaust air in summer.
USA, South Korea	Chae et al. (2014)	window	a-Si (ST)	Numerical	• Semi-transparent PV windows may reduce annual cooling load. • Semi-transparent PV windows may reduce annual HVAC energy load in low and medium latitude locations.	• Three types of semi-transparent a-Si cells are fabricated and their optical properties are evaluated. • Energy performance of typical office buildings installed with the PV windows is assessed in 6 climate conditions in the US.
BIPV/T water systems						
USA	Yin et al. (2013); Yang et al. (2012)	Roof	c-Si	Experimental	• Double than single serpentine water tube connection may achieve better PV temperature distribution uniformity. • Thermal efficiency may reach 53.9% with 1100 W/m2 and 66 ml/min.	• A water-based BIPV/T roofing panel is constructed and tested. The multifunctional system provides energy, insulation, structural strength and waterproofing. • Water tube is embedded in the polyethylene with high aluminum content. This allows for heat transfer to water tubes in all directions.

Country	References	Integration	PV	Approach	Findings	Highlights
China	Chow et al. (2007b); Chow et al. (2008); Chow et al., (2009)	Façade	c-Si	Numerical experimental	• Natural over forced water circulation is more suitable for the system in Hong Kong. • The BIPV/T façade reduces thermal loads in summer and winter. • Annual thermal and electrical efficiencies are 37.5% and 9.4% in Hong Kong.	• The BIPV/T water collector is installed on the façade of a test chamber and tested. • Aluminum-alloy flat-box type of thermal absorber was used in the BIPV/T design.
UK	Herrando et al. (2014)	Roof	c-Si	Numerical	• The investigated BIPV/T system may cover 52% of the electrical and 36% of the hot water demands annually. • High PV packing factor and low water flow rate are recommended.	• The suitability of BIPV/T system for the provision of electricity and hot water for a typical terraced house in the UK is assessed.
New Zealand, Australia	Anderson et al. (2009)	Roof	c-Si	Numerical experimental	• Low cost materials such as pre-coated color steel may be utilised in the BIPV/T design without significant efficiency decrease. • Good thermal contact between the PV and the absorber need to be made; this could be achieved using thermally conductive adhesives.	• A BIPV/T water system is developed by integrating the PV with troughed sheet roof.
USA	Corbin and Zhai (2010)	Roof	c-Si	Numerical experimental	• Thermal and overall efficiencies are 19% and 34.9%. • A correlation is developed relating electrical efficiency to inlet water temperature, ambient air temperature and insolation.	• Full-scale experimentation is carried out on a BIPV/T water system. • The BIPV/T system is installed for a Solar Decathlon competition house.
UK	Buker et al. (2014)	Roof	c-Si	Numerical experimental	• A thermal efficiency of 20.25% may be achieved with water temperature increase of 16 °C for the BIPV/T system.	• A BIPV/T system is formed by laying polyethylene water tubes under the PV panels, offering an inexpensive and requiring minimum maintenance heat extraction solution to existing PV systems.

Country	References	Integration	PV	Approach	Findings	Highlights
					Heat pipe BIPV/T systems	
China	Pei et al. (2011); Pei et al. (2012)		c-Si	Numerical experimental	• Thermal, electrical and exergy efficiencies are 41.9%, 9.4% and 6.8%. • Annual solar thermal contribution of the system is 69%, 81% and 65% for Hong Kong, Lhasa and Beijing, respectively.	• A glazed heat pipe PV/T system was constructed and tested outdoors. • Temperature difference between the hot and cold ends of the heat pipe is less than 3 °C. • Freezing problem may be avoided with a carefully selected heat pipe working fluid.
China	Wu et al. (2011)		c-Si	Numerical	• Thermal, electrical and exergy efficiencies are 63.7%, 8.5% and 10.3%	• PV module temperature difference range less than 2.5 °C. • Radial fins are used on heat pipe condenser section.
UK, China	Zhang et al. (2013)	Roof	c-Si	Experimental	• The electrical, thermal and exergy efficiencies of the PV/T system are 9.1%, 39.3% and 15.0%. • The thermal COP is 5.5. The thermal and electrical combined COP is 8.7. • The aluminum-alloy based PV temperature is 62.4 °C. It is 5.2 °C lower than that of the Tedlar based PV module.	• A loop-heat-pipe integrated PV/T system is fabricated for use in connection with the heat pump. • A coated aluminium-alloy sheet over the conventional Tedlar material was used as the backsheet of the PV module for enhanced heat dissipation.
					Heat pump BIPV/T evaporator system	
UK, China	Zhao et al. (2011)	Roof	c-Si	Numerical	• Electrical and thermal efficiencies are 19% and 55% in the UK climate. The heat pump efficiency is over 70%. • Evaporation and condensation temperatures are recommended to be 10 °C and 60 °C for UK.	• A roofing system design that incorporates the roof element, the PV module and the evaporator of a heat pump is developed.

Country	References	Integration	PV	Approach	Findings	Highlights
China	Ji et al. (2008), Liu et al. (2009)		c-Si	Numerical experimental	• Average COP of the tested system is 6.5. • The PV/T evaporator system significantly improves the COP of the heat pump. • The average COP of the system reaches 6.0 on a typical sunny winter day in Tibet, with electrical and thermal efficiencies to be 47.9% and 13.5%.	• The performance of a PV/T evaporator system working in connection with a heat pump is experimentally tested in outdoor conditions.
Nether-lands	Bakker et al. (2005)	roof	c-Si	Numerical	• A 25 m2 PV/T system and a ground coupled heat pump may cover the total heat demand for a typical Dutch one-family dwelling. • PV generated electricity may cover 96% of electricity use of the pumps, heater, and heat pump.	• PV/T panels are made by laminating PV modules onto a sheet-and-tube absorber as the evaporator of a heat pump and installed on an office building.
Concentrating BIPV/T systems						
Spain	Chemisana et al. (2013)	Façade		Numerical	• The BIPV/T system integrated with the absorption chiller may cover up to 39% of the cooling load of the building. • The heat rejection of the proposed system is less than 75% of a single-effect absorption chiller assisted by evacuated tube collectors. This means reduced cost of the cooling tower.	• The concentrating BIPV/T collector is coupled with double-effect absorption chillers to provide solar cooling. • The Fresnel reflectors are similar to vertical lattices from aesthetic point of view, enhancing integrability and compactness.
Sweden	Davidsson et al. (2010)	window		Numerical experimental	• Electricity generation per unit PV area in the window system is 35% higher compared to a vertical PV module. • Diffuse radiation accounts for 40% of the electricity generation. • U-value of the window may be adjusted by tilting the BIPV/T system, which improves building's energy performance.	• A concentrating BIPV/T water system suitable for window integration is developed. • A full-scale system is installed in a family home and its performance is monitored.

Country	References	Integration	PV	Approach	Findings	Highlights
China	Xu et al. (2011)		c-Si	Experimental	• The system achieves an average COP of 4.8 for heating water from 30 °C to 70 °C on sunny summer days. • Electrical efficiency of the cooled PV is 17.5%, which is 1.36 times that of the non-cooled PV.	• The concentrating PV/T collector incorporates the refrigerant evaporator of the heat pump for hot water production. • The fixed truncated parabolic concentrator used in the system opens building integration opportunities.
					BIPV with thermal influences	
Greece	Mandalaki et al. (2012)	Shading device		Numerical	• Lowest energy need for heating, cooling and lighting corresponds to surrounding shading, Brise-Soleil full façade and canopy inclined double for both Chania and Athens. • Surrounding shading is the most energy efficient system when PV electricity generation is also considered for both cities.	• Energy impact on the building of a large range of window shading device designs are studied in the Mediterranean climate.
USA	Dominguez et al. (2011)	Roof	c-Si	Experimental	• Daytime ceiling temperatures under the PV arrays are 2.5 K cooler than under the exposed roof. • The PV covered roof may enable a 38% reduction in annual cooling load over exposed roof. • The reduced daily variability in rooftop temperature under the PV arrays reduces thermal stresses of the roof.	• A building rooftop partially covered by a horizontal and flush PV array and a tilted PV arrays is investigated.
USA, Canada	Ban-Weiss et al. (2013)	Roof	a-Si	Experimental	• Summertime daily mean roof upper surface temperature is lowered by 5 °C due to reduced solar absorptance and increased insulation of the BIPV system. • Summertime daily heat flux through the roof deck falls to ±0.1 kWh/m2 from 0.3-1.0 kWh/m2.	• A BIPV retrofit system is installed on an office building and investigated.

Country	References	Integration	PV	Approach	Findings	Highlights
Switzer-land	Pola et al. (2007)	Roof	a-Si	Experimental	• Flat roof integrated PVs that are thermally insulated are hotter than PVs mounted on a tilted open rack. • Amorphous silicon PV modules are more suitable for thermally insulated applications than c-Si PVs.	• A roofing system consisting of PV modules laminated with polyolefin membranes as a waterproof system is installed on a school building.

Note: ST is semi-transparent.

2.8.2 Research Needs and Recommendations

The following topics are areas of further BIPV/T system research as identified by the literature reviewed in this work:

(1) Improved design of BIPV/T systems and modules and their performance investigation through experimental and numerical approaches remain an important need. Many factors need to be taken into account, including but not limited to working medium, heat transfer enhancement, materials, structure and climate.

(2) It is necessary to develop compact plug-and-play BIPV/T modules to allow standard and easy installation of BIPV/T systems. Pre-fabricated BIPV/T modules enable the construction at high precision and are vital for cold climate regions where it is nearly impossible to perform outdoor construction work in snowy months.

(3) It is necessary to explore the use of a-Si PV modules in BIPV/T systems with high-temperature applications such as solar cooling. The a-Si PV technology may represent a better choice than c-Si for high-temperature BIPV/T applications not only because of the lower temperature coefficient, but also due to the annealing mechanism that reverses the degradation process under hot conditions. In addition, the yellowing of EVA in c-Si PV modules may be avoided because EVA is not used in a-Si PV modules.

(4) The enhancement of heat transfer from the PV panel to the working medium is important for lowering PV panel temperature and increasing thermal efficiency of the BIPV/T system. Current commercial PV panels use low thermal conductivity materials such as

Tedlar as the backsheet, which do not provide good thermal contact between PV panels and the working medium.

(5) Means for avoiding overheating need to be studied since temperatures of PV over 70 ºC cause deterioration.

(6) Methods for effective building integration need to be studied. They enable BIPV/T systems to be an attractive building design option and aiding BIPV/T becoming a standard building component.

(7) Integration of the BIPV/T system with heat pumps needs to be studied, so that more of the produced heat can be used potentially in winter.

This thesis will address topics (1), (5) and (6).

3. A study of design options for a building integrated photovoltaic/thermal (BIPV/T) system with glazed air collector and multiple inlets[2]

3.1 Chapter Overview

This chapter propose a BIPV/T system enhanced with a series-connected vertical glazed air collector whose channel may be packed with wire mesh (a metal matrix) and multiple inlets. To demonstrate the performance of a typical BIPV/T system and obtain data for model verification, experimental study is conducted in a full-scale solar simulator. A lumped parameter thermal network model is developed for the tested BIPV/T system and further used to assess the performance of the proposed system. Relevant studies are published in one journal paper (Yang and Athienitis, 2014) and two conference papers (Yang and Athientis, 2012a; 2012b).

3.2 Abstract

In this section (paper), a prototype open loop air-based building integrated photovoltaic thermal BIPV/T system with a single inlet is studied through a comprehensive series of experiments in a full scale solar simulator recently built at Concordia University. A numerical control volume model is developed and validated based on the results from the experiments. Improved designs of a BIPV/T system with multiple inlets and other means of heat transfer enhancement are

---

studied through simulations. Simulation results indicate that the application of two inlets on a BIPV/T collector increases thermal efficiency by about 5% and increases electrical efficiency marginally. An added vertical glazed solar air collector improves the thermal efficiency by about 8%, and the improvement is more significant with wire mesh packing in the collector by an increase of about 10%. The developed model is applied to a BIPV/T roof of an existing solar house with four simulated inlets, and the thermal efficiency is improved by 7%.

3.3 Introduction

For a photovoltaic module, a portion of the incident solar energy is converted into useful electricity, while the rest is either reflected or dissipated as heat. The photovoltaic module can be used as the absorber in a solar thermal collector and such a device is also known as a photovoltaic/thermal (PV/T) collector. Photovoltaic panels can also be used as the building component provided their framing and attachment systems are modified for attachment as the outer layer of facades or roofs. There are two ways of incorporating the PV into the building envelope– BAPV (building-added photovoltaic) and BIPV (building-integrated photovoltaic). In a BAPV system, the PV modules are fixed onto the existing building envelope (such as PV panels installed over an asphalt shingle roof). In a building-integrated PV (BIPV) system, PV modules are part of the building envelope in a BIPV system – forming the outer layer and also performing the function of cladding such as shedding water. In either BAPV or BIPV systems, the PVs need to be cooled, otherwise they may overheat. When active heat recovery is utilized with BIPV systems – either in a closed loop (like PV/T – with a liquid loop) or in an open loop with forced air they are known as building-integrated photovoltaic/thermal (BIPV/T) systems.

BIPV/T systems can be readily integrated with building envelopes and with HVAC systems (into which the recovered heat or heated air can be transferred) while producing simultaneously electricity and useful thermal energy. In addition to generating electricity and useful heat, BIPV/T systems also reduce the building heating loads and possibly the cooling loads compared to conventional building envelope elements (Chow et al., 2007; Zogou and Stapountzis, 2011).

The most common types of BIPV/T systems are air-based (normally open loop) or closed loop water-based. Water-based BIPV/T systems have been studied for regions such as Hefei (Ji et al., 2011) and Hong Kong, China (Chow et al., 2009). A dual-function BIPV/T collector (Ji et al., 2011) is sometimes used to provide passive space heating in winter, and water heating in warm seasons through natural circulation. A variety of models have been developed for BIPV/T and PV/T systems. Ji et al. (2011) developed a finite difference model considering characteristics of both the collector and the building. This model was further validated with field experiments. Natural water circulation (thermosyphon) was found more efficient than forced water circulation in terms of system thermal performance. The annual thermal and electrical efficiency reached 37.5% and 9.39% respectively under the climate of Hong Kong. In addition, the BIPV/T system brought overall heat transmission down to 38% of that of the conventional building wall. Tripanagnostopoulos (2012) performed an extensive study on water-based PV/T systems and their integration with buildings.

Chen et al. (2010) designed and studied an air-based open-loop BIPV/T system that was thermally coupled with a ventilated concrete slab in a prefabricated, two-storey detached low energy solar house in Quebec, Canada. It was found that a BIPV/T system can significantly lower the temperature of PV panels and showed great potential in assisting space heating.

Athienitis et al. (2011) developed a prototype BIPV/T system that was integrated with unglazed transpired collector (UTC). The value of energy generated by the BIPV/T system was between 7% and 17% higher than the UTC covering the same area, assuming that electricity is about four times more valuable than heat. The concept of this prototype formed the foundation for a full-scale demonstration project in Montreal (latitude 45 N), in which crystalline silicon PV modules covered 70% of the UTC area. The BIPV/T system acts as the facade of the building, while also generating up to 25kW electricity and 75kW heat for preheating ventilation fresh air. Also in the cold climate of Hokkaido, Japan, Nagano et al. (2003) developed a wall-mounted BIPV/T system to replace the flat roof incorporated system and reduce system cost and roof leak because of snow. Their study involved six BIPV/T prototypes different from each other in terms of PV type (amorphous or polycrystalline silicon), PV protecting material (glass or Teflon), with or without a cover glass in front of the PV. Chow et al. (2003) designed a BAPV system for a hypothetical (but typical) subtropical hotel building in Macau, which was mounted onto the west-facing façade of the hotel. The PV modules were fixed at a gap distance of 250 mm from the building facade, allowing air movement in the gap driven by buoyancy as well as wind-induced effects. The warm air can be collected and pre-heat water in the hotel restaurant. ESP-r simulation results showed that this BAPV system could reduce the building's cooling load compared to a BIPV system that had no air gap. Chow et al. (2007) studied a BIPV air system in Hong Kong, which was integrated to the window of an office building. In addition to a conventional glass assembly, a semi-transparent amorphous PV module was mounted as the outer layer. The bottom and top ends were left open so that the gap between the glass and PV was naturally ventilated. The screening effect of the PV and the air ventilating effect were shown to reduce solar heat gain of

the office significantly, improve visual comfort and minimize local thermal discomfort.

In solar thermal collecting systems, a variety of ways can be employed to boost system performance - double channels (Hegazy, 2000; Shahsavar and Ameri, 2010), fins (Kumar and Rosen, 2011b; Moummi et al., 2004), slat (Ammari, 2003; Ibrahim et al., 2009), packing materials (Kolb et al., 1999; Sopian et al., 2009), corrugated surfaces (Gao et al., 2007; El-Sebaii et al., 2011) and ribs (Promvonge et al., 2011). In addition to the heat transfer enhancement measures mentioned above, new ways of performance enhancement in BIPV/T systems are emerging. Agrawa and Tiwari (2010) investigated different ways of connecting the air channel in a BIPV/T system and their effects on energy and exergy production. Pantic et al. (2010) proposed three different open-loop air BIPV/T roof systems. By comparing the system performance, they found that linking a short vertical solar air heater to the unglazed BIPV/T system results in a higher thermal energy production in winter. This section (paper) aims to further investigate ways to enhance BIPV/T system performance, particularly for sloped roofs in a cold climate.

In open-loop air-cooled BIPV/T systems which often involve large-scale PV areas covering complete roof or façade surfaces, the temperature of PV arrays can rise to high values (exceeding 70 ºC), resulting in a significant decrease in electrical efficiency and degradation of PV panels with time. It is desirable to enhance heat removal from the PV panels by using multiple inlets instead of a single inlet. The introduction of extra inlets breaks the exterior and interior air boundary layers and increases the heat transfer coefficient. In winter, the air outlet temperature can be further increased by adding a vertical glazed air collector section packed with wire mesh. The vertical glazed section takes advantage of the low winter sun altitude, resulting in significant air temperature increase.

This study considers several designs as follows:

1. A prototype BIPV/T system consisting of a single inlet studied previously outdoors by Candanedo et al. (2011) is studied through a comprehensive series of experiments in a full scale solar simulator recently built in Concordia University. This collector simulates the BIPV/T system in the EcoTerra house (a low energy solar demonstration house in Quebec, Canada) (Chen et al., 2010) which has a metal roof with amorphous silicon photovoltaic panels, with outdoor air passing through a cavity under the metal layer, extracting heat from the BIPV/T top layer where the PV is adhered to the metal layer. The prototype is half the length of the EcoTerra roof (2.8m long versus 5.6m long for EcoTerra) and can be tested at different angles in the solar simulator. An explicit finite difference control volume model is developed and validated based on the results from the solar simulator.

2. Improved designs with multiple inlets and other means of heat transfer enhancement are studied through simulations. In the design shown in Figure 3.1, air is drawn from two inlets in the BIPV/T section connected in series with a vertical glazed collector section packed with wire mesh.
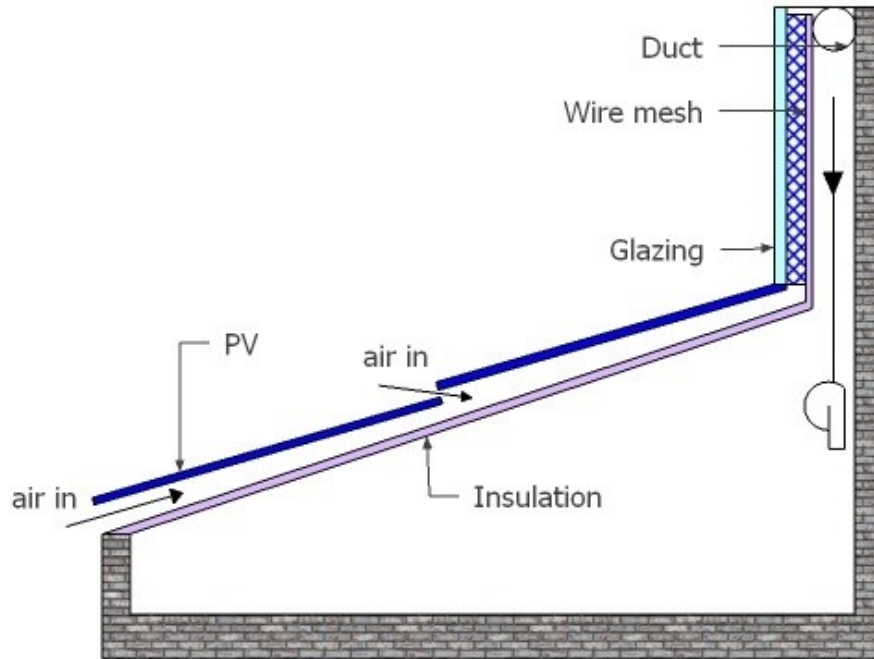
Figure 3.1. Schematic of the two-inlet BIPV/T system connected in series with glazed air

collector packed with wire mesh

3.4 Experiments in a Solar Simulator

3.4.1 Experimental Setup

The experiments with the amorphous silicon BIPV/T system prototype are carried out in a

recently built Solar Simulator and Environmental Chamber Laboratory (SSEC) at Concordia

University in Montreal as shown in Figure 3.2a. The lamp field consisting of eight special metal

halide (MHG) lamps with an artificial sky illuminates the test area. To simulate natural sunlight,

the lamps provide a spectral distribution in accordance with relevant standards EN 12975:2006

and ISO 9806-1:1994. The heat input of the lamps reaches up to 27.6 kW, and the heat is taken

away by a cooling unit in the mechanical room next to the test room. The lamps in the lamps

field can be moved and continuously dimmed, allowing test areas of different dimensions to be

illuminated at various radiations levels as uniform as possible. In the experiments conducted in this paper, the homogeneity is controlled within ±3%. For this class B solar simulator, homogeneity of ±3% can be reached for a test surface that measures 2.0 m by 2.4 m, at an irradiance level of approximately 1100 W/m^2. The lamp field as well as the platform can be tilted at any angle between 0° and 90°, simulating the conditions of different building envelop elements; Figure 3.2b shows the solar simulator testing the BIPV/T collector at a tilt angle of 45°. In order to remove the long-wave infrared irradiation emitted by the high-temperature lamps, an artificial sky is set up between the lamps and the test area. The artificial sky is formed by two panes of low-iron glass with anti-reflective coating, with cooled air passing in between. A pyranometer and an anemometer are mounted on an x-y scanner above the test area to measure the radiation and the wind speed, respectively.

A total of forty-eight special limit T-type thermocouples are distributed in the system. Eleven thermocouples are attached under the center of each PV cell; another eleven are installed onto the insulation surface (see Figure 3.1 for general concept, but with a single inlet). Fourteen thermocouples measure the air temperature in the channel, and another twelve are placed on top of the PV to measure the temperatures just above the collector. Figure 3.2c shows the positions of the thermocouples. Artificial wind is blown parallel to the collector from the inlet side to the top.

A schematic of the Solar Simulator configuration and the experimental setup of the BIPV/T system is presented in Figure 3.3.
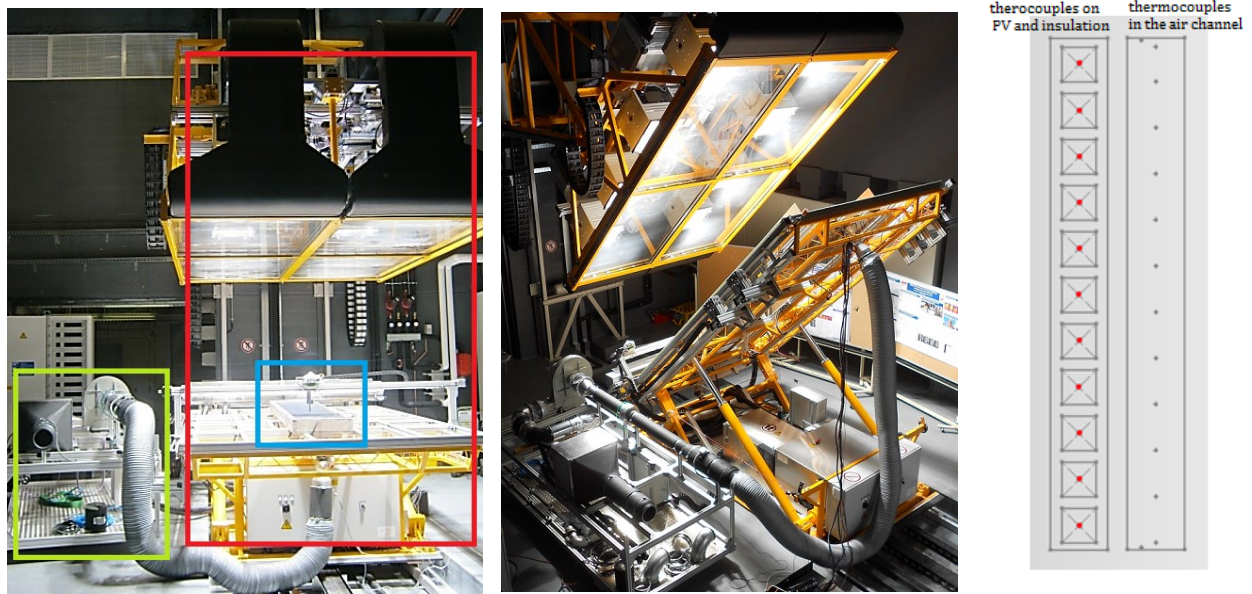
Figure 3.2. (a) BIPV/T air collector (in blue rectangle) tested horizontally in the solar simulator (in red rectangle) and air collector testing platform (in green rectangle); (b) BIPV/T system tested at 45 degrees slope; (c) Thermocouple positions in the BIPV/T collector (The red dots represent thermocouples attached under the PV cells and onto the insulation; the gray dots represent thermocouples in the BIPV/T channel)
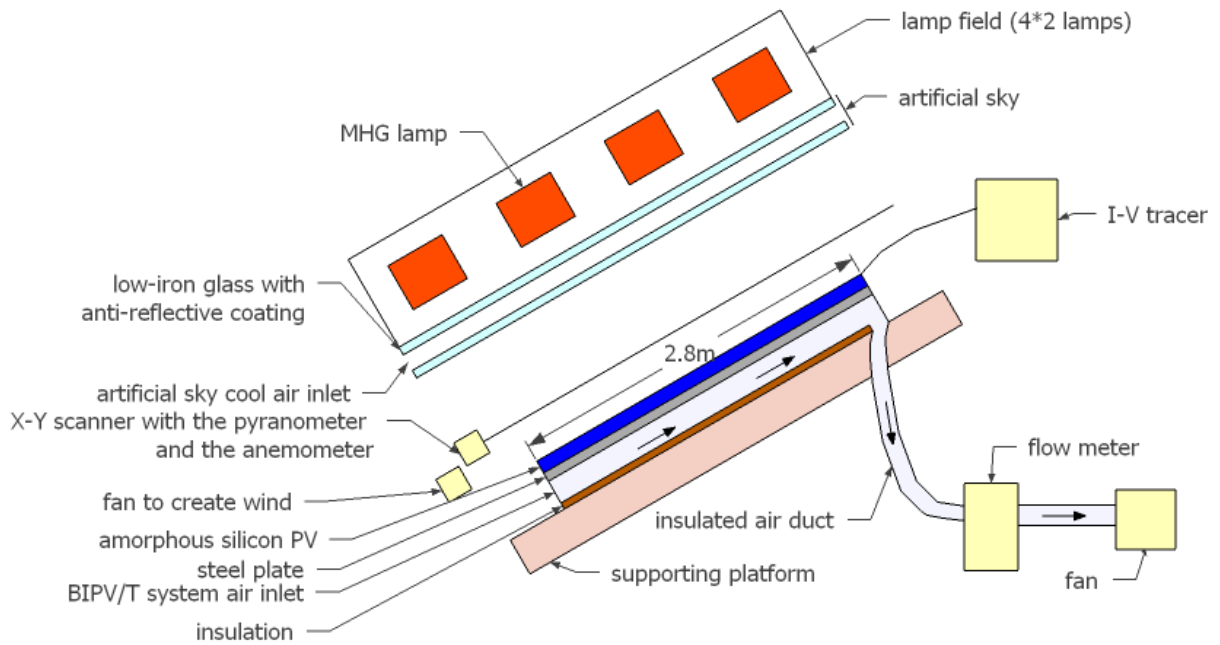
Figure 3.3. Schematic of the Solar Simulator and the experimental setup of the BIPV/T system

(the BIPV/T prototype is 2.89 m long by 0.39 m wide; the PV is attached to a metal roof layer

and air is drawn under this 4 cm thick layer with a fan)

3.4.2 Mathematical Model (for BIPV/T with Single Inlet)

Flowing air in the BIPV/T system extracts heat from both the top and bottom surfaces of the

cavity of the BIPV/T system. The total thermal energy extracted by the air in each control

volume is given by

$$Q_{air} = \dot{m}c_p(T_{out} - T_{in}) \qquad (3.1)$$

The bottom surface of the cavity receives radiative energy from the top surface of the cavity. The

radiative heat gain by the bottom surface is discharged to air, assuming that heat conduction

93

through the bottom is negligible. Thus, we have

$$\frac{F\sigma(T_{plate}^4 - T_{insu}^4)}{\dfrac{1}{\varepsilon_{plate}} + \dfrac{1}{\varepsilon_{insu}} - 1} = h_{bot}(T_{insu} - \overline{\overline{T}}_{air}) \tag{3.2}$$

Convective heat transfer from the top surface to air is given by

$$Q_{air} - \frac{F\sigma(T_{plate}^4 - T_{insu}^4)}{\dfrac{1}{\varepsilon_{plate}} + \dfrac{1}{\varepsilon_{insu}} - 1} \cdot wdx = h_{top}(T_{plate} - \overline{T}_{air}) \cdot wdx \tag{3.3}$$

The hot PV module releases heat into the ambient through both radiative and convective heat transfer. The combined radiative and convective heat transfer coefficient was decided by

$$h_{ambient}(T_{pv} - T_{wind}) \cdot wdx = \alpha G \cdot wdx - P_{elec} - Q_{air} \tag{3.4}$$

Curve fitting was performed on the temperature readings of PV, air and insulation. Experimental data were fitted in an exponential formula:

$$T(x) = A(1 - e^{-\frac{x}{B}}) + C \tag{3.5}$$

where x denotes the distance away from the inlet.

Figure 3.4 is an example of the experimental measurement and fitted curves when the incident solar radiation was 1080 W/m^2, the average wind speed was 1.6 m/s and the average air speed in the BIPV/T channel was set at 0.26 m/s. Note that air temperature shows a sudden rise at the second node, which was caused by the entrance effect.
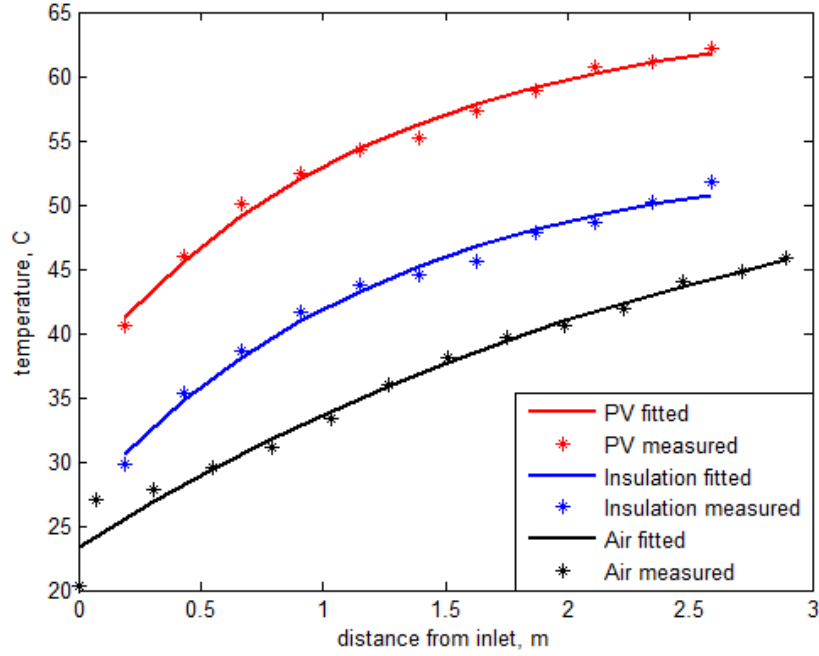
Figure 3.4. Experimental data and curve fits of the temperatures of PV, insulation and air in prototype with single inlet

The heat transfer coefficients between air and the top and bottom surfaces of the BIPV/T channel tilted at 45 degrees are presented in the form of local Nusselt numbers. The format of the following formulas is referenced from the work of Candanedo et al. (2011).

In the turbulent region

$$Nu_{top}(x) = 8.188\,\mathrm{Re}^{0.77}\,\mathrm{Pr}^{3.85}\,e^{-\frac{x^{0.2}}{2.8D_h}} + 0.061\,\mathrm{Re}^{0.77}\,\mathrm{Pr}^{3.85} \quad 2300 < \mathrm{Re} < 9500 \tag{3.6}$$

$$Nu_{bot}(x) = 4.02\,\mathrm{Re}^{1.09}\,\mathrm{Pr}^{19.3}\,e^{-\frac{x^{0.2}}{14D_h}} + 0.005\,\mathrm{Re}^{1.09}\,\mathrm{Pr}^{19.3} \quad 2300 < \mathrm{Re} < 9500 \tag{3.7}$$

And in the laminar region we have the following fitted equations

$$Nu_{top}(x) = 0.6883 \, \text{Re}^{0.7} \, \text{Pr}^{0.8} \, e^{-\frac{x^{0.3}}{6.45 D_h}} + 0.0124 \, \text{Re}^{0.7} \, \text{Pr}^{0.8} \qquad 1190 < \text{Re} < 2300 \qquad (3.8)$$

$$Nu_{bot}(x) = 50 \, \text{Re}^{0.5} \, \text{Pr}^{0.2} \, e^{-\frac{x^{0.3}}{1.37 D_h}} + 0.428 \, \text{Re}^{0.5} \, \text{Pr}^{0.2} \qquad 1190 < \text{Re} < 2300 \qquad (3.9)$$

3.4.3 Experimental Results

A comprehensive set of experiments have been conducted in the solar simulator. Different irradiance levels were considered. The flow rate in the BIPV/T channel is controlled, with a Reynolds number ranging from 1200 to 10000, which was chosen based on previous experience with a BIPV/T system that the practical operating Reynolds number was under 10000 (to keep friction losses low). The artificial wind is parallel to the collector, with a controlled speed ranging from 1.6 to 3.5 m/s. Figure 3.5 compares the thermal efficiencies of the BIPV/T collector with different wind speeds on top of the PV surface. As expected, with increasing wind speed, the thermal efficiency is reduced.

96
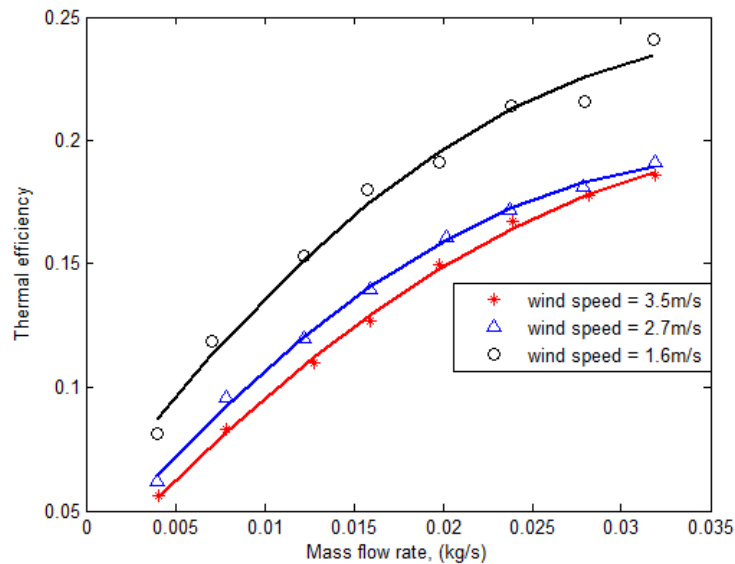
Figure 3.5. Thermal efficiencies of the BIPV/T system at different wind speeds, with a tilt angle

of 45 degrees and incident solar radiation of 1080 W/m^2

In the original BIPV/T prototype, four steel bars (shown in Figure 3.6a) were placed immediately

under the amorphous PV module to support its weight. Later, these bars were removed from the

collector. The impact of the steel support on the thermal efficiency of the BIPV/T system is

illustrated in Figure 3.7. It can be seen that the steel bars act as fins, increasing the thermal

efficiency of the BIPV/T system. The dimensions of the BIPV/T cavity are illustrated in Figure

3.6b.

(a)

(b)
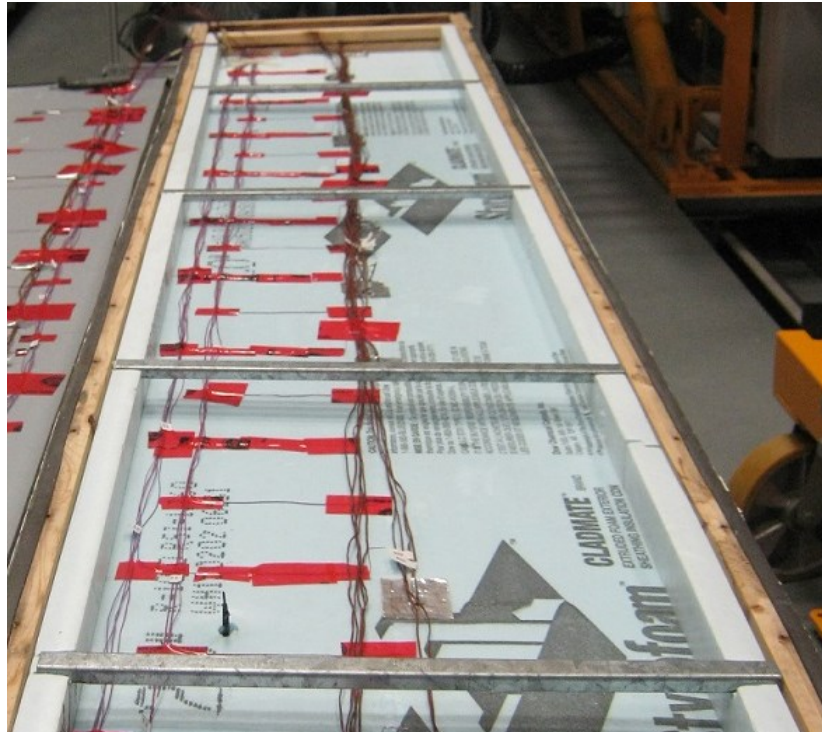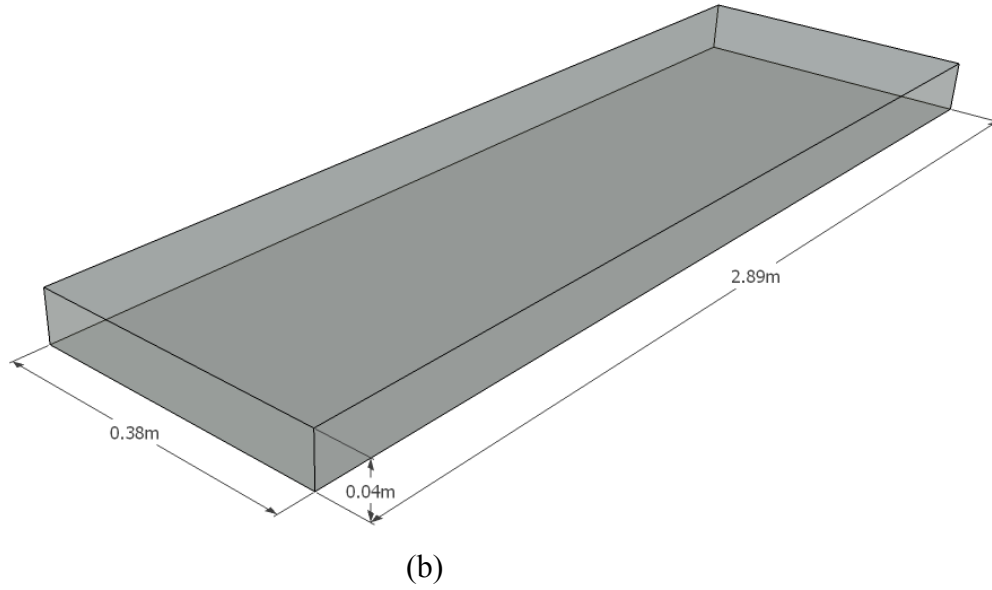
Figure 3.6. (a) Photo of the steel bars placed underneath the PV module as structural

support; (b) Dimensions of the BIPV/T channel (drawing not to scale)
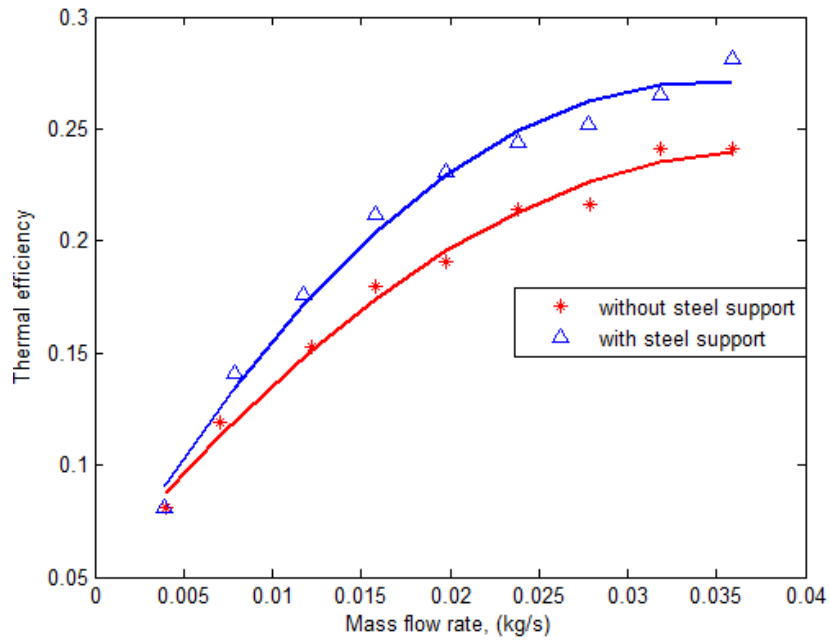
Figure 3.7. Thermal efficiency of the BIPV/T system with and without the structural support

steel bars under the PV module, when the tilt angle is 45 degrees, the incident solar radiation is

$1080W/m^2$ and the average wind speed is 1.6 m/s

3.5 Numerical Modeling and Verification

3.5.1 Mathematical Model

The mathematical model for the BIPV/T system is based on a simplified model of the amorphous silicon photovoltaic module (other PV modules can be similarly modelled). As shown in Figure 3.8a, from top to bottom, the layers of the amorphous photovoltaic module are Tefzel (encapsulation material), anti-reflective coating, silicon, backing substrate, Tefzel, adhesive and steel sheet. In a typical control volume as shown in Figure 3.8b, the layers under silicon are combined as one equivalent layer with no significant thermal capacity.

The following assumptions have been applied to the model:

- The system is in quasi steady state

- The bottom insulation and the side walls are adiabatic

- Heat flow is assumed to be one-dimensional perpendicular to the PV

A set of energy balance equations are written for the components in the BIPV/T system.

(a)   (b)
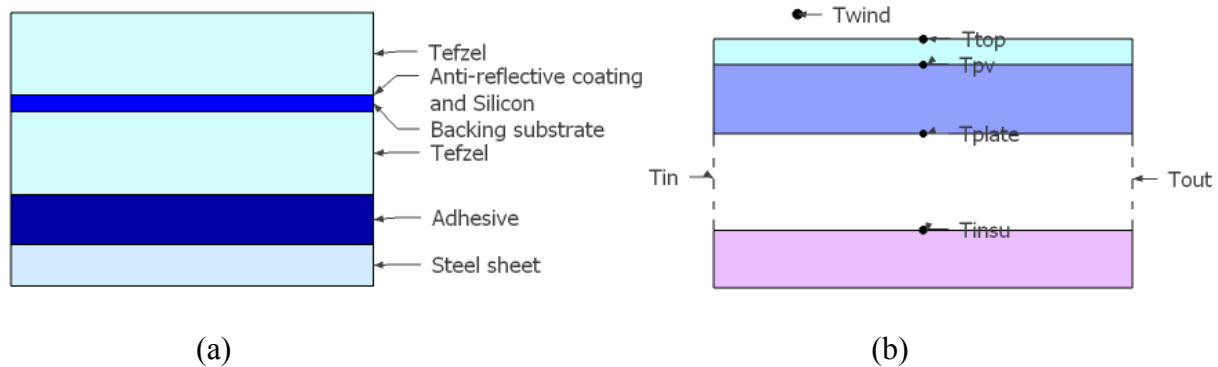
Figure 3.8. (a) Composition of the amorphous PV module attached to steel roof layer; (b) Temperature nodes of the BIPV/T system (white layer indicates flowing air, T_{plate} is the temperature of the steel sheet)

For the temperature node on the outer surface of the PV module,

$$\frac{T_{pv} - T_{top}}{R_{Tefzel}} = h_{ambient}(T_{top} - T_{wind}) \tag{3.10}$$

For the PV node in the middle of the PV module,

$$\alpha G \cdot wdx = P_{elec} + \frac{T_{pv} - T_{top}}{R_{Tefzel}} \cdot wdx + \frac{T_{pv} - T_{plate}}{R_{mix}} \cdot wdx \tag{3.11}$$

For the temperature node on the bottom of the PV module,

$$\frac{T_{pv} - T_{plate}}{R_{mix}} = h_{top}(T_{plate} - \overline{T}_{air}) + \frac{F\sigma(T_{plate}^4 - T_{insu}^4)}{\dfrac{1}{\varepsilon_{plate}} + \dfrac{1}{\varepsilon_{insu}} - 1} \tag{3.12}$$

For the temperature node on the insulation surface,

$$\frac{F\sigma(T_{plate}^4 - T_{insu}^4)}{\dfrac{1}{\varepsilon_{plate}} + \dfrac{1}{\varepsilon_{insu}} - 1} = h_{bot}(T_{insu} - \overline{T}_{air}) \tag{3.13}$$

For the air passing through the control volume,

$$\dot{m}c_p(T_{out} - T_{in}) = h_{top}(T_{plate} - \overline{T}_{air}) \cdot wdx + h_{bot}(T_{insu} - \overline{T}_{air}) \cdot wdx \tag{3.14}$$

The heat transfer process in the vertical solar air heater packed with wire mesh is shown in Figure 3.9. Compared to the conventional solar air heater, the added wire mesh absorbs the

incident solar radiation and releases it to the passing air by convection. The following equations demonstrate the calculation of heat transfer coefficient between air the wire mesh (Prasad et al., 2009). Similar approaches to study wire mesh packed solar air heater have been applied by Mittal and Varshney (2006), and Ho et al. (2013).
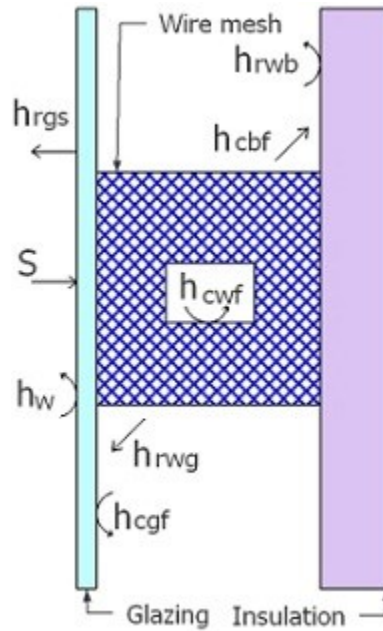
Figure 3.9. Cross-section view of the wire mesh packed solar air collector

The porosity of the wire screen matrix is determined by

$$P = 1 - \frac{\pi}{2} \frac{nd_w^2}{p_t D} (1 + \frac{d_w^2}{p_t^2})^{1/2}$$ (3.15)

The effective heat transfer area between the wire mesh and air is determined by

$$A = \frac{4A_f L(1-P)}{d_w}$$ (3.16)

The hydraulic radius for the packed bed duct is given by

$$r_h = \frac{Pd_w}{4(1-P)} \tag{3.17}$$

The Colburn factor is expressed by

$$J_h = 0.2563(\frac{1}{nP})^{0.609}(\frac{P_t}{d_w})^{0.7954}\text{Re}_p^{-0.63} \tag{3.18}$$

The relation between the heat transfer coefficient and the Stanton number is evaluated by

$$St_p = \frac{h}{G_0 c_p} \tag{3.19}$$

where the relative mass flow rate for a packed bed G_0 is given by

$$G_0 = \frac{\dot{m}}{A_f P} \tag{3.20}$$

The relation between the Colburn factor and Stanton number is evaluated by

$$J_h = St_p \text{Pr}^{2/3} \tag{3.21}$$

In the vertical solar air heater, the convective heat transfer coefficient between the plate and the air flow is decided by Eq. (3.22) – (3.24).

$$h_c = \frac{k_{air}}{D_h}(1.86 \cdot (\frac{\text{Re Pr} D_h}{L})^{1/3} \cdot (\frac{\mu}{\mu_s})^{0.14}) \qquad \text{Re} < 2300 \tag{3.22}$$

$$h_c = \frac{k_{air}}{D_h}(0.116 \cdot (\text{Re}^{2/3}-125) \cdot \text{Pr}^{1/3} \cdot (1+(\frac{D_h}{L})^{2/3}) \cdot (\frac{\mu}{\mu_s})^{0.14}) \qquad 2300 < \text{Re} < 6000 \tag{3.23}$$

$$h_c = \frac{k_{air}}{D_h}\left(\frac{\frac{f}{8} \cdot (\text{Re}-1000) \cdot \text{Pr}}{1+12.7 \cdot \sqrt{\frac{f}{8}} \cdot (\text{Pr}^{2/3}-1)}\right) \cdot (1+(\frac{D_h}{L})^{2/3}) \qquad 6000 < \text{Re} < 10^6 \tag{3.24}$$

where the friction factor f is given by

$$f = (1.82 \log \text{Re}-1.64)^{-2} \tag{3.25}$$

The electrical efficiency of PV is expressed in terms of solar cell temperature

$$\eta_{electric} = 0.16(1-0.0045(T_{pv,s} - T_{ref})) \tag{3.26}$$

where T_{ref} is the reference temperature.

In smooth ducts, the friction factor is calculated as shown in Eq. (3.27)-(3.29) (Prasad et al., 2009)

$$f = \frac{64}{\text{Re}} \qquad \text{Re} < 2300 \tag{3.27}$$

$$f = 0.316 \text{Re}^{-1/4} \qquad 2300 < \text{Re} < 3000 \tag{3.28}$$

$$f = (0.790 \ln \text{Re}-1.64)^{-2} \qquad 3000 < \text{Re} < 5\times10^6 \tag{3.29}$$

In the wire mesh packed duct, the friction factor is given by

$$f_p = 3.5722(\frac{1}{nP})^{1.0431}(\frac{p_t}{d_w})^{1.1507} \text{Re}_p^{-0.43} \tag{3.30}$$

The relation between pressure drop and friction factor is

$$\Delta p_1 = f \cdot \frac{L}{D_h} \cdot \frac{\rho V^2}{2} \tag{3.31}$$

For packed duct, the hydraulic radius r_h is used as the hydraulic diameter, and velocity is defined as $u = G_0 / \rho$.

The entrance loss at the air inlet is given by

$$\Delta p_2 = K_L \cdot \frac{\rho V^2}{2}$$

(3.32)

where the loss coefficient K_L for a square-edged entrance is approximately 0.5.

Total pressure drop is calculated by

$$\Delta P = \Delta p_1 + \Delta p_2$$

(3.33)

Thus, fan power can be calculated by

$$P_p = \frac{\dot{m} \Delta P}{\rho_f}$$

(3.34)

3.5.2 Verification of the Model

The indoor Solar Simulator facility enables accurate and repeatable test conditions, allowing for the prototype being tested under a stable environment close to room temperature (at lower or higher temperatures the environmental chamber needs to be used with a mobile solar simulator). A cooling unit maintains the ambient temperature according to the lab thermostat setting; the sunlight-simulating lamps provide radiation close to the solar spectrum at a stable; the fan creates different wind speeds parallel to the PV surface in the same direction as the flow in the cavity. At the same time, there are some special requirements. The intensity and location of each lamp (8 in total) need to be adjusted in order that the irradiance on the test surface is in an acceptable

uniformity range. The uniformity achieved was 3%. The lab temperature was set around 20 ºC.

Numerical simulations were performed using the model described above and are compared against experimentally measured data from the simulator, as shown in Figure 3.10. The operating conditions are: 1080 W/m^2 of solar radiation, 1.6 m/s of average wind speed and 1.5 m/s of air speed in the BIPV/T cavity.
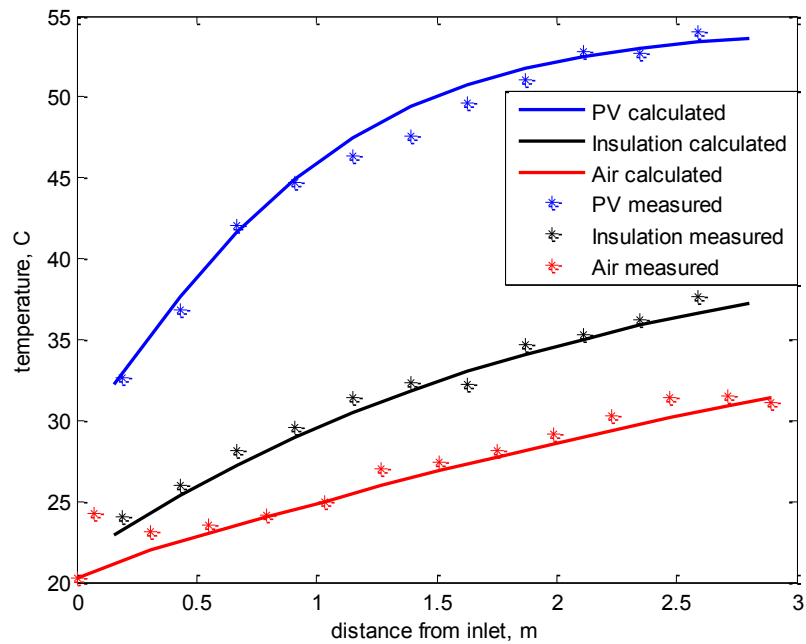
Figure 3.10. Comparison between calculated and measured temperatures in the BIPV/T system

3.6 Results

A two-inlet BIPV/T system (without the vertical glazed collector) was studied based on the validated model. The inlet air flow of the second section is a mixture of the outlet air of the first section and the ambient air. The local Nusselt number for the second section is calculated assuming that the boundary layer restarts at the second inlet.

By using the 2-inlet BIPV/T system, the thermal efficiency is increased by 5%. Although the electrical efficiency increase is marginal, it can be seen in Figure 3.11 that the peak PV temperature in the 2-inlet system is lower than that in the 1-inlet system, which means that PV degradation with high temperature is reduced in the 2-inlet system and by extension in a multi-inlet system. The addition of a vertical glazed solar air heater will increase the thermal output of the whole system, especially in low latitude areas where the winter sun is low.

The effect of using a glazed solar air heater is presented in Figure 3.12, which shows that using wire mesh in the glazed solar air heater will increase thermal efficiency by 2%. However, the fan power consumption in the wire mesh packed system increases noticeably when the air flow rate is increased, resulting in a decrease in electrical efficiency.

The results also show that the vertical air collector improves the thermal efficiency compared to a PV covered BIPV/T system – by about 8% with a smooth solar air collector and by about 10% with a wire mesh packed solar air collector.
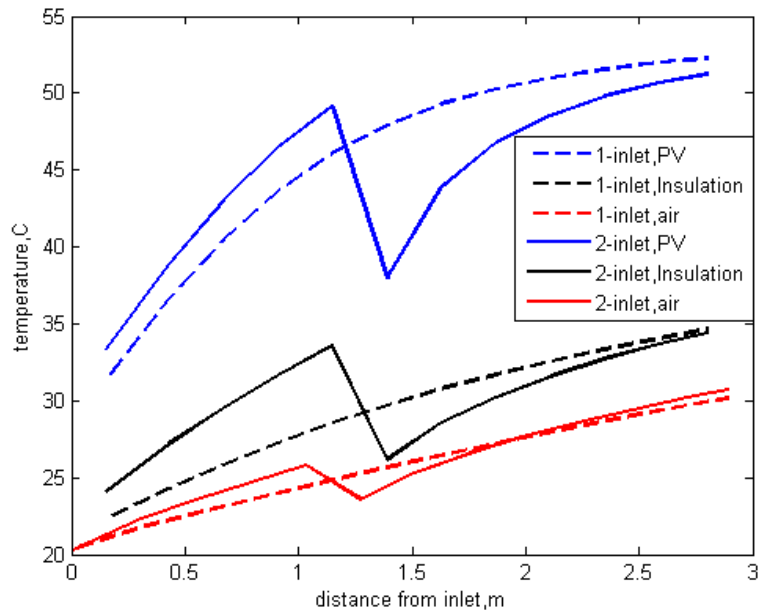
Figure 3.11. Comparison of the temperatures of the 1-inlet and 2-inlet BIPV/T systems
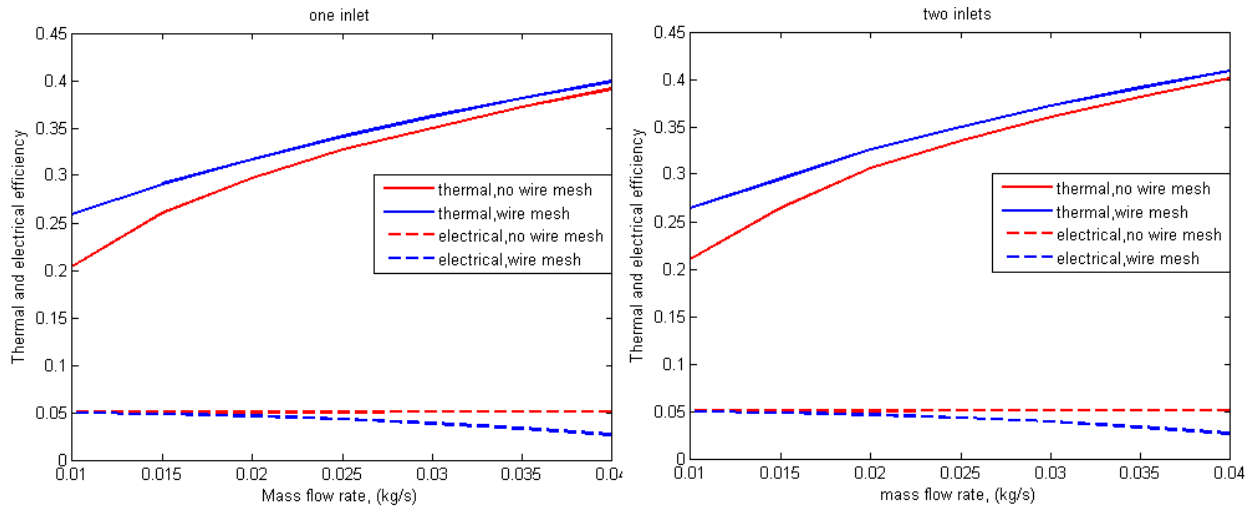
Figure 3.12. (a) Thermal and electrical production in a one-inlet BIPV/T system with the glazed solar air collector with or without wire mesh; (b) Thermal and electrical production in a two-inlet BIPV/T system with the glazed solar air collector with or without wire mesh

The thermal performance of the solar air collector can be expressed in a Hottel-Whillier-Bliss

107

form (Duffie and Beckman, 2006). The heat removal factor of a solar air collector can be expressed as

$$F_R = \frac{Q_{air}}{A_c(\alpha G - U_L(T_i - T_a))} \tag{3.35}$$

Some typical heat removal factors are summarized in Table 3.1.

Table 3.1. Heat removal factors of the solar air heater with/without wire mesh

flow velocity	without mesh	with mesh
0.85 m/s	54.8%	80.9%
1.7 m/s	73.7%	82.8%
2.55 m/s	78.6%	84.1%
3.4 m/s	81.1%	84.9%

As a preliminary study, the concept of using multiple inlets is examined for the BIPV/T system installed on the EcoTerra house. Chen et al. (2010) reported that the typical efficiency of this BIPV/T system was about 20%, and the temperature of the PV panels peaked at 65 ºC with an outdoor temperature of about 20 ºC and low wind speed on a warm sunny day. The original system measures 5.8 m and takes in air by one inlet (Figure 3.13). The new design divides the whole length evenly into four parts (Figure 3.13), assuming that flow rate through each inlet equals. The temperature distributions of the PV and air flow are presented in Figure 3.14. Depending on each section, the local heat transfer coefficient between PV and the channel air varies approximately between 5 ~ 50 W/(m²•K). The mixed heat transfer coefficient of PV with wind (convection) and with surroundings is approximately 20 W/(m²•K). It was found that the thermal efficiency is 27.1% for the four-inlet BIPV/T system. Experimental work is underway with a crystalline silicon based BIPV/T system.
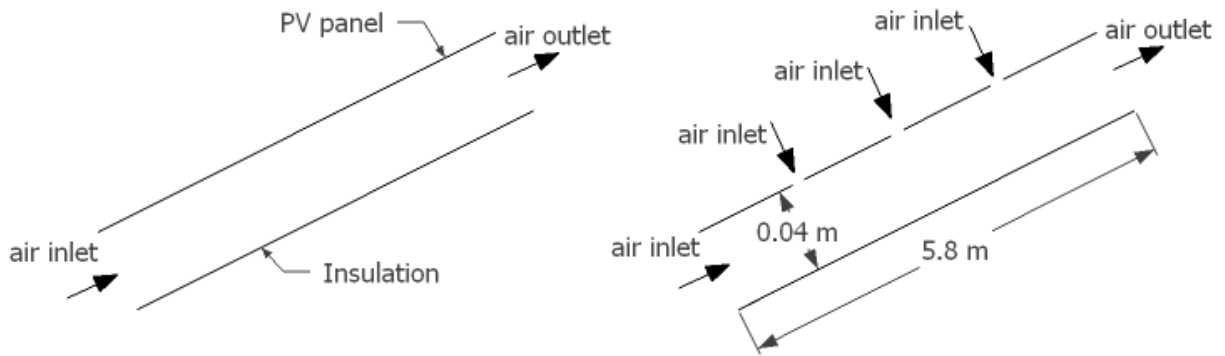
Figure 3.13. Schematics of the original EcoTerra BIPV/T system with one air inlet (left) and the new BIPV/T system with four inlets (the roof length is put actual length here; the new simulated inlets are at equal distances)
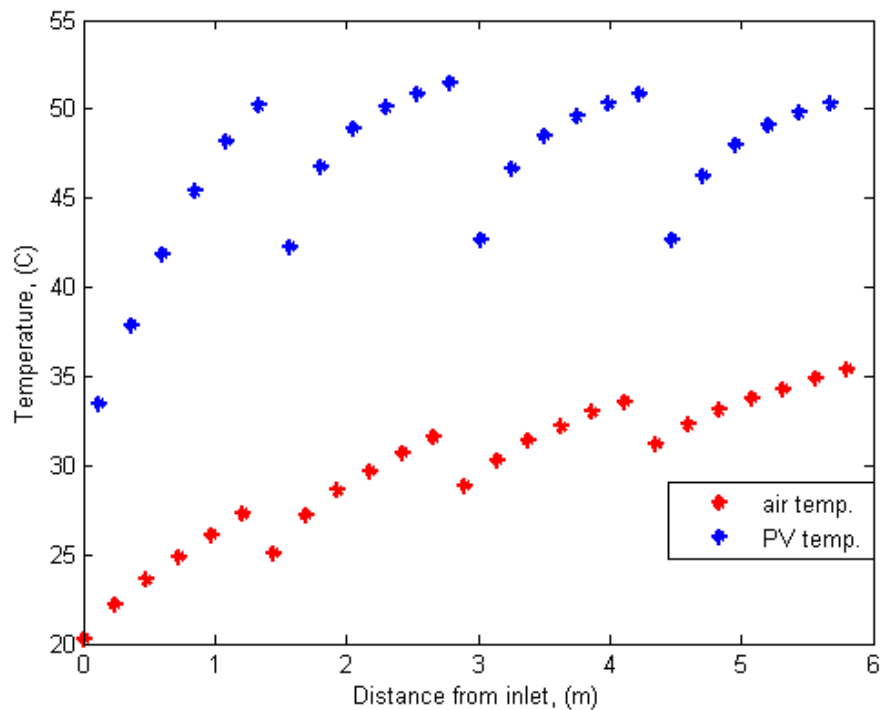
Figure 3.14. Temperature distributions of PV and air in the cavity along the flow direction

3.7 Conclusion

A prototype BIPV/T system consisting of a single inlet was experimentally studied in a full scale

solar simulator. The influence of wind speed on the thermal efficiency of the BIPV/T system was studied. As expected, with higher wind speed, the thermal efficiency of the BIPV/T system is reduced significantly. Addition of structural support steel bars in the BIPV/T collector channel was shown to increase the thermal efficiency of the BIPV/T system significantly by acting as fins to dissipate heat into the flowing air.

A control volume model for the BIPV/T system was developed and validated with experimental results. This model was first used to study the performance of a BIPV/T system with two inlets. The two-inlet design increases thermal efficiency by up to about 5% and increases electrical efficiency marginally. It was found out that by using two inlets, the peak temperature of the PV module is reduced by about 1.5 ℃ for the small prototype length, and this will reduce the degradation of the PV module. For actual roofs where the length is 5-6 m, the reduction of maximum PV temperature is expected to be at least 5-10 ℃ depending on flow rate and wind conditions.

A vertical glazed solar air collector was simulated connected to the end of the BIPV/T system, for the purpose of increasing thermal efficiency in winter when the solar altitude is low. By adding wire mesh in this section, thermal performance is further increased significantly, particularly for heating applications in the winter when the solar altitude is lower, and the additional heat is needed. The addition of the solar air heater increases the system thermal efficiency by about 8% with a smooth air channel, and by 10% with a wire mesh packed air cavity.

4. Experimental investigation of a two-inlet air-based building integrated photovoltaic/thermal (BIPV/T) system[3]

The design concept of using two or more air inlets was preliminarily studied in Chapter 3, and Chapter 4 further investigates this topic through experimentation carried out in the solar simulator.

4.1 Chapter Abstract

An experimental study of a novel two-inlet air-based open-loop building integrated photovoltaic/thermal (BIPV/T) system using a full-scale solar simulator is presented. Experimental prototypes of one-inlet and two-inlet BIPV/T systems were constructed for conducting comparative experiments. Variations of BIPV/T systems are also investigated including systems employing opaque mono-crystalline silicon photovoltaic (PV) panels and systems employing semi-transparent mono-crystalline PV panels. Experimental results demonstrate that an equivalent two-inlet system can increase the thermal efficiency by 5% compared to a conventional one-inlet system, and that the BIPV/T system with semi-transparent PV panels achieves higher thermal efficiency due to the absorption of some solar radiation at the bottom surface in the BIPV/T system cavity. Also, the two-inlet BIPV/T design is easily implemented and does not add significant cost. Detailed air temperature measurements reveal

---

that the mixing of the warm outlet air from the first section and the cool ambient air drawn in from the second inlet contributes to the improved performance of the two-inlet system. Based on a thermal network model of the BIPV/T system and experimental data, correlations are developed for the convective heat transfer coefficients in the two sections. These are necessary for further analysis and development of BIPV/T system with multiple inlets.

4.2 Introduction

A building-integrated photovoltaic/thermal (BIPV/T) system captures solar radiation on the building envelope and converts a fraction of this energy into both electricity and useful thermal energy. A typical commercial crystalline photovoltaic (PV) module converts about 15-20% of the incident solar energy into electricity, with the rest either reflected (5-10%) or largely converted into heat. For a large installation of the BIPV/T system such as a residential roof, the peak PV temperature could reach up to 60 °C or higher on hot sunny days Chen et al. (2010). The rise in PV temperature not only reduces electricity generation, but also reduces the life-span of the module itself. Integrating the PV and solar thermal technology into a single component could reduce the overheating of PV as well as provide useful thermal energy for the building. This energy can be used for ventilation air pre-heating (Nagano et al., 2003; Candanedo et al., 2011; Yang and Athienitis, 2014), domestic hot water heating (Chow et al., 2007; Kalogirou and Tripanagnostopoulos, 2006), and heat storage for later use (Bakker et al., 2005).

Conventional building materials may be exploited as a practical element of BIPV/T systems (Anderson et al., 2009; Yin et al., 2013). Assoa et al. (2014) described a roof-integrated BIPV/T air heating system constructed by attaching PV modules to a ribbed sheet steel plate. Anderson et

al. (2009) designed a roof-integrated BIPV/T water system by using troughed sheet roofs as the structural support and fluid passageways. Their numerical investigation indicated that the low-cost steel sheet incurred negligible system thermal efficiency reduction compared to a copper and aluminum sheet, despite its relatively low thermal conductivity. Further, compact BIPV/T systems are being developed as the functional building component to facilitate modular assembly and plug-and-play operation. Yin et al. (2013) presented a hybrid BIPV/T water roofing panel that performed multiple functions of waterproofing, insulation, structural strength and energy generation. Numerical simulation results showed that the overall electrical and thermal efficiency of the system was 71% (Yang et al., 2012). Zhao et al. (2011) proposed a BIPV/T roof module that may serve as the roofing element, electricity generator and the evaporator of the heat pump. The sandwiched BIPV/T component comprised an outer clear glazing, a PV layer, evaporator coil and copper plate adhered to the rear of the PV panel, a vapor control layer and an insulation layer. Numerical studies showed that the BIPV/T system had an electrical efficiency of 19% and a thermal efficiency of 55% whereas the heat pump system had an overall efficiency of above 70% under typical UK operating conditions. In general the fully incorporated BIPV/T system may replace roof shingles or expensive construction materials such as natural stone, marble, ceramic and granite on the building façade, while providing weatherproofing and insulation layers (Zogou and Stapountzis, 2011; Aste et al., 2008).

For an open-loop air-based BIPV/T system, fresh air is continuously drawn from the ambient environment whereas a closed-loop BIPV/T system repeatedly circulates the same volume of air. Although the outlet temperature of an open-loop system may be lower compared to a closed loop system, the risk of PV delamination may be reduced while the electrical performance is enhanced

since the panel temperature is lower in an open-loop system.

In a cold climate, an air-based BIPV/T system has the advantage of providing space heating for most of the year due to low ambient temperatures (Chow, 2010; Athienitis et al., 2011). Nagano et al. (2003) developed an air-based BIPV/T system integrated with vertical exterior wallboards to cope with the snow coverage encountered during the cold winter period. Comparative outdoor experiments of different BIPV/T systems were carried out for the full two months from December 1999 through January 2000. Although an additional glass cover in front of the PV modules increased thermal efficiency from about 22% to 29%, electrical efficiency was reduced from about 11% to 9% due to the condensation on the inner surface of the glass, higher PV temperature, and less solar radiation transmitted onto the PV surface. Argawal and Tiwari (2011) attempted to optimize BIPV/T system performance under cold climate conditions in India by assessing the energy and exergy gains of different system configurations where the air channels may be connected in series or in parallel. Numerical simulations results showed that the serial air channel connection was more suitable for a constant air mass flow rate whereas the parallel connection was better in the case of constant air velocity. Above all, the serial connection at constant mass flow rate was found to generate the most annual energy and exergy including thermal and electrical outputs. Pantic et al. (2010) explored the opportunity of enhancing BIPV/T system performance by connecting a 1.5 m vertical glazed solar air collector in series with the outlet of the BIPV/T system. The added solar air collector received high amounts of solar irradiance in winter when the solar altitude was low, generating hot air suitable for coupling with a rockbed heat storage. Located in Quebec, Canada, the EcoTerra low energy solar demonstration house adopted a roof-integrated air-based BIPV/T system to transform solar

114

energy into electricity and thermal energy simultaneously (Chen et al., 2010). Part of the heat from the BIPV/T system could be stored in a ventilated concrete slab, heat domestic hot water with an air-to-water heat exchanger or used to dry clothes. Although not optimized, the BIPV/T system achieved a thermal efficiency of 20%, and with other passive solar design measures, the annual space heat energy demand of the house was about 5% of the national average.

The design option of integrating air-based BIPV/T system with a UTC (unglazed transpired collector) has been studied (Athienitis et al., 2011; Naveed et al., 2006). The UTC is a highly efficient solar thermal energy collector, and the BIPV/T combined design could add the bonus of producing useful electricity all year round. Athienitis et al. (2011) carried out comparative experiments between a bare UTC and a BIPV/T prototype with 70% of UTC area covered by PV modules. The results showed that the BIPV/T system was 7-17% higher in overall equivalent efficiency, assuming that electricity is four times more valuable than heat. The horizontal corrugation of the UTC plate promoted turbulence of the air flow field; the pores in the UTC created numerous air inlets into the plenum and may break the boundary layer to increase heat transfer rate. Special consideration was given to the PV module construction by selecting a black frame and a black backsheet, and this was shown to increase the thermal efficiency of the BIPV/T system compared to an unpainted aluminum frame and a white backsheet. This concept was also applied on the façade of a new office building using a BIPV/T system with peak power generation of 24.5 kW electrical and 75 kW thermal.

The BIPV/T systems may be tested in an outdoor environment to characterize their transient performance with varying ambient conditions. Bloem (2008) pointed out that convective and radiative heat exchanges on the rear side of the PV module in the building-integrated application

were different from those for the open rack mounted PV. An outdoor air-based BIPV/T Test Reference Environment (TRE) was developed that facilitated changing materials such as metal, brick and wood at the surface facing the rear of the PV panel. Experiments performed with forced airflow showed that the glass-Tedlar PV module could achieve higher electrical yield than the Tedlar-glass one. The experimental data from the TRE were used to correlate convective heat transfer coefficients, validate TRNSYS models and calibrate CFD models of the BIPV/T system by a number of researchers (Bloem et al., 2012). Sohel et al. (2014) monitored the performance of the BIPV/T air system installed for two functional buildings under real operation conditions. The collected data was used to calibrate a dynamic model capable of predicting the transient behavior of the BIPV/T installation. Zogou and Stapountzis (2011) assessed the performance of a BIPV/T air system by conducting outdoor tests in Volos, Greece. They recorded the typical dynamic behavior of the system in summer and autumn and also observed the cooling effect of the fan-induced air flow on PV panels. To further characterize the air flow field in the BIPV/T collector, they carried out indoor tests using flow visualization instruments as well as the hot wire anemometry system (Zogou and Stapountzis, 2012). A significant flow entrance effect was demonstrated in the cases studied in their work. The measurements were used for the fine tuning of the CFD modeling of the system.

The utilization of an indoor solar simulator test facility may allow for accurate and repeatable experimentation of the BIPV/T system by offering stable and controllable operating conditions. Chen et al. (2012) investigated experimentally a thin-film semi-transparent BIPV glazing by the use of an indoor calorimetric hot box while simulating the climate with a solar simulator and an external air curtain. Solanki et al. (2009) studied the thermal and electrical performance of PV/T

116

air collectors connected in series using a solar simulator. Dupeyrat et al. (2014) obtained energy efficiency curves of glazed and unglazed PV/T water prototypes at the indoor solar simulator of Fraunhofer ISE. Krauter et al. (1999) explored the electrical and thermal performance as well as the thermal insulating property of a façade-integrated BIPV/T system through the use of a solar simulator. Mei et al. (2009) examined the overheating problem of roof-integrated BIPV systems in a solar simulator at Loughborough University, UK. They pointed out the effective black body temperature of the sky that exchanged radiation with the PV surface is not properly represented by the hot lighting devices at the indoor facility. To compensate for this, energy exchange models were developed for both the test arrangement and a typical outdoor exposure. In the solar simulator facility where the present research was conducted, an artificial sky comprising two glass panes with cool air circulated in between was installed in front of the lamps, which simulated a more realistic sky temperature.

The air-based BIPV/T system usually involves large-scale installation to cover one roof surface with the outer layer performing the function of building envelope cladding or roof tiles. As air extracts heat from the PV panel, its temperature keeps increasing along the flow path until such heat absorption capacity is greatly hindered due to the high air temperature. At this point, the air temperature profile reaches a plateau and air has a negligible cooling effect on the PV panel. To address this issue, the present authors (Yang and Athienitis, 2014) designed a structure with two-inlets with the second inlet halfway along the air path. The preliminary calculation showed that the thermal efficiency could be raised by about 5% by adding an extra inlet in the middle of a BIPV/T air collector. An analogy may be made between the UTC integrated BIPV/T system previously investigated by Athienitis et al. (2011) and the proposed system − the former

117

introduces continuous multiple air inlets by the perforated UTC sheet whereas the latter leaves air inlets as opposed to applying sealing at the conjunction of PV modules. The proposed system is easy to be implemented and does not add significant cost since an UTC and the mounting clamps are not used.

In addition, modular assembly of the air-based BIPV/T system is important for cold regions with a limited outdoor construction period (Chen et al., 2010; Nagano et al., 2003). The design discussed in this paper could be pre-fabricated in a factory environment and assembled on-site.

The purpose of this paper is to present the experimental investigation of the modified air-based BIPV/T system with two-inlets using a full-scale solar simulator. Through experimentation, the thermal performance of the two-inlet air-based BIPV/T system is determined, and Nusselt correlations are derived which are important for further analysis of BIPV/T systems with multiple inlets.

4.3 Experimental Setup

4.3.1 Solar Simulator

The solar simulator is a major component of the Solar Simulator – Environmental Chamber Laboratory at Concordia University, Montreal, Canada. The solar simulator enables the testing of various energy systems such as photovoltaic systems, solar thermal collectors, photovoltaic/thermal collectors and insulation components. It offers accurate and repeatable test conditions in terms of solar radiation, wind speed and ambient temperature, all of which are unpredictable and unstable in outdoor conditions.

The solar simulator mainly consists of three parts – lamp field, artificial sky and collector support. These components can be rotated between 0° and 90°, allowing solar systems to be tested at different building roof/façade angles. Eight metal halide lamps are used as the light source, and their emitting spectrum is very similar to that of natural sunlight according to standards EN 12975:2006 and ISO 9806-1:1994. The intensity and location of each individual lamp can be adjusted so that the test area is illuminated as homogeneously as possible. An artificial sky is installed in front of the lamps to simulate the sky temperature that is encountered in the outdoor environment. The artificial sky consists of two panes of clear glass assembled in parallel, with a gap in between for cold air to circulate and cool down the glass surfaces.

The collector support provides a platform onto which the test prototype can be mounted. An x-y scanner with two degrees of freedom is installed above the collector support surface, and it is able to reach any point in the horizontal plane. Once the test area of the BIPV/T system is designated, the pyranometer (Kipp & Zonen CMP11) mounted on the x-y scanner sweeps through the zone and measures the irradiance. By examining the radiation distribution on the scanned plane, a more uniform distribution can be achieved by changing the location and/or the intensity of each lamp. This process can be repeated a number of times to ensure a satisfactory solar radiation homogeneity.

A ventilation unit was installed at one end of the collector support to generate wind on top of the BIPV/T system. The main parts of this unit are two cross-flow fans that create wide and uniform air stream above the PV panels. An anemometer (Airflow Lufttechnik GmbH D12 -65) was attached to the x-y scanner to measure the wind speed over the BIPV/T test surface.

Since the high-power lamps add a large amount of heat into the room, a cooling unit is installed

to remove the heat and maintain a stable indoor temperature.

4.3.2 Experimental BIPV/T Prototype

Two types of the BIPV/T system based on two different PV panels were tested: panels made from semi-transparent modules and panels made from opaque modules. The sandwiched composition for both types of PV modules is the same; they are 3.2 mm tempered glass, EVA (ethylene-vinyl acetate), mono-crystalline silicon solar cells, EVA and PVF (polyvinyl fluoride) backsheet from top to bottom. The PVF may take on a clear or pigmented form. The clear PVF is utilized in semi-transparent crystalline silicon PV modules, while the pigmented white or black PVF is used in opaque PV modules that are commercially popular. In the BIPV/T system using clear PVF, a portion of the incoming solar radiation is transmitted inside the BIPV/T system by passing through the transparent area and being absorbed by the insulation and this increases the thermal efficiency. Photos and schematic drawings of the two types of PV modules are shown in Figure 4.1.

(a)   (b)
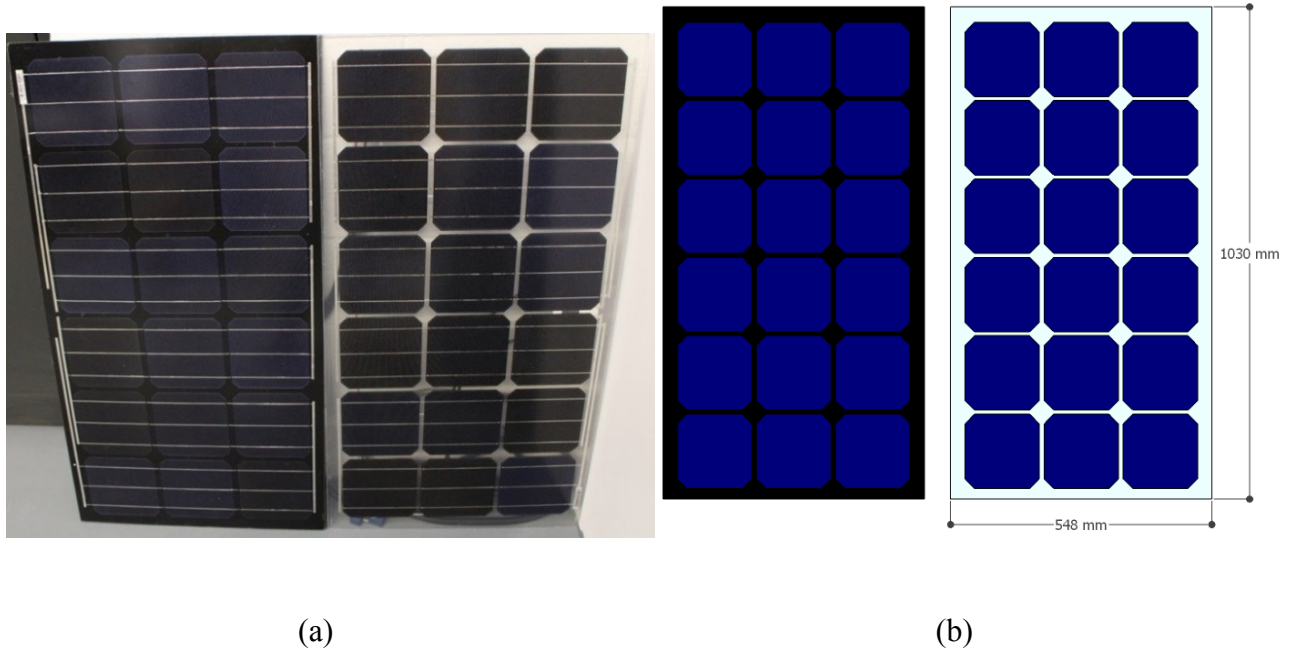
Figure 4.1. (a) Photo of the opaque and semi-transparent PV panels used in BIPV/T systems; (b)

Schematic of the opaque and semi-transparent PV panels

In order to take into account both electrical power generation and PV panel temperature, a packing factor (the percentage of the PV panel area covered by solar cells) of 80% was used for both semi-transparent and opaque PV types. Vats et al. (2012) studied the effect of packing factor on the performance of a semi-transparent BIPV/T system and found that a decrease of module temperature can be achieved by reducing the packing factor of the PV module.

Frameless PV panels were used in this experimental research. Most photovoltaic modules have a frame around the outer edge to provide structural support and ease of installation onto racks. Such frames will obstruct the air flow near the two ends of the module, creating hot spots on the PV panels (Gan, 2009). The framed BIPV/T system can be improved by eliminating the framing structure and applying curtain wall technologies to the PV installation process.

In sizing the experimental BIPV/T prototypes, the following factors were considered:

(1) The length of the PV module should allow the generation of a fully developed flow pattern.

(2) The size of the PV module should facilitate fixation to the collector support platform of the solar simulator and radiation uniformity adjustment.

(3) The length of the tested BIPV/T system is a maximum of about 3 m.

The schematic of the experimental semi-transparent BIPV/T prototype consisting of two custom designed and manufactured mono-crystalline PV panels is shown in Figure 4.2. Each PV panel contains three columns of six solar cells, with length × width × thickness of 1030 mm × 548mm × 4mm. The two sides of the air channel were made of 31 mm thick solid pine wood with grooves for installing the PV panels. The PV panels were slit along the grooves and then fixed with 9.5 mm of the panel width embedded in the groove on each side, leaving the air channel width of 529 mm. The bottom of the channel consists of 25.4 mm thick (1 inch) rigid polystyrene insulation with an RSI value of 0.88 $m^2 \cdot K/W$ and a 11 mm (7/16 inch) thick oriented strand board (OSB).

The first PV panel is parallel to the bottom insulation surface, creating a uniform channel height of 45 mm. Considering that the BIPV/T system is intended to be used as the building envelope and should reduce rain/snow/dust penetration, the second PV module overlaps the first one at the conjunction and leaves a gap of 12 mm in height as the second air inlet. Along the air flow path, the second PV module tilts down so that in a large-scale project more PV panels could be set at the same elevation as the second module and maintains a uniform look. The BIPV/T channel

covered by the parallel PV is called the first section, and the channel covered by the tilted PV is named the second section.
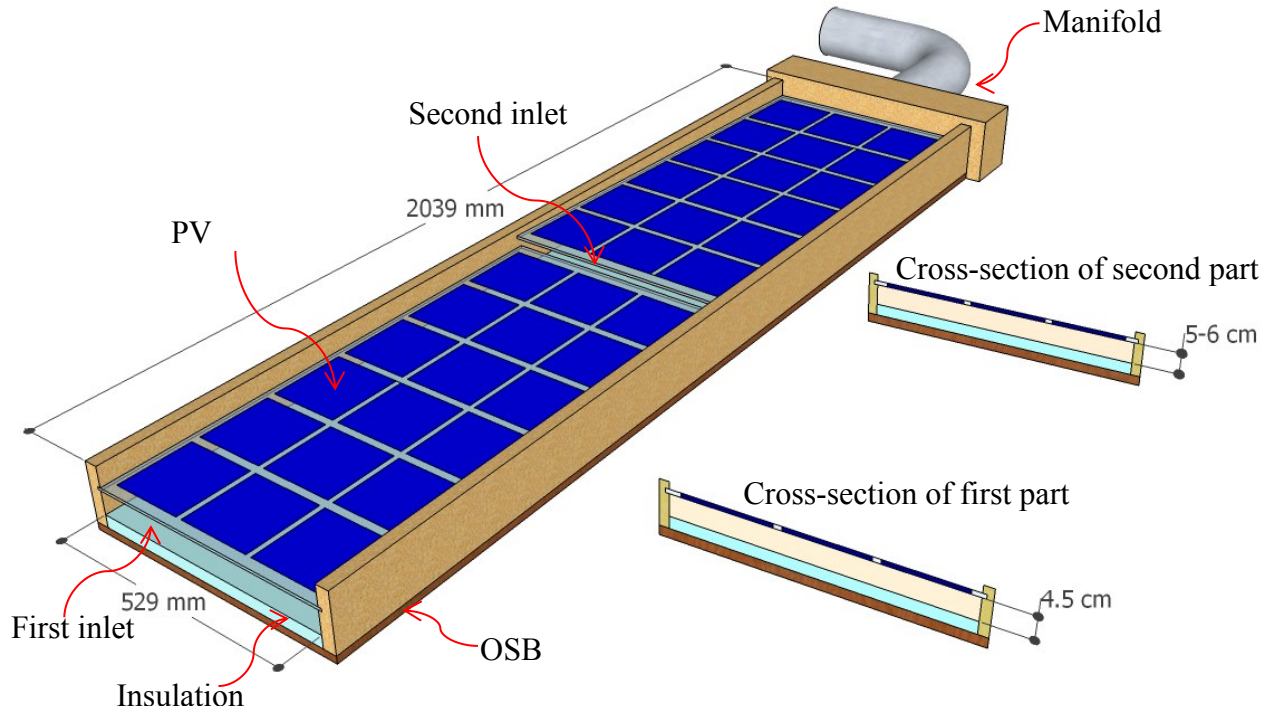
Figure 4.2. Schematic of the semi-transparent BIPV/T system prototype with two inlets

With the BIPV/T system mounted onto the collector support of the solar simulator, it can be tilted between 0° and 90° to reproduce different roof/façade slopes. Figure 4.3 shows photos taken during the testing of the semi-transparent and black opaque BIPV/T systems, both at a 45° tilt angle.
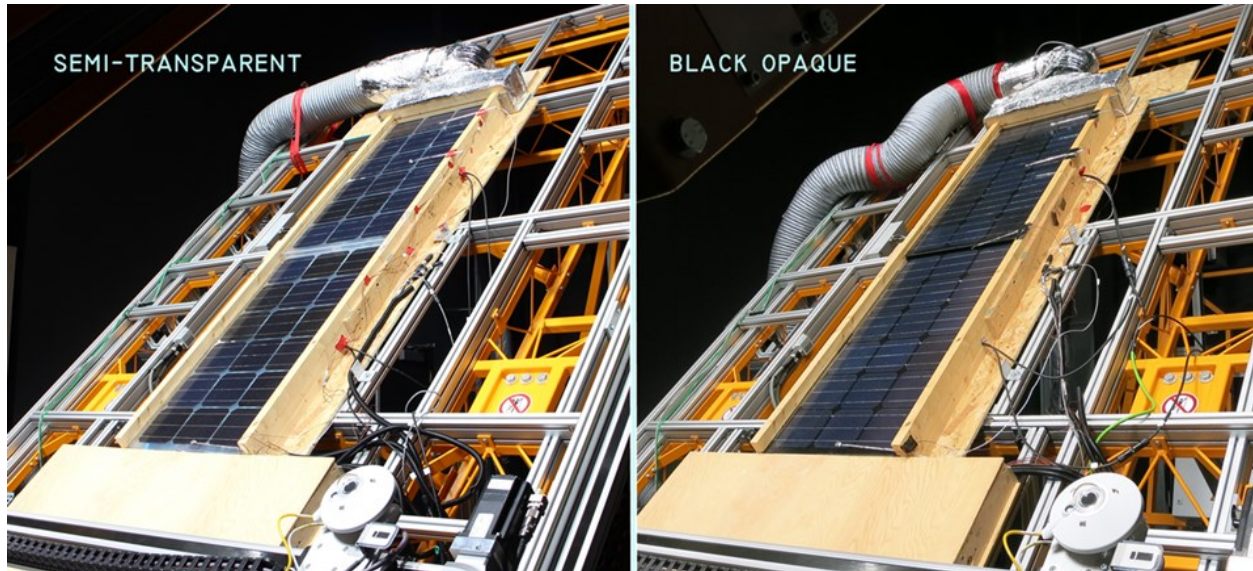
Figure 4.3. Photos of BIPV/T systems using semi-transparent or black opaque PV panels being tested at a tilt angle of 45° (left: semi-transparent, right: black opaque)

4.3.3 Temperature Measurement

Fifty five type-T thermocouples and three RTD temperature sensors were distributed throughout the system. Four system parameters were measured: the bottom surface temperature of the PV module, the channel air temperature, the inner surface temperature of the insulation and the artificial wind temperature just above the top surface of the PV module (the simulator creates an artificial wind along the length of the collector).

The outlet air from the first section and ambient air from the second inlet mixes in the second section of the system. To examine the mixed air temperature profile, three thermocouples were grouped at different heights and five such groups were distributed along the air flow direction in the second section of the BIPV/T system. The tip of the thermocouple is shielded by aluminum foil in order to block the radiation from the PV and insulation hot surfaces.

124

4.4 Experimental Procedure and Numerical Model

The BIPV/T system prototypes were tested to compare the performances of one-inlet and two-inlet systems. The effect of PV panel transparency was also evaluated experimentally using the previously described PV panels.

When studying the performance of a two-inlet system, one challenge is to determine the air flow rate in the first section, while knowing the total flow rate in the second section from readings of LabView program controlling the fan. For a given channel geometry, the flow velocity at a certain point has a single-valued relationship with the flow rate in the channel. If the relationship is known and the velocity can be measured, the flow rate can be determined. A small hole was drilled in the side wood of the BIPV/T channel near the middle of the first section to facilitate the use of a velocity meter. With the second air inlet closed, the flow rate in the first section equals the total flow rate which was known from the fan controlling program. The uncertainty of the air mass flow rate measurement is less than 2%. A TSI VelociCalc meter 8346 was used to measure air velocity through the hole. The anemometer had an accuracy of 3.0% of reading or ±0.015 m/s, and its measurement showed a deviation of 1.25% when calibrated in a wind tunnel against a 4-hole cobra probe.

The measured air velocity in the first section was plotted against mass flow rate in Figure 4.4. The correlation between them is given below:

$$\dot{m} = 90.6V^{1.038} \qquad\qquad (4.1)$$
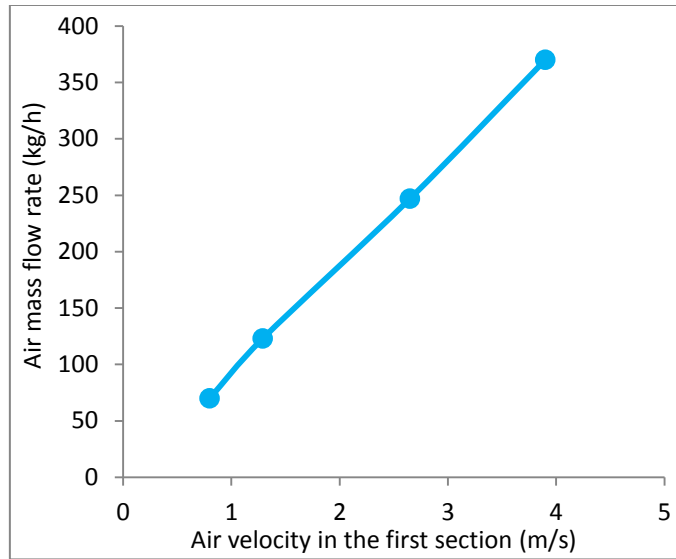
Figure 4.4. Air mass flow rate in relation to air velocity in the first BIPV/T section

When experiments were conducted on the two-inlet system, the above correlation was used to determine air mass flow rate in the first section using measured velocity.

Thermal efficiency η_{th} was calculated using Eqn. 4.2 below.

$$\eta_{th} = \frac{\dot{m}c_p(T_{out} - T_{in})}{G \cdot A} \qquad (4.2)$$
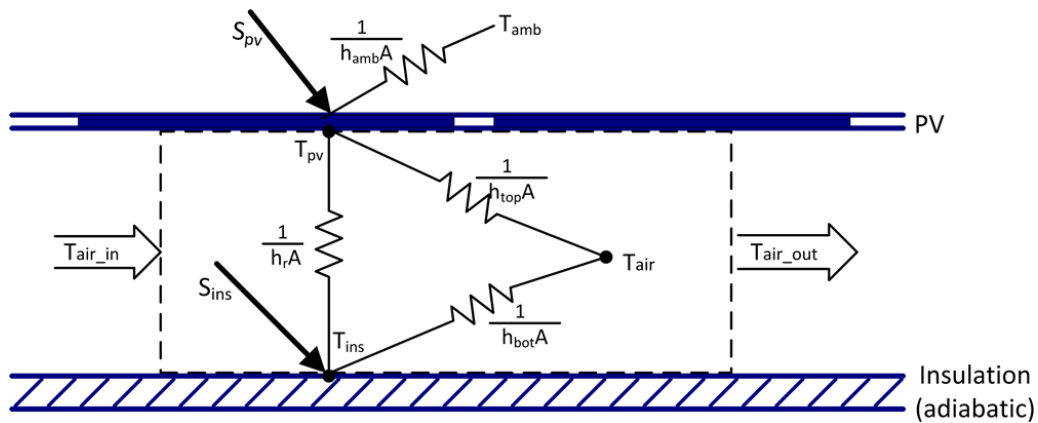
Figure 4.5. Thermal network model of the BIPV/T system

126

A thermal network model is commonly used for analyzing solar thermal systems. Fig. 5 illustrates a thermal network schematic for the BIPV/T system studied in this paper. The PV panel, insulation, channel air, and ambient surroundings of the BIPV/T system make up a network, in which their interactions achieve a balanced steady state in the experiment. The governing equations for each component of the semi-transparent BIPV/T system are shown below.

For the PV panel, the energy balance equation is

$$S_{pv} = \frac{A\sigma(T_{pv}^4 - T_{ins}^4)}{\frac{1}{\varepsilon_{pv}} + \frac{1}{\varepsilon_{ins}} - 1} + Ah_{amb}(T_{pv} - T_{amb}) + Ah_{top}(T_{pv} - T_{air}) \qquad (4.3)$$

For air in the BIPV/T channel, the energy balance equation is

$$\dot{m}c_p(T_{out} - T_{in}) = Ah_{top}(T_{pv} - T_{air}) + Ah_{bot}(T_{ins} - T_{air}) \qquad (4.4)$$

For insulation inner surface, the energy balance equation is

$$S_{ins} + \frac{A\sigma(T_{pv}^4 - T_{ins}^4)}{\frac{1}{\varepsilon_{pv}} + \frac{1}{\varepsilon_{ins}} - 1} = Ah_{bot}(T_{ins} - T_{air}) \qquad (4.5)$$

The PV panel absorbs solar energy on the upper surface, and its lower surface also receives radiation reflected by the insulation, thus S_{pv} can be given by

$$S_{pv} = G \cdot A \cdot PF \cdot \alpha_{pv} + G \cdot A \cdot (1 - PF) \cdot \alpha_g + G \cdot A \cdot (1 - PF) \cdot \tau_g \cdot \rho_{ins} \cdot \alpha_{pv} - E \qquad (4.6)$$

where *PF* stands for packing factor, and E denotes the generated electricity.

The solar radiation incident on the insulation is

$$S_{ins} = G \cdot A \cdot (1 - PF) \cdot \tau_g \cdot \alpha_{ins} \tag{4.7}$$

It was assumed that the insulation did not receive reflected radiation from the PV's back surface, because both insulation and PV have high absorptivity.

This thermal network model is then used to determine the convective heat transfer coefficients using experimentally obtained data.

The electrical efficiency of the PV module is expressed as a function of temperature as follows

$$\eta_e = \eta_{ref}(1 - 0.4\%(T_{pv} - 25)) \tag{4.8}$$

The transmissivity τ_g is set to zero for the opaque BIPV/T system in the thermal network equations.

4.5 Experimental Results

4.5.1 Comparison of Temperature between 1-inlet and 2-inlet BIPV/T Systems Using Semi-Transparent or Opaque PV Panels

The system performances of a two-inlet and a single-inlet BIPV/T system are compared. A one-inlet system is set up by blocking the second inlet in front of the second section using a thin clear acrylic bar. The comparison of such two systems is based on the fact that the total flow rates flowing out of the systems are the same, which was accomplished by controlling the fan speed. A RTD temperature sensor is placed next to the prototype on the collector support, shaded from direct sunlight from the lamps. The measurement given by this sensor is considered as the ambient air temperature, under which the BIPV/T system works. The experimental data showed that this temperature was stable when the cooling unit for the room was operating. Under an

average incident solar radiation of 1040 W/m², the outlet air temperatures of the one-inlet and two-inlet semi-transparent BIPV/T systems are compared in Figure 4.6. Wind speeds of 2.1 m/s and 3.1 m/s were tested and the results are presented in Figure 4.6a and 4.6b respectively.

(a)
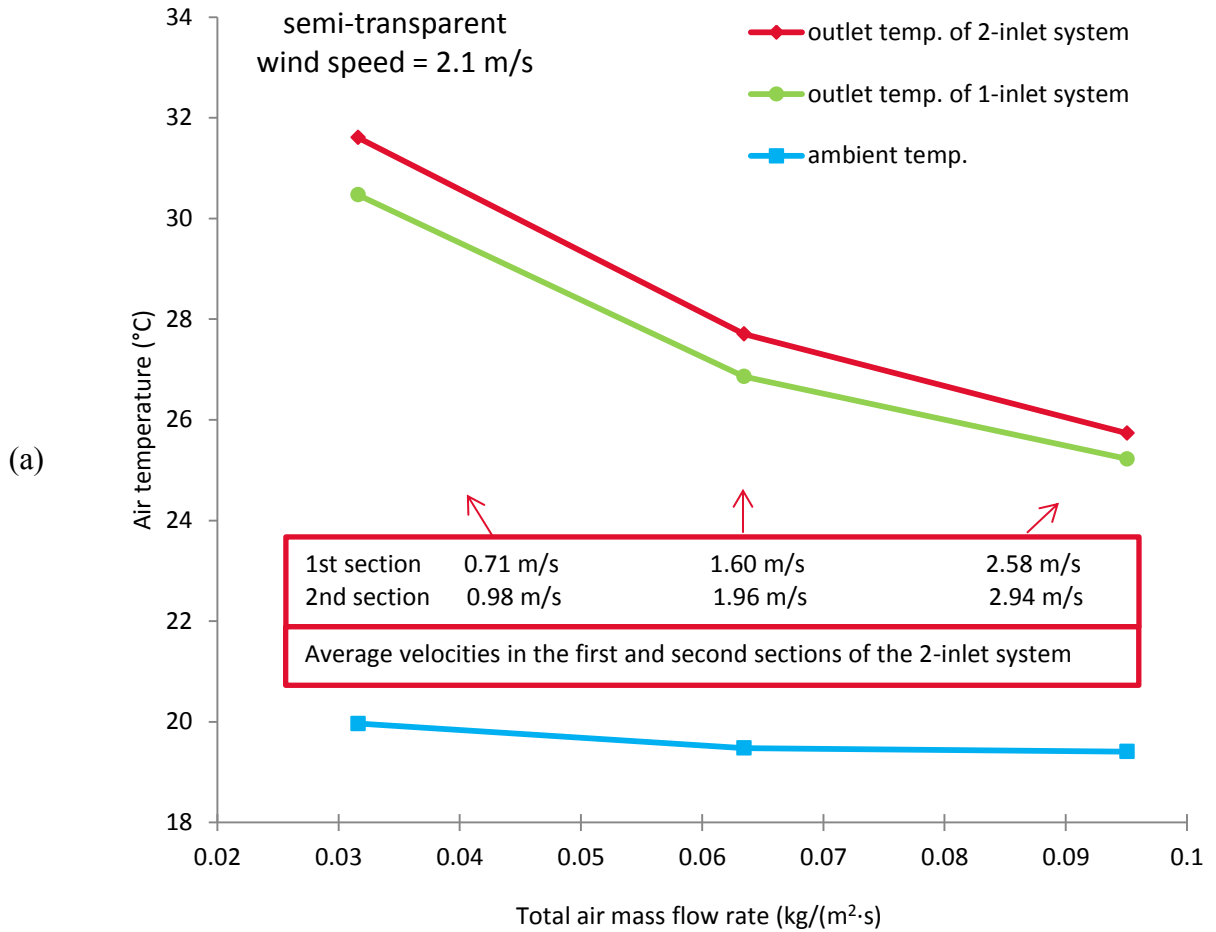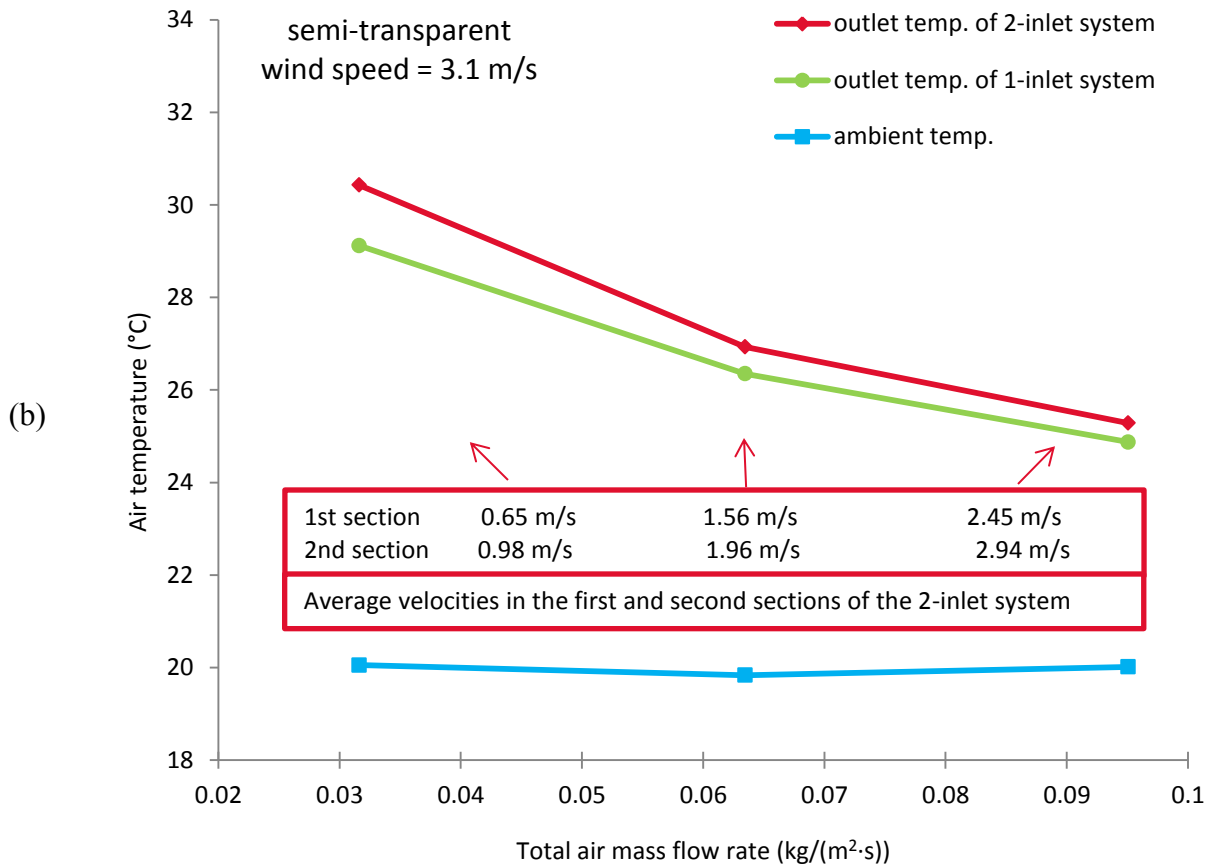
Figure 4.6. Comparison of outlet air temperatures between one-inlet and two-inlet semi-transparent BIPV/T systems: (a) wind speed at 2.1 m/s; (b) wind speed at 3.1 m/s

The ambient temperature was maintained around 20 °C for the duration of the experiment. It can be observed from Figure 4.6 that the outlet temperatures of the two-inlet system are higher than the one-inlet system, regardless of the air flow rate in the BIPV/T channel and the wind speed. It can also be seen from Figure 4.6 that the introduction of two inlets increases outlet air temperature more significantly at smaller air flow rate. For example, the outlet air temperature of the two-inlet system is 1.4 °C higher than that of the one-inlet system when the air mass flow rate is 123 kg/s, while this temperature difference is 0.5 °C when the air mass flow rate is 370

kg/s.

Figure 4.7 depicts the outlet air temperatures of the opaque BIPV/T systems having one inlet and two inlets, respectively, under a solar radiation of 1040 W/m^2 and wind speed of 2.1 m/s. It can also be observed that air outlet temperature is increased by applying two inlets in the opaque BIPV/T system.
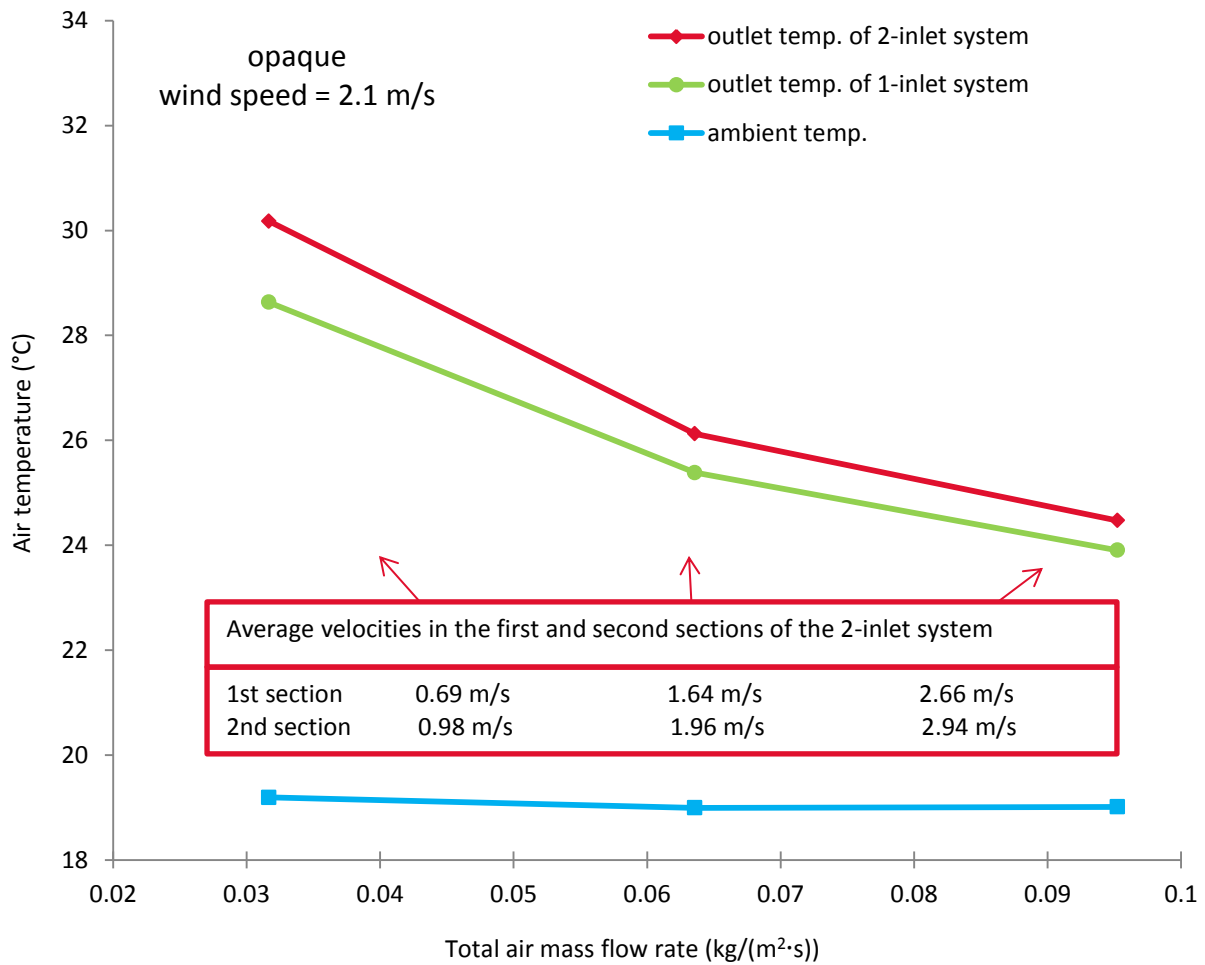
Figure 4.7. Comparison of outlet air temperatures between one-inlet and two-inlet opaque BIPV/T systems

4.5.2 Comparison of Thermal Efficiency between 1-inlet and 2-inlet BIPV/T Systems

The thermal efficiencies of one-inlet and two-inlet semi-transparent BIPV/T systems are compared under different wind speeds, as shown in Figure 4.8. It can be concluded that using two inlets achieves higher thermal efficiency than one inlet, with other conditions unchanged. As expected, the system thermal efficiency decreases with increasing wind speed. For the wind speed of 2.1 m/s, the curves for one-inlet and two-inlet are nearly parallel to each other, suggesting that the two-inlet design improved the thermal efficiency by about 5% regardless of the total air mass flow rate. In addition, at both high wind speed (3.1 m/s) and high channel air flow rate (370 kg/h), the thermal efficiencies for one-inlet and two-inlet designs are close compared to other cases. This is because with high air velocities at the top and bottom of PV panels, heat extraction approaches a limit and design alterations do not impact system performance significantly.
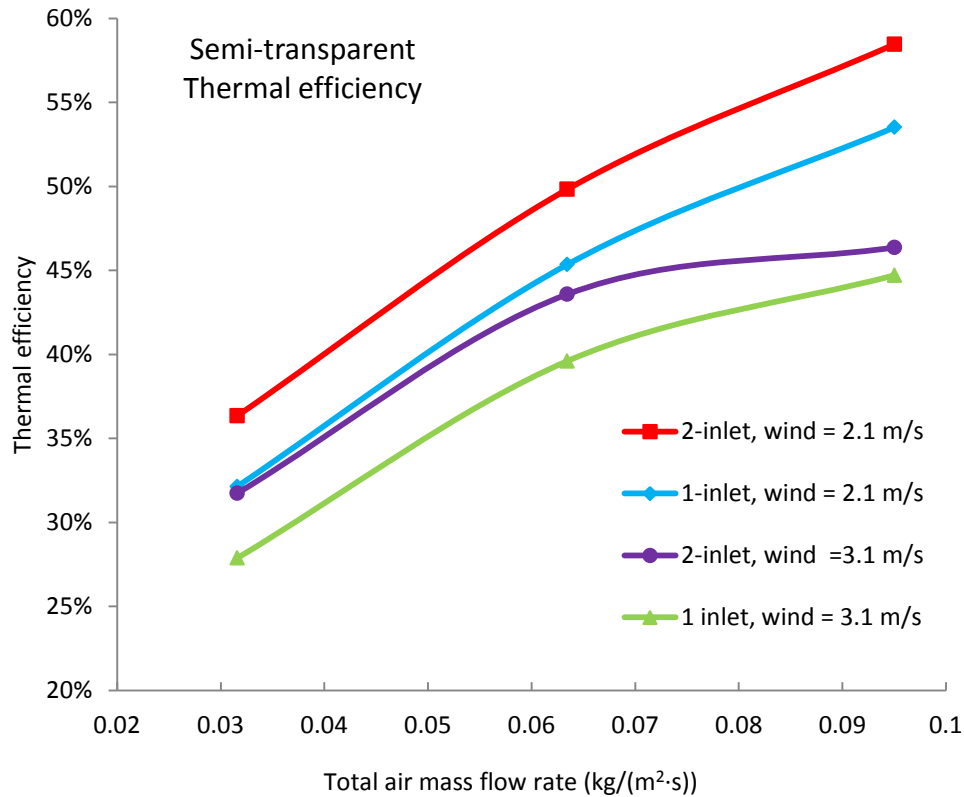
Figure 4.8. Comparison of thermal efficiency between one-inlet and two-inlet semi-transparent

BIPV/T systems under wind speeds of 2.1 m/s and 3.1 m/s

The effect of using semi-transparent or opaque PV panels in one-inlet and two-inlet BIPV/T systems is illustrated in Figure 4.9. The comparison is made with a solar radiation of 1040 W/m^2 and a wind speed of 2.1 m/s. It can be seen that the two-inlet design out-performed the one-inlet design in terms of thermal efficiency, for both PV panel types (semi-transparent and opaque). It is also evident that using semi-transparent PV panel improves thermal efficiency in both one-inlet and two-inlet BIPV/T systems. The opaque PV panel is the most significant heat exchange interface, where the air obtains most of the thermal energy while absorbing a smaller amount of heat from the insulation surface. The semi-transparent PV panel allows a portion of the incoming

133

solar radiation to pass through and reach the insulation surface, creating two major heat transfer surfaces – PV panel and insulation. As shown in Figure 4.9, the thermal efficiency of the BIPV/T system can be increased from 50.9% using opaque PV to 58.5% using semi-transparent PV at a total mass flow rate of 0.095 kg/(m^2·s).
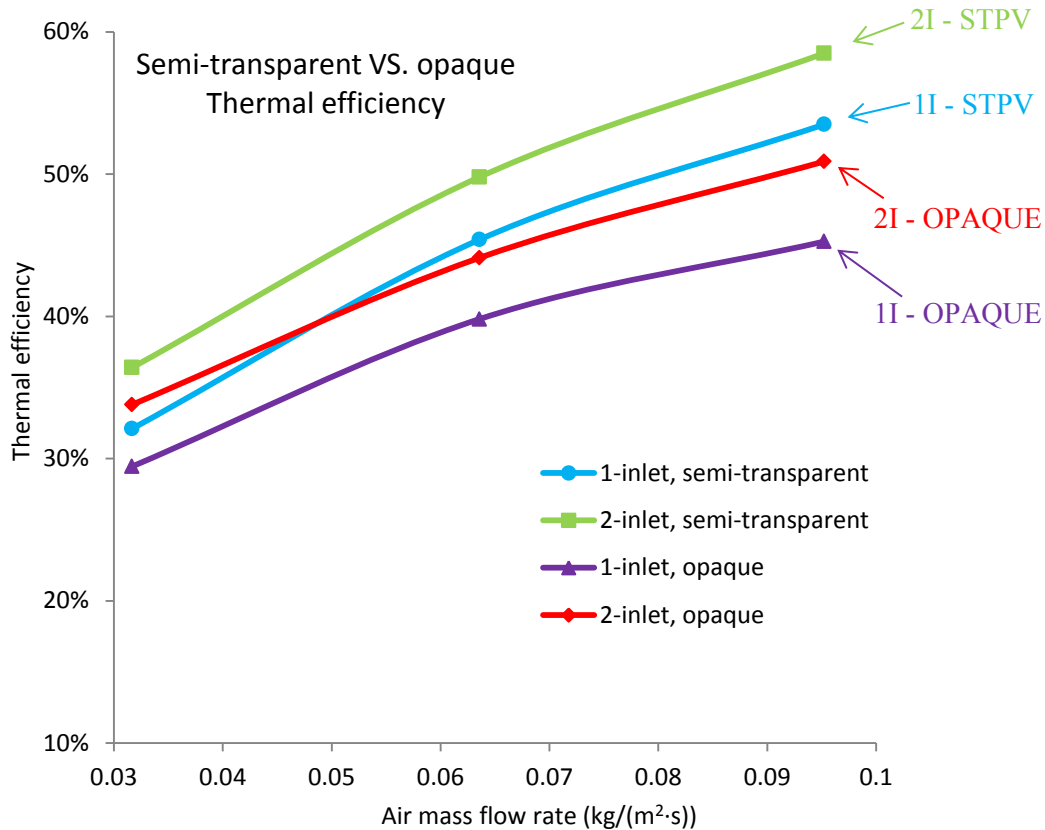
Figure 4.9. Thermal efficiency comparison between one-inlet and two-inlet BIPV/T systems using semi-transparent or opaque PV panels

4.5.3 Air Mixing in the Second Section of the BIPV/T System

Cold ambient air enters the second section from a top opening near the PV, while warmed air from the first section enters near the insulation side. The bottom warm air has the tendency to

rise, and the top cold air will drop down. Their mixing can be observed from the measured temperatures. Figure 4.10 shows the side view along the BIPV/T channel and the thermocouple distribution in the system. Thermocouples were attached to the bottom of the PV panels, the insulation inner surface and fixed in the air stream. In the second section, three thermocouples were grouped at different heights to measure the temperature changes from top to bottom. Along the channel, there are five groups of thermocouples. In Figure 4.10, the BIPV/T channel is roughly divided into three layers from top to bottom: top layer, middle layer and bottom layer.
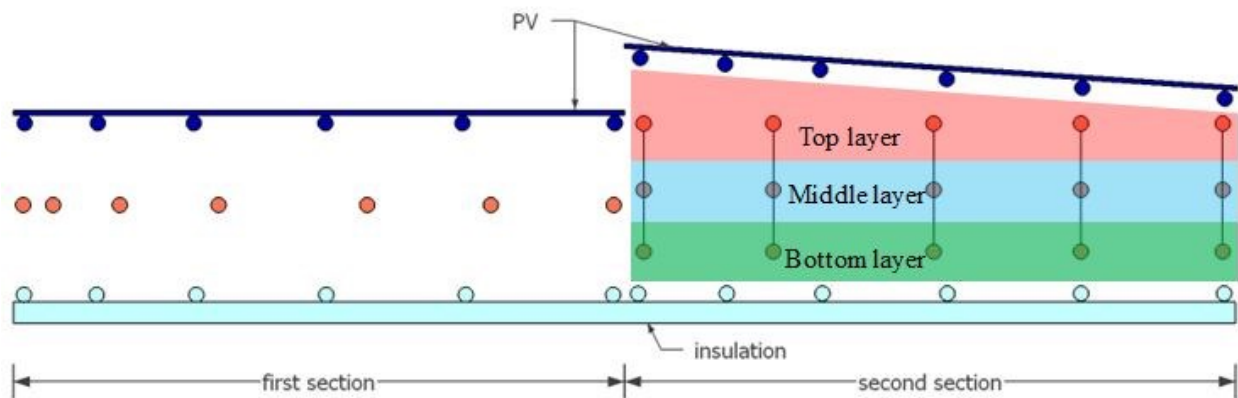
Figure 4.10. Side view of the BIPV/T channel with thermocouple positions

Typical temperature trends in the top, middle and bottom layers of the second section along the flow path are plotted in Figure 4.11. Affected by the mixing of cool ambient air and warmed air, as well as heat absorption from PV panel and insulation, the temperatures in different layers follow independent trends. The cool air entering from the second inlet immediately under the second PV panel got heated by the PV panel, making the air temperature in the top layer show a continuous growing pattern. In the middle layer, the warm air from the first section mixed with the cold air from the second inlet, resulting in a sharp temperature decrease at the second

thermocouple of the middle. The temperature shows a slowly increasing trend after half-length in the middle layer mainly due to the heat transfer from the top layer. The air temperature in the bottom layer is slightly influenced by the cool air jet, as can be seen from the gradually decreasing trend between the first and third thermocouples. It can be generally observed that the mixing of cool ambient air and warm outlet air from the first section occurs before the half-length, which is about 0.5 m away from the second inlet.
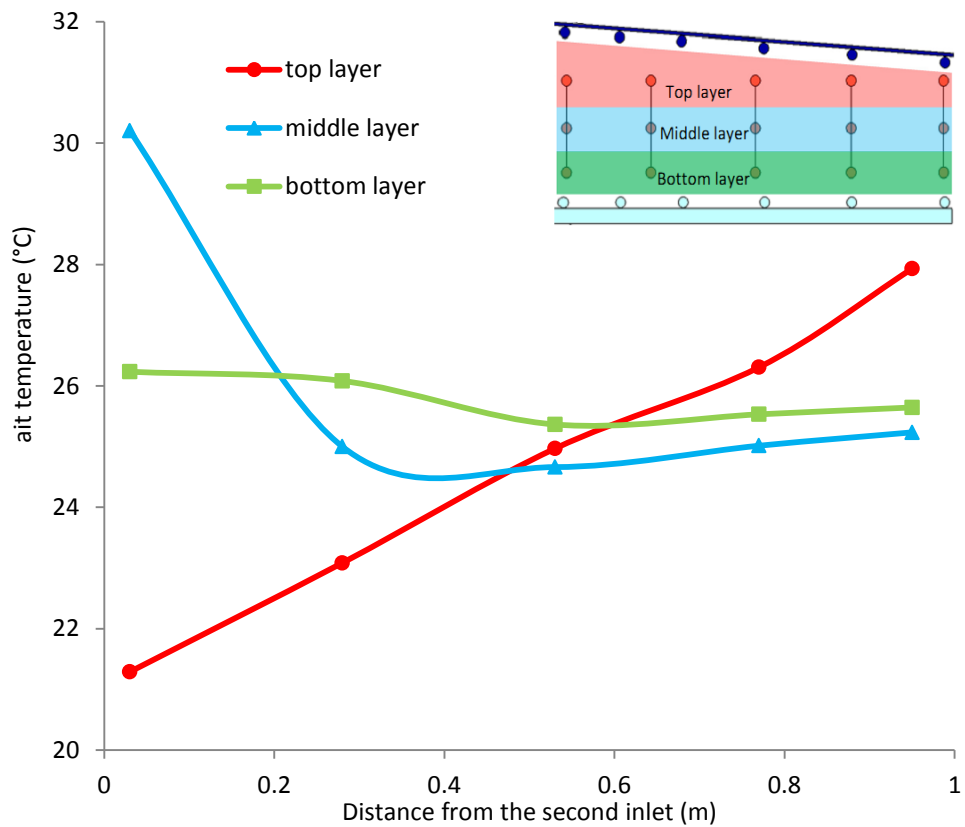
Figure 4.11. Temperature variations in each layer when air is mixed in the second BIPV/T section

4.5.4 Inlet Air Temperature at the Second Inlet of the BIPV/T System

136

For a conventional one-inlet BIPV/T system, the ambient air is heated up by the PV's top surface and is lost to the ambient afterwards. In the case of a BIPV/T system with two inlets, the pre-heated ambient air is drawn through the second inlet into the system and improves system performance. A thermocouple is placed at the second inlet and shielded by aluminum foil to avoid direct sunlight. As shown in Figure 4.12, the ambient air temperature stabilizes around 19.5 °C, while the inlet air temperature at the second BIPV/T inlet is notably higher by 1-3 °C depending on the air flow rate in the BIPV/T channel.
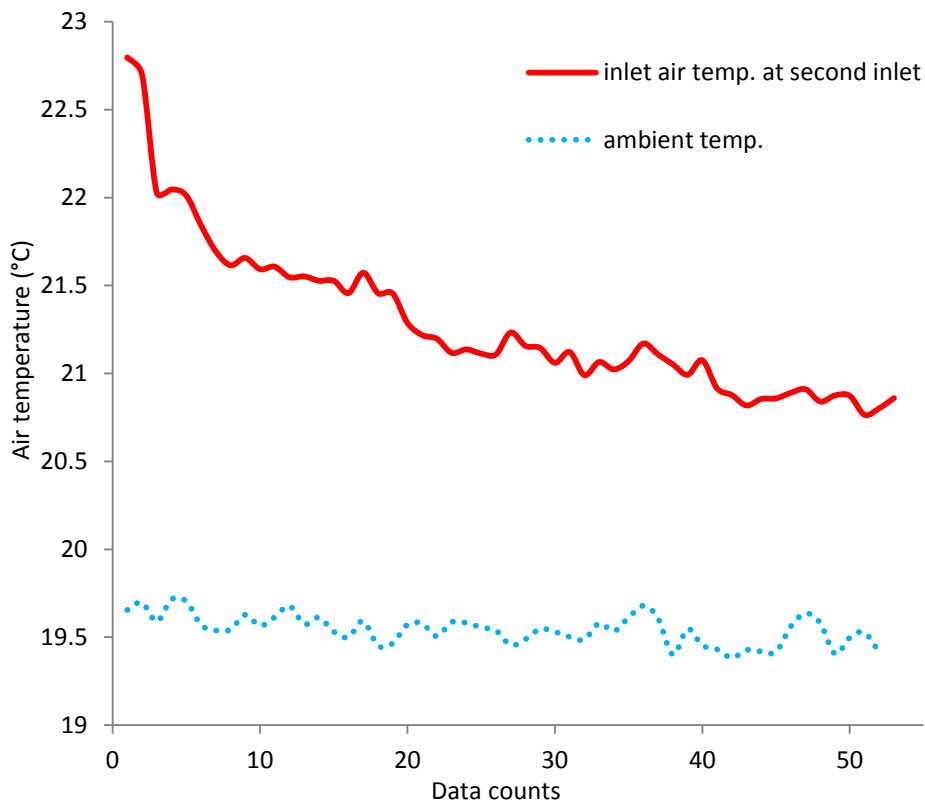
Figure 4.12. Comparison of the inlet air temperature at the second inlet with the ambient air temperature

4.5.5 Convective Heat Transfer Coefficient (CHTC) Correlation and Nusselt

Number Correlation for Opaque BIPV/T System

The CHTC identifies the level of heat exchange between the PV and the channel air and can be used to study different heat transfer phenomena. In the current investigation, CHTCs between the PV's bottom surface and the channel air in the two-inlet system for both the first and second sections are plotted against average air velocities in Figure 4.13. It is evident that the convective heat transfer is more effective in the second section, which is due to the broken boundary layer and local heat transfer enhancement by the extra air inlet.

In order to verify the procedure of calculating mass flow rate in each section, the CHTC in the 1-inlet system whose mass flow rate is readily known is also shown in Figure 4.14. The good agreement between CHTCs in the first sections of both 1-inlet and 2-inlet systems suggested a reliable calculation procedure of mass flow rates when air is drawn in from more than one inlet.
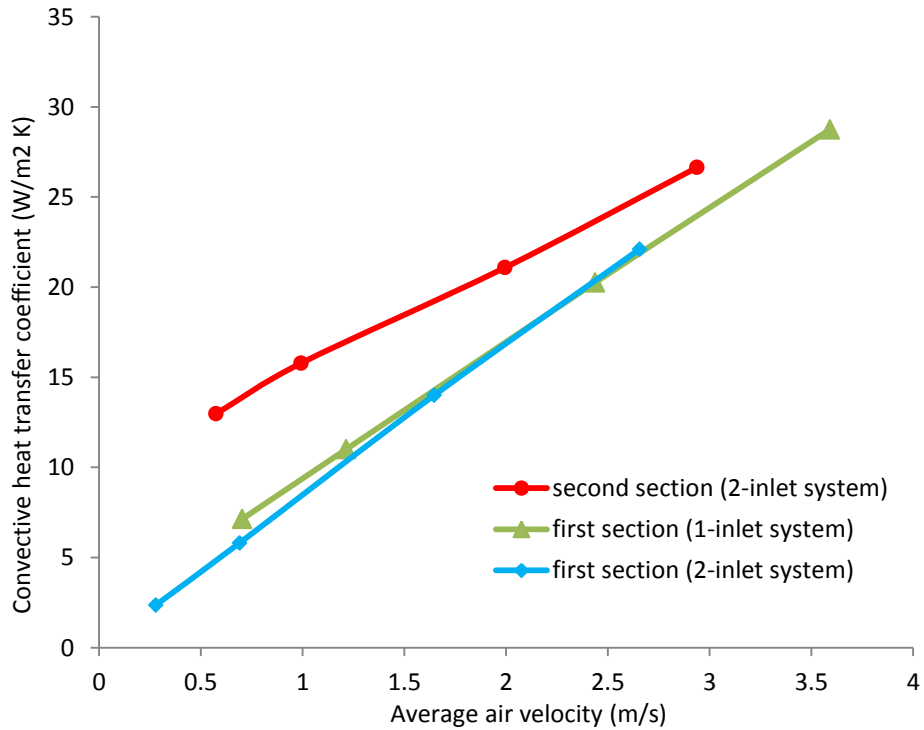
Figure 4.13. Heat transfer coefficient as a function of average channel air velocity in both one-inlet and two-inlet systems

The Nusselt number calculation is based on the experimentally obtained CHTC and uses the following formula (Incropera and DeWitt, 2002)

$$Nu = \frac{hD_h}{k} \qquad (4.9)$$

Where h is the convective heat transfer coefficient, D_h is the hydraulic diameter of the BIPV/T channel, and k is the conductivity of air.

As a reference, the Dittus-Boelter equation is plotted along with the Nusselt numbers in the two-inlet BIPV/T system (Figure 4.14). The Nusselt number in the first section is greater than predicted by the Dittus-Boelter equation because it involves entrance region. It is believed that the second section of the BIPV/T system achieves higher convective heat transfer coefficients and Nusselt number than the first section mainly due to the increased turbulence. Under the joint force of the wind thrust and the fan suction, the air enters the second inlet at a velocity higher than the channel flow. This high-speed air stream mixes with the channel air and induces turbulence, creating a different flow pattern compared to the conventional one-inlet channel flow. Figures 4.13 and 4.14 show that the effectiveness of the added inlet is more significant at lower flow rate. This is attributed to the fact that the wind force may impose much higher air speed at the second inlet than inside the channel especially when the air mass flow in the BIPV/T system is low.
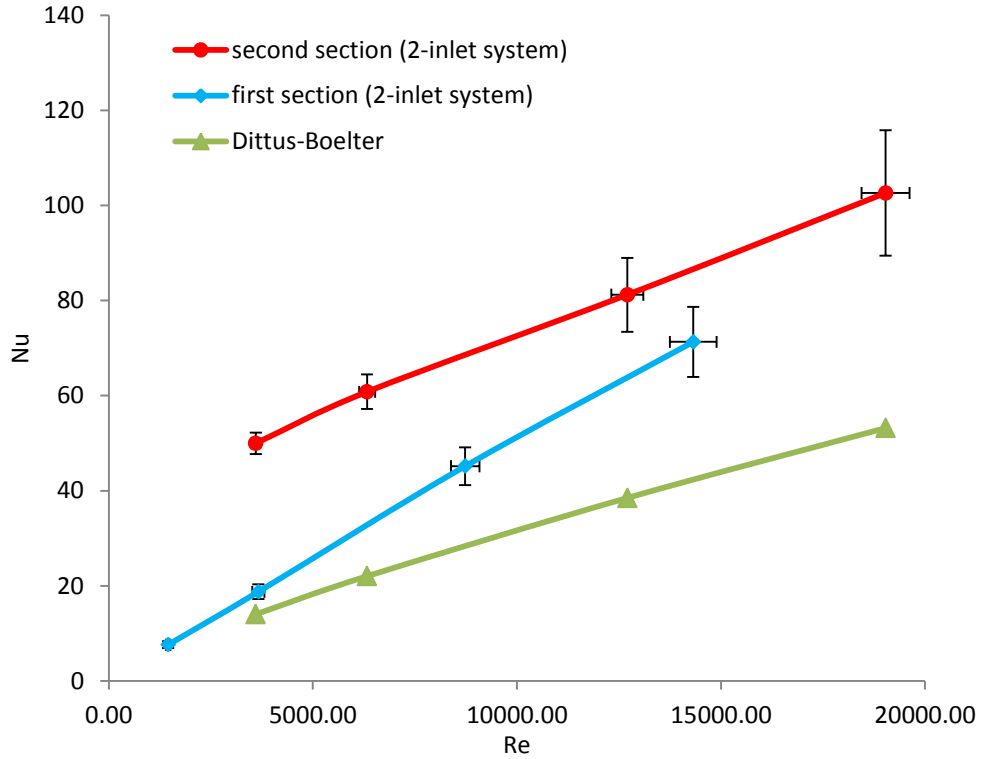
Figure 4.14. Nusselt number plotted against Reynolds number in the first and second sections of

the BIPV/T system

For the first and second sections of a two-inlet BIPV/T system, the Nusselt number between

PV's bottom surface and the channel air, fitted with coefficients of determinations around 99%,

can be expressed as:

First section: $Nu_{pv-air} = 0.0149Re^{0.9}Pr^{0.43}$ $\qquad\qquad$ $1453 < Re < 14322$ $\qquad$ (4.10)

Second section: $Nu_{pv-air} = 1.451Re^{0.44}Pr^{0.4}$ $\qquad\qquad$ $3600 < Re < 19034$ $\qquad$ (4.11)

At low flow rates corresponding to air flow velocities of 0.28 m/s in the first section and 0.58

m/s in the second section (related to the first points in Figure 4.14), natural convection of air

plays an increased role. In real operational practice, the air velocity is usually higher than these

values to ensure more efficient heat removal from the PV.

The procedure of uncertainty analysis of the Nusselt number and Reynolds number is presented in Appendix A3. It should be noted that although the above correlations were derived from a 2-inlet BIPV/T system, they can also possibly be applied in a BIPV/T system with multiple inlets due to the similar nature of heat transfer and fluid flow.

4.6 Conclusion

The open-loop air-based BIPV/T system has great potential where there is a high space heating demand. This paper presents an improved design concept of BIPV/T systems using multiple inlets to enhance the heat transfer between flowing air and PV modules. Experimental prototypes of one-inlet and two-inlet BIPV/T systems were constructed and a solar simulator was used to investigate the feasibility of the multiple-inlet concept and its heat transfer characteristics. Two types of custom-made frameless mono-crystalline silicon PV modules, semi-transparent and opaque, were used in the experimental prototypes to study effects of transmittance on the system performances. The results are summarized below:

(1) The two-inlet BIPV/T system is able to increase thermal efficiency by 5% compared to the one-inlet counterpart, and it is easy to be implemented and does not add significant cost.

(2) The thermal performance of a BIPV/T system can be significantly improved by using semi-transparent crystalline silicon PV modules to replace opaque ones due to the absorption of some solar radiation at the bottom surface in the BIPV/T system cavity. The

heterogeneous appearance of semi-transparent PV modules can be compensated by painting the inner surface of the insulation black.

(3) The advantages of the two-inlet BIPV/T system over the one-inlet counterpart are attributed to the following factors:

a. Along the flow path, the CHTC is highest near the inlet due to the entrance effect. Adding extra inlets in the BIPV/T system results in more areas with a higher CHTC between air and the PV, enhancing the heat transfer from the PV to the air.

b. In the conventional one-inlet BIPV/T system, the PV panel heats up both air beneath in the channel and free air on the top. However, heat transferred to the outside free air is unavailable for collection and therefore lost to the ambient. In a BIPV/T system with more inlets, the extra inlets could draw in free air that has been pre-heated by the PV panels resulting in improved thermal efficiency.

c. The cool ambient air enters the extra inlets at a location higher than the warmed air stream. Since cool air tends to descend due to higher density and warm air tends to rise, there is a good mixing of air in the BIPV/T channel. Furthermore, cool air enters the channel in the vicinity of the PV panel, creating a greater temperature difference between air and the PV than in conventional systems. Such temperature difference also leads to greater heat extraction from the PV.

(4) The Nusselt number correlations of the convective heat transfer between PV and air are developed as a function of Reynolds number and Prandtl number. As expected, the Nusselt number for the second section of the air flow path is higher than that in the first

section. The new correlations are helpful for further analysis and optimization of BIPV/T

system with multiple inlets.

5. Conclusion

5.1 Summary

The objective of this thesis is to propose enhanced open-loop air-based BIPV/T systems and evaluate their performances. These enhanced systems provide improved PV operating conditions, increased electrical production and higher outlet air temperature, enabling these systems to be an attractive building design option and aiding BIPV/T becoming a standard building component.

A literature review of a variety of BIPV/T systems is presented. A diverse range of working media and working principles of these systems are discussed and summarized. In particular, active open-loop air-based BIPV/T systems are discussed and analysed in detail. The survey of literature demonstrates that there is a need for BIPV/T design improvements, due to some PV/T and solar air heater designs being incompatible with a BIPV/T application constrained by aesthetical and envelope requirements. The review also provides suggestions for future research and improvement opportunities of BIPV/T systems.

The use of an additional vertical glazed solar air heater connected in series with a conventional BIPV/T collector and the application of multiple inlets to the PV covered section is proposed and investigated. Further, a glazed solar air heater may be packed with the wire mesh (a metallic matrix) to increase thermal gains. To demonstrate the performance of a conventional BIPV/T system and provide data for model verification, a comprehensive series of experiments were conducted using a solar irradiance simulator. Thermal efficiency curves for variable wind speed

and air mass flow rate of the BIPV/T prototype are presented. The thermal ramifications of the steel bars used as structural support are also discussed. By working as fins to conduct heat and induce air turbulence, these steel bars can improve the system thermal performance.

A lumped parameter thermal network model is developed to analyse the PV covered BIPV/T section and the glazed solar air heater section with and without packing material. The vertical glazed solar air collector, being able to receive high amount of solar energy especially in winter when the solar altitude is low, is shown to increase thermal efficiency by 8-10%, where the maximum of 10% is achieved when a wire mesh is used. However, the wire mesh substantially increases fan power consumption at high air mass flow rates in channel. The lumped thermal model is also applied to a BIPV/T roof of an existing solar house with four simulated inlets, and this model computed a thermal efficiency improvement of 7%.

A BIPV/T prototype with two air inlets was constructed and experimentally investigated. Comparative experiments carried out between one-inlet and two-inlet BIPV/T systems show a 5% increase in thermal efficiency due to the use of the two inlet design. This improvement is mainly attributed to the increased air inlet temperature at the second inlet and enhanced air turbulence near the second inlet. Moreover, the thermal performance of a BIPV/T system can be significantly improved by using semi-transparent crystalline silicon PV modules to replace opaque modules due to solar radiation absorption at the bottom surface in the BIPV/T system cavity.

Finally, the Nusselt number correlations of the convective heat transfer between PV and air are developed as a function of the Reynolds number and Prandtl number. These new correlations are helpful for further analysis and optimization of BIPV/T system with multiple inlets, and they can

be readily integrated in building energy simulation software such as EnergyPlus, TRNSYS and ESP-r.

5.2 Contributions

The main contributions of this research are summarized as follows:

1. Comprehensive review of BIPV/T systems. The BIPV/T technology with different working media and working principles are discussed and summarized, and recommendations for future research and improvement opportunities are provided.

2. Development of open-loop air-based BIPV/T system with improved performance using multiple inlets. The proposed system can achieve significantly higher thermal efficiency by improving the convective heat transfer in channel and reduce the PV operating temperature to avoid deterioration.

3. A lumped parameter thermal network model for BIPV/T systems. It was used to analyse the PV covered BIPV/T section and the glazed solar air heater section with and without packing material. It may be further used to evaluate variant BIPV/T systems. The model was verified with experimental data.

4. The Nusselt number correlations of the convective heat transfer in the BIPV/T channel. These correlations are obtained through experiments under well-controlled conditions. These new correlations are helpful for further analysis and optimization of BIPV/T system with multiple inlets, and they can be readily integrated in building energy simulation software such as EnergyPlus, TRNSYS and ESP-r.

5. The design methodology of the experimental setup in a solar simulator, including the

146

design of thermocouples placement. It enables the examination of detailed temperature profile and the thermal performance in a BIPV/T system.

With experimental results that validate performance enhancement using multiple inlets in a BIPV/T system, the above experimental and numerical procedures may be used for extended study of BIPV/T systems with multiple inlets.

5.3 Future Work

Further research in the following areas is recommended:

- The computational fluid dynamics (CFD) modeling of the two-inlet BIPV/T systems may be carried out to study the flow and temperature conditions of the channel air and further understand the mechanism that facilitate heat dissipation into the air. An optimised system design may be achieved from the numerical study.

- The determination of the packing factor of the semi-transparent PV module used in the BIPV/T installation needs to be evaluated. Electrical and thermal production should be balanced according to the energy requirements of specific applications.

- The sizes of the inlet openings need to be controlled, which offset wind distractions.

- The procedure of installing BIPV/T system with multiple air inlets should be explored. Standard assembling procedure may facilitate high-quality construction work and achieve desired system performance.

- Research on the backsheet material of the PV module is necessary. Low-conductivity polymer sheets are currently applied in PV panels, which obstruct the heat flow from PV to the flowing air. Using metallic substrate as the PV's backsheet

147

may result in improved system performance.

- Performance of a BIPV/T air system integrated with a heat pump to obtain useful thermal energy especially in winter may be investigated.

- The integration of the enhanced BIPV/T systems into building energy simulation softwares such as EnergyPlus, TRNSYS and ESP-r may be studied.

References

ABAQUS [computer program]. France: Dassault Systemes Simulia.

Aelenei, L., Pereira, R., Goncalves, H., Athienitis, A., 2014. Thermal performance of a hybrid BIPV-PCM: modeling, design and experimental investigation. Energy Procedia 48, 474-483.

Agrawal, B., Tiwari, G.N., 2010a. Life cycle cost assessment of building integrated photovoltaic thermal (BIPVT) systems. Energy and Buildings 42, 1472-1481.

Agrawal, B., Tiwari, G.N., 2010b. Optimizing the energy and exergy of building integrated photovoltaic thermal (BIPVT) systems under cold climatic conditions. Applied Energy 87, 417-426.

Al-Alili, A., Hwang, Y., Radermacher, R., Kubo, I., 2011. A high efficiency solar air conditioner using concentrating photovoltaic/thermal collectors. Applied Energy 93, 138-147.

Ammari, H.D., 2003. A mathematical model of thermal performance of a solar air heater with slats. Renewable Energy 28, 1597-1615.

Anderson, T.N., Duke, M., Morrison, G.L., Carson, J.K., 2009. Performance of a building integrated photovoltaic/thermal (BIPVT) solar collector. Solar Energy 83, 445-455.

Arcuri, N., Reda, F., De Simone, M., 2014. Energy and thermo-fluid-dynamics evaluations of photovoltaic panels cooled by water and air. Solar Energy 105, 147-156.

Assoa, Y.B., Menezo, C., 2014. Dynamic study of a new concept of photovoltaic-thermal hybrid

collector. Solar Energy 107, 637-652.

Assoa, Y.B., Menezo, C., Fraisse, G., Yezou, R., Brau, J., 2007. Study of a new concept of photovoltaic-thermal hybrid collector. Solar Energy 81, 1132-1143.

Aste, N., Chiesa, G., Verri, F., 2008. Design, development and performance monitoring of a photovoltaic-thermal (PVT) air collector. Renewable Energy 33, 914-927.

Athienitis, A.K., 2007. Design of a solar home with BIPV-Thermal system and ground source heat pump. 2nd Canadian Solar Buildings Conference, Calgary, June 10-14, 2007.

Athienitis, A.K., 2008. Design of advanced solar homes aimed at net-zero annual energy consumption in Canada, ISES-AP-3rd International Solar Energy Society Conference-Asia Pacific Region, Sidney, Australia, Nov., 14 pages.

Athienitis, A.K., Bambara, J., O'Neill, B., Faille, J., 2011. A prototype photovoltaic/thermal system integrated with transpired collector. Solar Energy 85, 139-153.

Bakar, M.N.A., Othman, M., Din, M.H., Manaf, N.A., Jarimi, H., 2014. Design concept and mathematical model of a bi-fluid photovoltaic/thermal (PV/T) solar collector. Renewable Energy 67, 153-164.

Bakker, M., Zondag, H.A., Elswijk, M.J., Strootman, K.J., Jong, M.J.M., 2005. Performance and costs of a roof-sized PV/thermal array combined with a ground coupled heat pump. Solar Energy 78, 331-339.

Ban-Weiss, G., Wray, C., Delp, W., Ly, P., Akbari, H., Levinson, R., 2013. Electricity production and cooling energy savings from installation of a building-integrated photovoltaic roof on an office building. Energy and Buildings 56, 210-220.

Bergene, T., Lovvik, O.M., 1995. Model calculations on a flat-plate solar heat collector with integrated solar cells. Solar Energy 55, 453-462.

Bernardo, L.R., Perers, B., Hakansson, H., Karlsson, B., 2011. Performance evaluation of low concentrating photovoltaic/thermal systems: A case study from Sweden. Solar Energy 85, 1499-1510.

Bigot, D., Miranville, F., Fakra, A.H., Boyer, H., 2009. A nodal thermal model for photovoltaic systems: Impact on building temperature fields and elements of validation for tropical and humid climatic conditions. Energy and Buildings 41, 1117-1126.

Bloem, J.J., 2008. Evaluation of a PV-integrated building application in a well-controlled outdoor test environment. Building and Environment 43, 205-216.

Bloem, J.J., Lodi, C., Cipriano, J., Chemisana, D., 2012. An outdoor Test Reference Environment for double skin applications of building integrated photovoltaic systems. Energy and Buildings 50, 63-73.

Brinkworth, B.J., Marshall, R.H., Ibrahim, Z., 2000. A validated model of naturally ventilated PV cladding. Solar Energy 69, 67-81.

Brogren, M., Wennerberg, J., Kapper, R., Karlsson, B., 2003. Design of concentrating elements with CIS thin-film solar cells for façade integration. Solar Energy Materials & Solar Cells 75, 567-575.

Buker, M.S., Mempouo, B., Riffat, S.B., 2014. Performance evaluation and techno-economic analysis of a novel building integrated PV/T roof collector: An experimental validation. Energy and Buildings 76, 164-175.

Candanedo, L.M., Athienitis, A., Park, K.W., 2011. Convective heat transfer coefficients in a building-integrated photovoltaic/thermal system. Journal of Solar Energy Engineering 133, 021002 (1-14).

Chae, Y.T., Kim, J., Park, H., Shin, B., 2014. Building energy performance evaluation of building integrated photovoltaic (BIPV) window with semi-transparent solar cells. Applied Energy 129, 217-227.

CHAM [computer program]. London, UK: CHAM Ltd; 2006.

Charron, R., Athienitis, A.K., 2006. Optimization of the performance of double-facades with integrated photovoltaic panels and motorized blinds. Solar Energy 80, 482-491.

Chemisana, D., Lopez-Villada, J., Coronas, A., Rosell, J.I., Lodi, C., 2013. Building integration of concentrating systems for solar cooling applications. Applied Thermal Engineering 50, 1472-1479.

Chemisana D., Rosell, J.I., 2011. Design and optical performance of a nonimaging Fresnel transmissive concentrator for building integration applications. Energy Conversion and Management 52(10), 3241-3248.

Chen, D.T., Chaturvedi, S.K., Mohieldin, T.O., 1992. An approximate method for calculating laminar natural convective motion in a trombe-wall channel. Energy 19 (2), 259-268.

Chen F.Z., Wittkopf, S.K., Ng, P.K., Du, H., 2012. Solar heat gain coefficient measurement of semi-transparent photovoltaic modules with indoor calorimetric hot box and solar simulator. Energy and Buildings 53, 74-84.

Chen, Y, Athienitis, A.K., Galal, K., 2010. Modeling, design and thermal performance of a

BIPV/T system thermally coupled with a ventilated concrete slab in a low energy solar house: Part 1, BIPV/T system and house energy concept. Solar Energy 84, 1892-1907.

Chow, T.T., 2010. A review on photovoltaic/thermal hybrid solar technology. Applied Energy 87, 365-379.

Chow, T.T., Chan, A.L.S., Fong, K.F., Lin, Z., He, W., Ji, J., 2009c. Annual performance of building-integrated photovoltaic/water-heating system for warm climate application. Applied Energy 86, 689-696.

Chow, T.T., Fong, K.F., He, W., Lin, Z., Chan, A.L.S., 2007a. Performance evaluation of a PV ventilated window applying to office building of Hong Kong. Energy and Buildings 39, 643-650.

Chow, T.T., Hand, J.W., Strachan, P.A., 2003. Building-integrated photovoltaic and thermal applications in a subtropical hotel building. Applied Thermal Engineering 23, 2035-2049.

Chow, T.T., He, W., Chan, A.L.S., Fong, K.F., Lin, Z., Ji, J., 2008. Computer modeling and experimental validation of a building-integrated photovoltaic and water heating system. Applied Thermal Engineering 28, 1356-1364.

Chow, T.T., He, W., Ji, J., 2007b. An experimental study of façade-integrated photovoltaic/water-heating system. Applied Thermal Engineering 27, 37-45.

Chow, T.T., He, W., Ji, J., 2006. Hybrid photovoltaic-thermosyphon water heating system for residential application. Solar Energy 80, 298-306.

Chow, T.T., Pei, G, Fong, K.F., Lin, Z., Chan, A.L.S., Ji, J., 2009b. Energy and exergy analysis of

photovoltaic-thermal collector with and without glass cover. Applied Energy 2009, 310-316.

Chow, T.T., Qiu, Z., Li, C., 2009a. Potential application of "see-through" solar cells in ventilated glazing in Hong Kong. Solar Energy Materials & Solar Cells 93, 230-238.

Clarke, J.A., Hand, J.W., Johnstone, C.M., Kelly, N., Strachan, P.A., 1996. Photovoltaic-integrated building facades. Renewable Energy 8, 475-479.

Cipriano, J., Houzeaux, G., Chemisana, D., Lodi, C., Marti-Herrero, J., 2013. Numerical analysis of the most appropriate heat transfer correlations for free ventilated double skin photovoltaic facades. Applied Thermal Engineering 57, 57-68.

Corbin, C.D., Zhai, Z.J., 2010. Experimental and numerical investigation on thermal and electrical performance of a building integrated photovoltaic-thermal collector system. Energy and Buildings 42, 76-82.

Coventry, J.S., 2005. Performance of a concentrating photovoltaic/thermal solar collector. Solar Energy 78, 211-222.

Crawley, D.B., Lawrie, L.K., Winkelmann, F.C., Buhl, W.F., Huang, Y.J., et al., 2001. EnergyPlus: creating a new-generation building energy simulation program. Energy and Buildings 33, 319-331.

CSEM. White solar modules: a revolution for building integration. [http://www.csem.ch/docs/Show.aspx/28546/docname/CP14-white-pv-EN.pdf]. Accessed 11, Nov, 2014.

Davidsson, H., Perers, B., Karlsson, B., 2010. Performance of a multifunctional PV/T hybrid

solar window. Solar Energy 84, 365-372.

Davidsson, H., Perers, B., Karlsson, B., 2012. System analysis of a multifunctional PV/T hybrid solar window. Solar Energy 86, 903-910.

De Soto, W., Klein, S.A., Beckman, W.A., 2006. Improvement and validation of a model for photovoltaic array performance. Solar Energy 80, 78-88.

DeBlois, J., Bilec, M., Schaefer, L., 2013. Simulating home cooling load reductions for a novel opaque roof solar chimney configuration. Applied Energy 112, 142-151.

Dehra, H., 2009. A two dimensional thermal network model for a photovoltaic solar wall. Solar Energy 83, 1933-1942.

Dhiman, P., Thakur, N.S., Kumar, A., Singh, S., 2011. An analytical model to predict the thermal performance of a novel parallel flow packed bed solar air heater. Applied Energy 88, 2157-2167.

Dominguez, A., Kleissl, J., Luvall, J.C., 2011. Effects of solar photovoltaic panels on roof heat transfer. Solar Energy 85, 2244-2255.

Dubey, S., Sandhu, G.S., Tiwari, G.N., 2009. Analytical expression for electrical efficiency of PV/T hybrid air collector. Applied Energy 86, 697-705.

Duffie, J.A., Beckman, W.A., 2006. Solar engineering of thermal processes. Wiley, New York.

Dupeyrat, P., Menezo, C., Fortuin, S., 2014. Study of the thermal and electrical performances of PVT solar hot water system. Energy and Buildings 68, 751-755.

Dupeyrat, P., Menezo, C., Rommel, M., Henning, H-M, 2011. Efficient single glazed flat plate

photovoltaic-thermal hybrid collector for domestic hot water system. Solar Energy 85, 1457-1468.

Eiffert, P., 2000. U.S. guidelines for the economic analysis of building-integrated photovoltaic power system. National Renewable Energy Laboratory: Colorado (USA). NREL/TP-710-25266.

Eiffert, P., Kiss, J.G., 2000. Building-integrated photovoltaic designs for commercial and institutional structures: A sourcebook for architects. U.S. Department of Energy's (DOE's): Oak Ridge (USA). NREL/BK-520-25272.

Evola, G., Marletta, L., 2014. Exergy and thermoeconomic optimization of a water-cooled glazed hybrid photovoltaic/thermal (PVT) collector. Solar Energy 107, 12-25.

Fleck, B.A., Meier, R.M., Matovic, M.D., 2002. A field study of the wind effects on the performance of an unglazed transpired solar collector. Solar Energy 73, 209-216.

Florschuetz, L.W., 1979. Extension of the Hottel-Whiller model to the analysis of combined photovoltaic/thermal flat plate collectors. Solar Energy 22, 361-366.

Fossa, M., Menezo, C., Leonardi, E., 2008. Experimental natural convection on vertical surfaces for building integrated photovoltaic (BIPV) applications. Experimental Thermal and Fluid Science 32, 980-990.

Fraisse, G., Menezo, C., Johannes, K., 2007. Energy performance of water hybrid PV/T collectors applied to combisystems of Direct Solar Floor type. Solar Energy 81, 1426-1438.

Friling, N., Jimenez, M.J., Bloem, H., Madsen, H., 2009. Modelling the heat dynamics of

building integrated and ventilated photovoltaic modules. Energy and Buildings 41, 1051-1057.

Fudholi, A., Sopian, K., Yazdi, M.H., Ruslan, M.H., Ibrahim, A., Kazem, H.A., 2014. Performance analysis of photovoltaic thermal (PVT) water collectors. Energy Conversion and Management 78, 641-651.

Fujisawa, T., Tani, T., 1997. Annual exergy evaluation on photovoltaic-thermal hybrid collector. Solar Energy Materials and Solar Cells 47, 135-148.

Gaillard, L., Giroux-Julien, S., Menezo, C., Pabiou, H., 2014. Experimental evaluation of a naturally ventilated PV double-skin building envelope in real operating conditions. Solar Energy 103, 223-241.

Gajbert, H., Hall, M., Karlsson, B., 2007. Optimisation of reflector and module geometries for stationary, low-concentrating, façade-integrated photovoltaic systems. Solar Energy Materials and Solar Cells 91, 1788-1799.

Gan, G., 2009a. Effect of air gap on the performance of building-integrated photovoltaics. Energy 34, 913-921.

Gan, G.H., 2009b. Numerical determination of adequate air gaps for building-integrated photovoltaics. Solar Energy 83, 1253-1273.

Gao, W.F., Lin, W.X., Liu, T., Xia, C.F., 2007. Analytical and experimental studies on the thermal performance of cross-corrugated and flat-plate solar air heaters. Applied Energy 84, 425-441.

Ghani, F., Duke, M., Carson, J.K., 2012a. Effect of flow distribution on the photovoltaic

performance of a building integrated photovoltaic/thermal (BIPV/T) collector. Solar Energy 86, 1518-1530.

Ghani, F., Duke, M., Carson, J.K., 2012b. Estimation of photovoltaic conversion efficiency of a building integrated photovoltaic/thermal (BIPV/T) collector array using an artificial neural network. Solar Energy 86, 3378-3387.

Guiavarch, A., Peuportier, B., 2006. Photovoltaic collectors efficiency according to their integration in buildings. Solar Energy 80, 65-77.

Han, J., Lu, L., Yang, H., 2010. Numerical evaluation of the mixed convective heat transfer in a double-pane window integrated with see-through a-Si PV cells with low-e coatings. Applied Energy 87, 3431-3437.

Han, J., Lu, L., Peng, J., Yang, H., 2013. Performance of ventilated double-sided PV façade compared with conventional clear glass façade. Energy and Buildings 56, 204-209.

Hao, G.Q., Yu, X.T., Huang, Y., Xu, Y., Zhao, X.K., et al., 2009. Application and development of building-integrated photovoltaic (BIPV) system in China. In: Proceedings of ISES World Congress 2007, 1685-1689.

Hayter, S.J., Martin, R.L., 1998. Photovoltaics for buildings: Cutting-edge PV. Presented at UPVG Utility PV Experience (UPEx) '98, San Diego, California, Septermber 28-30.

Hazi, A., Hazi, G., 2014. Comparative study of indirect photovoltaic thermal solar-assisted heat pump systems for industrial applications. Applied Thermal Engineering 70, 90-99.

He, W., Zhang, Y.X., Sun, W., Hou, J.X., Jiang, Q.Y., Ji, J., 2011. Experimental and numerical investigation on the performance of amorphous silicon photovoltaic window in East

China. Building and Environment 46, 363-369.

Hegazy, A.A., 2000. Comparative study of the performances of four photovoltaic/thermal solar air collectors. Energy conversion and management 41, 861-881.

Herrando, M., Markides, C.N., Hellgardt, K., 2014. A UK-based assessment of hybrid PV and solar-thermal systems for domestic heating and power: System performance. Applied Energy 122, 288-309.

Ho, C.J., Tanuwijava, A.O., Lai, C.M., 2012. Thermal and electrical performance of a BIPV integrated with a microencapsulated phase change material layer. Energy and Buildings 50, 331-338.

Huang, M.J., 2011. The effect of using two PCMs on the thermal regulation performance of BIPV systems. Solar Energy Materials & Solar Cells 95, 957-963.

Huang, M.J., Eames, P.C., Norton, B., 2004. Thermal regulation of building-integrated photovoltaics using phase change materials. International Journal of Heat and Mass Transfer 47, 2715-2733.

Huang, M.J., Eames, P.C., Norton, B., Hewitt, N.J., 2011. Natural convection in an internally finned phase change material heat sink for the thermal management of photovoltaics. Solar Energy Materials & Solar Cells 95, 1598-1603.

Ibrahim, A., Fudholi, A., Sopian, K., Othman, M.Y., Ruslan, M.H., 2014. Efficiencies and improvement potential of building integrated photovoltaic thermal (BIPVT) system. Energy Conversion and Management 77, 527-534.

Infield, D., Eicker, U., Fux, V., Mei, L., Schumacher, J., 2006. A simplified approach to thermal

performance calculation for building integrated mechanically ventilated PV facades. Building and Environment 41, 893-901.

Jelle, B.P., 2012. Accelerated climate ageing of building materials, components and structures in the laboratory. Journal of Materials Science 47, 6475-6496.

Jelle, B.P., Breivik, C., 2012. State-of-the-art building integrated photovoltaics. Energy Procedia 20, 68-77.

Jelle, B.P., Breivik, C., Rokenes, H.D., 2012. Building integrated photovoltaic products: A state-of-the-art review and future research opportunities. Solar Energy Materials & Solar Cells 100, 69-96.

James, P.A.B., Jentsch, M.F., Bahaj, A.S., 2009. Quantifying the added value of BiPV as a shading solution in atria. Solar Energy 83, 220-231.

Ji, J., He, H.F., Chow, T.T., Pei, G., He, W., Liu, K.L., 2009. Distributed dynamic modeling and experimental study of PV evaporator in a PV/T solar-assisted heat pump. International Journal of Heat and Mass Transfer 52, 1365-1373.

Ji, Ji, Lu, J.P., Chow, T.T., He, W., Pei, G., 2007. A sensitivity study of a hybrid photovoltaic/thermal water-heating system with natural circulation. Applied Energy 84, 222-237.

Ji, J., Pei, G., Chow, T.T., Liu, K.L., He, H.F., et al., 2008. Experimental study of photovoltaic solar assisted heat pump system. Solar Energy 82, 43-52.

Ji, J., Yi, H., He, W., Pei, G., Lu, J., Jiang, B., 2007a. Modeling of a novel Trombe wall with PV cells. Building and Environment 42, 1544-1552.

Ji, J., Yi, H., Pei, G., Lu, J., 2007b. Study of PV-Trombe wall installed in a fenestrated room with heat storage. Applied Thermal Engineering 27, 1507-1515.

Ji, J., Yi, H., He, W., Pei, G., 2007c. PV-Trombe wall design for buildings in composite climates. Journal of Solar Energy Engineering 129, 431-437.

Jiang, B., Ji, J., Yi, H., 2008. The influence of PV coverage ratio on thermal and electrical performance of photovoltaic-Trombe wall. Renewable Energy 33, 2491-2498.

Kalogirou, S.A., Tripanagnostopoulos, Y., 2006. Hybrid PV/T solar systems for domestic hot water and electricity production. Energy Conversion and Management 47, 3368-3382.

Kamel, R.S., Fung, A.S., Modeling, simulation and feasibility analysis of residential BIPV/T + ASHP system in cold climate – Canada. Energy and Buildings 82, 758-770.

Karagiorgas, M., Galatis, K., Tsagouri, M., Tsoutsos, T., Botzios-Valaskakis, A., 2010. Solar assisted heat pump on air collectors: A simulation tool. Solar Energy 84, 66-78.

Karava, P., Jubayer, C.M., Savory, E., 2011. Numerical modelling of forced convective heat transfer from the inclined windward roof of an isolated low-rise building with application to photovoltaic/thermal system. Applied Thermal Engineering 31, 1950-1963.

Kazanci, O.B., Skrupskelis, M., Sevela, P., Pavlov, G.K., Olesen, B.W., 2014. Sustainable heating, cooling and ventilation of a plus-energy house via photovoltaic/thermal panels. Energy and Buildings, http://dx.doi.org/10.1016/j.enbuild.2013.12.064

Kaiser, A.S., Zamora, B., Mazon, R., Garcia, J.R., Vera, F., 2014. Experimental study of cooling BIPV modules by forced convection in the air channel. Applied Energy 135, 88-97.

Kim, J.H., Kim, J.T., 2012. A simulation study of air-type building-integrated photovoltaic-thermal system. Energy Procedia 30, 1016-1024.

King, D.L., Boyson, W.E., Kratochvil, J.A., 2004. Photovoltaic array performance model, photovoltaic system R&D department. Sandia National Laboratories.

Kolb, A., Winter, E.R.F., Viskanta, R., 1999. Experimental studies on a solar air collector with metal matrix absorber. Solar Energy 65, 91-98.

Koyunbaba, B.K., Yilmaz, Z., 2012. The comparison of Trombe wall systems with single glass, double glass and PV panels. Renewable Energy 45, 111-118.

Koyunbaba, B.K., Yilmaz, Z., Ulgen, K., 2011. An approach for energy modeling of a building integrated photovoltaic (BIPV) Trombe wall system. Energy and Buildings 67,680-688.

Krauter, S., Araujo, R.G., Schroer, S., Hanitsch, R., Salhi, M.J., et al., 1999. Combined photovoltaic and solar thermal systems for façade integration and building insulation. Solar Energy 67, 239-248.

Kumar, N.S., Matty, K., Rita, E., Simon, W., Ortrun, A., Alex, C., et al., 2012. Experimental validation of a heat transfer model for concentrating photovoltaic system. Applied Thermal Engineering 33-34, 175-182.

Kumar, R., Rosen, M.A., 2011a. A critical review of photovoltaic-thermal solar collectors for air heating. Applied Energy 88, 3603-3614.

Kumar, R., Rosen, M.A., 2011b. Performance evaluation of a double pass PV/T solar air heater with and without fins. Applied Thermal Engineering 31, 1402-1410.

Lazzarin R.M., Schibuola L., 1986. Energy roof as heat pump source/sink. International Journal of Refrigeration 9, 108-112.

Leon, M. A., Kumar, S., 2007. Mathematical modeling and thermal performance analysis of unglazed transpired solar collectors. Solar Energy 81, 62-75.

Li, D.H.W., Lam, T.N.T., Chan, W.W.H., Mak, A.H.L., 2009. Energy and cost analysis of semi-transparent photovoltaic in office buildings. Applied Energy 86, 722-729.

Li, M., Ji, X., Li, G.L., Wei, S.X., Li, Y.F., Shi, F., 2011. Performance study of solar cell arrays based on a trough concentrating photovoltaic/thermal system. Applied Energy 88, 3218-3227.

Li, S., Karava, P., Currie, S., Lin, W.E., Savory, E., 2014a. Energy modeling of photovoltaic thermal systems with corrugated unglazed transpired solar collectors – Part 1: Model development and validation.

Li, S., Karava, P., 2014b. Energy modeling of photovoltaic thermal systems with corrugated unglazed transpired solar collectors – Part 2: Performance analysis. Solar Energy 102, 297-307.

Lin, W., Ma, Z., Sohel, M.I., Cooper, P., 2014. Development and evaluation of a ceiling ventilation system enhanced by solar photovoltaic thermal collectors and phase change materials. Energy Conversion and Management 88, 218-230.

Liu, K.L., Ji, J., Chow, T.T., Pei, G., He, H.F., Jiang, A.G., Yang, J.C., 2009. Performance study of a photovoltaic solar assisted heat pump with variable-frequency compressor – A case study in Tibet. Renewable Energy 34, 2680-2687.

163

Lodi, C., Cipriano, J., Bacher, P., Madsen, H., 2011. Modelling the heat dynamics of a monitored test reference environment for BIPV systems through deterministic and stochastic approaches, in: International Workshop on 'whole building testing, evaluation and modelling for energy assessment', Technical University of Denmark, Lyngby, Denmark.

Lu, L., Law K.M., 2013. Overall energy performance of semi-transparent single-glazed photovoltaic (PV) window for a typical office in Hong Kong. Renewable Energy 49, 250-254.

Maiti, S., Banerjee, S., Vyas, K., Patel, P., Ghosh, P.K., 2011. Self regulation of photovoltaic module temperature in V-trough using a metal-wax composite phase change matrix. Solar Energy 85, 1805-1816.

Malvi, C.S., Dixon-Hardy, D.W., Crook, R., 2011. Energy balance model of combined photovoltaic solar-thermal system incorporating phase change material. Solar Energy 85, 1440-1446.

Mandalaki, M., Zervas, K., Taoutsos, T., Vazakas, A., 2012. Assessment of fixed shading devices with integrated PV for efficient energy use. Solar Energy 86, 2561-2575.

Mei, L., Infield, D.G., Gottschalg, R., Loveday, D.L., Davies, D., Berry, M., 2009. Equilibrium thermal characteristics of a building integrated photovoltaic tiled roof. Solar Energy 83, 1893-1901.

Mittelman, G., Alshare, A., Davidson, J.H., 2009. A model and heat transfer correlation for rooftop integrated photovoltaics with a passive air cooling channel. Solar Energy 83,

1150-1160.

Mittelman, G., Kribus, A., Dayan, A., 2007. Solar cooling with concentrating photovoltaic/thermal (CPV/T) systems. Energy Conversion and Management 48, 2481-2490.

Miyazaki, T., Akisawa, A., Kashiwagi, T., 2005. Energy savings of office buildings by the use of semi-transparent solar cells for windows. Renewable Energy 30, 281-304.

Moradgholi, M., Nowee, S.M., Abrishamchi, I., 2014. Application of heat pipe in an experimental investigation on a novel photovoltaic/thermal (PV/T) system. Solar Energy 107, 82-88.

Moummi, N., Youcef-Ali, S., Moummi, A., Desmons, J.Y., 2004. Energy analysis of a solar air collector with rows of fins. Renewable Eenrgy 29, pp. 2053-2064.

Nagano, K., Mochida, T., Shimakura, K., Murashita, K., Takeda, S., 2003. Development of thermal-photovoltaic hybrid exterior wallboards incorporating PV cells in and their winter performances. Solar Energy Materials & Solar Cells 77, 265-282.

National Renewable Energy Laboratory (NREL), 1998. Federal technology alert: Transpired collectors (Solar preheaters for outdoor ventilation air).

Naveed, A.T., Kang, E.C., Lee, E.J., 2006. Effect of unglazed transpired collector on the performance of a polycrystalline silicon photovoltaic module. Journal of Solar Energy Engineering 128, 349-353.

Ng, P.K., Mithraratne, N., 2014. Lifetime performance of semi-transparent building-integrated photovoltaic (BIPV) glazing systems in the tropics. Renewable and Sustainable Energy

Reviews 31, 736-745.

Olivieri, L., Caamano-Martin, E., Moralejo-Vazquez, F.J., Martin-Chivelet, N., Olivieri, F., Neila-Gonzalez, F.J., 2014. Energy saving potential of semi-transparent photovoltaic elements for building integration. Energy, http://dx.doi.org/10.1016/j.energy.2014.08.054

Omer, S.A., Wilson, R., Riffat, S.B., 2003. Monitoring results of two examples of building integrated PV (BIPV) systems in the UK. Renewable Energy 28, 1387-1399.

OnyxSolar, Projects and References. [http://www.onyxsolardownloads.com/docs/ALL-YOU-NEED/Professional-Experience-Book-EN.pdf]. Accessed 12, Nov, 2014.

Pantic, S., Candanedo, L., Athienitis, A.K., 2010. Modeling of energy performance of a house with three configurations of building-integrated photovoltaic/thermal systems. Energy and Buildings 42, 1779-1789.

Pappas, A., Zhai, Z.Q., 2008. Numerical investigation on thermal performance and correlations of double skin façade with buoyancy-driven airflow. Energy and Buildings 40, 466-475.

Pei, G., Fu, H.D., Ji, J., Chow, T.T., Zhang, T., 2012a. Annual analysis of heat pipe PV/T systems for domestic hot water and electricity production. Energy Conversion and Management 56, 8-21.

Pei, G., Fu, H.D., Zhang, T., Ji, J., 2011. A numerical and experimental study on a heat pipe PV/T system. Solar Energy 85, 911-921.

Pei, G., Fu, H.D., Zhu, H.J., Ji, J., 2012b. Performance study and parametric analysis of a novel heat pipe PV/T system. Energy 37, 384-395.

Pei, G., Zhang, T., Yu, Z., Fu, H.D., Wang, J.Y., Ji, J., 2010. Comparative study of a heat pipe PV/T and a water-thermosiphon PV/T. Power and Energy Engineering Conference, Asia-Pacific. Chengdu, 28-31 March.

Peng, J., Lu, L., Yang, H., 2013a. An experimental study of the thermal performance of a novel photovoltaic double-skin façade in Hong Kong. Solar Energy 97, 293-304.

Photovoltaics and thin film electronics laboratory, 2012. The future of the PV module packaging. Ecole Poltechnique Federale de Lausanne. [http://pvlab.epfl.ch/pv_module_design/material_and_encapsulation/futur_packaging]. Accessed on 13, Nov, 2014.

Pola, I., Chianese, D., Bernasconi, A., 2007. Flat roof integration of a-Si triple junction modules laminated together with flexible polyolefin membranes. Solar Energy 81, 1144-1158.

Posnansky, M., Gnos, S., Coonen, S., 1994. The importance of hybrid PV-building integration. Paper presented at the IEEE Photovoltaic Specialists Conference, Hawaii.

Promvonge, P., Khanoknaiyakarn, C., Kwankaomeg, S., Thianpong, C., 2011. Thermal behaviour in solar air heater channel fitted with combined rib and delta-winglet. International Communications in Heat and Mass Transfer 38, 749-756.

Quan, Z.H., Li, N.J., Zhao, Y.H., 2011. Experimental study of solar photovoltaic/thermal (PV/T) system based on flat plate heat pipe. Power and Energy Engineering Conference, Asia-Pacific. Wuhan, 25-28 March.

Radhi, H., 2010. Energy analysis of façade-integrated photovoltaic systems applied to UAE commercial buildings. Solar Energy 84, 2009-2021.

Reijenga, T., 2000. Photovoltaic building integration concepts – what do architects need? IEA PVPS Task 7 workshop.

Rosell, J.I., Vallverdu, X., Lechon, M.A., Ibanez, M., 2005. Design and simulation of a low concentrating photovoltaic/thermal system. Energy Conversion and Management 46, 3034-3046.

Rosenthal, A., Sherwood, L., Brooks, B., Ghandi, P., Backstrom, B., 2010. Flammability testing of standard roofing products in the presence of standoof-mounted photovoltaic modules. Solar America Board for Codes and Standards Interim Report.

Roaf, S., Brotas, L., Nicol, F., 2015. Counting the costs of comfort. Building Research & Information 43, 269-273.

Ruther, R., Braun, P., 2009. Energetic contribution potential of building-integrated photovoltaics on airports in warm climates. Solar Energy 83, 1923-1931.

Sandberg, M., Moshfegh, B., 2002. Buoyancy-induced air flow in photovoltaic facades – effect of geometry of the air gap and location of solar cell modules. Buildings and Environment 37, 211-218.

Sandnes, B., Rekstad, J., 2002. A photovoltaic/thermal (PV/T) collector with a polymer absorber plate. Experimental study and analytical model. Solar Energy 72, 63-73.

Sanjuan, C., Suarez, M.J., Gonzalez, M., Pistono, J., Blanco, E., 2011. Energy performance of an open-joint ventilated façade compared with a conventional sealed cavity façade. Solar Energy 85, 1851-1863.

Santbergen, R., Rindt, C.C.M., Zondag, H.A., van Zolingen, R.J.Ch., 2010. Detailed analysis of

the energy yield of systems with covered sheet-and-tube PVT collectors. Solar Energy 84, 86-878.

Sarbry, M., Abdel-Hadi, Y.A., Ghitas, A., 2013. PV-integrated CPC for transparent facades. Energy and Buildings 66, 480-484.

Sarhaddi, F., Farahat, S., Ajam, H., Behzadmehr, A., Adeli, M.M., 2010. An improved thermal and electrical model for a solar photovoltaic thermal (PV/T) air collector. Applied Energy 87, 2328-2339.

Scott, K., Zielnik, A., 2009. Developing codes and standards for BIPV and integrated systems. International Photovoltaic Reliability Workshop, Tempe, AZ, USA.

Shahsavar, A., Ameri, M., 2010. Experimental investigation and modeling of a direct-coupled PV/T air collector. Solar Energy 84, 1938-1958.

Shan, F., Cao, L., Fang, G., 2013. Dynamic performances modeling of a photovoltaic-thermal collector with water heating in buildings. Energy and Buildings 66, 485-494.

Shan, F., Tang, F., Cao, L., Fang, G., 2014. Dynamic characteristics modeling of a hybrid photovoltaic-thermal solar collector with active cooling in buildings. Energy and Buildings78, 215-221.

Sharples, S., Charlesworth, P.S., 1998. Full-scale measurements of wind-induced convective heat transfer from a roof-mounted flat plate solar collector. Solar Energy 62, 69-77.

Sherwood, L., 2012. Fire rating for PV modules and roofs. PV Module Reliability Workshop. [http://www1.eere.energy.gov/solar/pdfs/pvmrw12_tuesam_solarabcs_sherwood.pdf]. Accessed on 11, Nov, 2014.

Sherwood, L., Backstorm, B., Sloan, D., Flueckiger, C., Brooks, B., Rosenthal, A., 2013. Fire classification rating testing of stand-off mounted photovoltaic modules and systems. Solar America Board for Codes and Standards Report.

Smolec, W., Thomas, A., 1991. Some aspects of Trombe wall heat transfer models. Energy Conversion and Management 32 (3), 269-277.

Sobhnamayan, F., Sarhaddi, F., Alavi, M.A., Farahat, S., Yazdanpanahi, J., 2014. Optimization of a solar photovoltaic thermal (PV/T) water collector based on exergy concept. Renewable Energy 68, 356-365.

Sohel, M.I., Ma, Z., Cooper, P., Adams, J., Scott, R., 2014. A dynamic model for air-based photovoltaic thermal systems working under real operating conditions. Applied Energy 132, 216-225.

Solanki, S.C., Dubey, S., Tiwari, A., 2009. Indoor simulation and testing of photovoltaic thermal (PV/T) air collectors. Applied Energy 86, 2421-2428.

SolarPV.co.uk. < http://www.solarpv.co.uk/solar-pv-facades.html> Accessed on Oct. 29, 2014].

Sun, W., Ji, J., Luo, C., He, W., 2011. Performance of PV-Trombe wall in winter correlated with south façade design. Applied Energy 88, 224-231.

SwissInso. [http://www.swissinso.com/]. Accessed on 12, Nov, 2014.

Timmerman, M., Bakker, M., Reinders, A., van der Meer, T., 2009. Plug-and-play liquid PV thermal panels – integrated design for easy manufacturing and installation. Photovoltaic Specialists Conference (PVSC), 34th IEEE. Philadelphia, PA, 7-12 June.

Tiwari A., Sodha, M.S., 2006. Performance evaluation of hybrid PV/thermal water/air heating system: a parametric study. Renewable Energy 31, 2460-2474.

Tripanagnostopoulos, Y., Nousia T.H., Souliotis M., Yianoulis P., 2002. Hybrid photovoltaic/thermal solar systems. Solar Energy 72, 217-234.

Tyagi, V.V., Kaushik, S.C., Tyagi, S.K., 2012. Advancement in solar photovoltaic/thermal (PV/T) hybrid collector technology. Renewable and Sustainable Energy Reviews 16, 1383-1398.

Ulavi, T., Hebrink, T., Davidson, J.H., 2014. Analysis of a hybrid solar window for building integration. Solar Energy 105, 290-302.

Underwritters Laboratories 2007. Trend for the solar photovoltaic market and product certification. [http://site.ul.com/asiaonthemark/as-en/2007-Issue24/page8.htm#top]. Accessed on 11, Nov, 2014.

Utzinger, D.M., Klein, S.A., Mitchell, J.W., 1980. The effect of air flow rate in collector-storage walls. Solar Energy 25, 511-519.

Vasan, N., Stathopoulos, T., 2014. Experimental study of wind effects on unglazed transpired collectors. Solar Energy 101, 138-149.

Vats, K., Tomar, V., Tiwari, G.N., 2012. Effect of packing factor on the performance of a building integrated semitransparent photovoltaic thermal (BISPVT) system with air duct. Energy and Buildings 53, 159-165.

Vokas, G., Christandonis, N., Skittides, F., 2006. Hybrid photovoltaic-thermal systems for domestic heating and cooling – A theoretical approach. Solar Energy 80, 607-615.

Wang, Y., Tian, W., Ren, J., Zhu, L., Wang, Q., 2006. Influence of a building's integrated-photovoltaics on heating and cooling loads. Applied Energy 83, 989-1003.

Warrington, R.O., Ameel, T.A., 1995. Experimental studies of natural convection in partitioned enclosures with a Trombe wall geometry. Journal of Solar Energy Engineering 117, 16-21.

Wennerberg, J., Kessler, J., Hedstrom, J., Stolt, L., Karlsson, B., Ronnelid, M., 2000. Thin film PV modules for low-concentrating systems. Solar Energy 69, 243-255.

Wilson, M.J., Paul, M.C., 2011. Effect of mounting geometry on conversion occurring under a photovoltaic panel and the corresponding efficiency using CFD. Solar Energy 85, 2540-2550.

Wolf, M., 1976. Performance analysis of combined heating and photovoltaic power systems for residences. Energy Conversion 16, 79-90.

Wong, P.W., Shimoda, Y., Nonaka, M., Inoue, M., Mizuno, M., 2008. Semi-transparent PV: Thermal performance, power generation, daylight modelling and energy saving potential in a residential application. Renewable Energy 33, 1024-1036.

Wu, S.Y., Zhang, Q.L., Xiao, L., Guo, F.H., 2011. A heat pipe photovoltaic/thermal (PV/T) hybrid system and its performance evaluation. Energy and Buildings 43, 3558-3567.

Xu, G.Y., Deng, S.M., Zhang, X.S., Yang, L., Zhang, Y.H., 2009. Simulation of a photovoltaic/thermal heat pump system having a modified collector/evaporator. Solar Energy 83, 1967-1976.

Xu, G.Y., Zhang, X.S., Deng, S.M., 2011. Experimental study on the operating characteristics of

a novel low-concentrating solar photovoltaic/thermal integrated heat pump water heating system. Applied Thermal Engineering 31, 3689-3695.

Xu, S., Liao, W., Huang, J., Kang, J., 2014. Optimal PV cell coverage ratio for semi-transparent photovoltaics on office building facades in central China. Energy and Buildings 77, 130-138.

Xuan, X.D., Zheng, X.Y., 2009. Façade design in building integrated photovoltaics. In: Proceedings of ISES World Congress 2007, 384-387.

Yang, D.J., Yuan, Z.F., Lee, P.H., Yin, H.M., 2012. Simulation and experimental validation of heat transfer in a novel hybrid solar panel. International Journal of Heat and Mass Transfer 55, 1076-1082.

Yang, T.T., Athienitis, A.K., 2012a. Investigation of performance enhancement of a building integrated photovoltaic/thermal system. eSim, May 1-4, Halifax, Canada.

Yang, T.T., Athienitis, A.K., 2012b. A study of design options for a building integrated photovoltaic/thermal (BIPV/T) system with glaed air collector and multiple inlets. 1st International conference on Solar Heating and Cooling for Buildings and Industry, San Francisco, USA.

Yang, T.T., Athienitis, A.K., 2014. A study of design options for a building integrated photovoltaic/thermal (BIPV/T) system with glazed air collector and multiple inlets. Solar Energy 104, 82-92.

Yin, H.M., Yang, D.J., Kelly, G., Garant, J., 2013. Design and performance of a novel building integrated PV/Thermal system for energy efficiency of buildings. Solar Energy 87, 184-

195.

Yun, G.Y., McEvoy, M., Steemers K., 2007. Design and overall energy performance of a ventilated photovoltaic façade, 81, 383-394.

Zakharchenko, R., Jimenez, L., Perez-Garcia, S.A., Vorobiev, P., Dehesa-Carrasco, U., et al., 2004. Photovoltaic solar panel for a hybrid PV/Thermal system. Solar Energy Materials & Solar Cells 82, 253-261.

Zeng, L.B., Li, M.H., Chen, Y.F., Shen, H., 2014. A simplified method to modulate colors on industrial multicrystalline silicon solar cells with reduced current losses. Solar Energy 103, 343-349.

Zhang, X.X., Zhao, X.D., Shen, J.C., Hu, X., Liu, X.Z., Xu, J.H., 2013. Design, fabrication and experimental study of a solar photovoltaic/loop-heat-pipe based heat pump system. Solar Energy 97, 551-568.

Zhao, X.D., Zhang, X.X., Riffat, S.B., Su, Y.X., 2011. Theoretical study of the performance of a novel PV/e roof module for heat pump operation. Energy Conversion and Management 52, 603-614.

Zhao, X.D., Wang, Z.Y., Tang, Q., 2010. Theoretical investigation of the performance of a novel loop heat pipe solar water heating system for use in Beijing, China. Applied Thermal Enginnering 30, 2526-2536.

Zogou, O., Stapountzis, H., 2011a. Energy analysis of an improved concept of integrated PV panels in an office building in central Greece. Applied Energy 88, 853-866.

Zogou, O., Stapountzis, H., 2011b. Experimental validation of an improved concept of building

integrated photovoltaic panels. Renewable Energy 36, 3488-3498.

Zogou, O., Stapountzis, H., 2012. Flow and heat transfer inside a PV/T collector for building application. Applied Energy 91, 103-115.

Zondag, H.A., De Vries, D.W., Van Helden, W.G.J., Van Zolingen, R.J.C., Van Steenhoven, A.A., 2002. The thermal and electrical yield of a PV-thermal collector. Solar Energy 72, 113-128.

Zondag, H.A., De Vries, D.W., Van Helden, W.G.J., Van Zolingen, R.J.C., Van Steenhoven, A.A., 2003. The yield of different combined PV-thermal collector designs. Solar Energy 74, 253-269.

Appendices

A1. Thermocouple placement in the second section in the two-inlet BIPV/T system

The unique design of adding an extra opening in the original course of the air flow will result in a different air flow pattern and heat transfer characteristic. To further resolve the temperature profile, three thermocouples are grouped at different height in the air channel. Figure A1.1 shows the image of such a thermocouple cluster, with each sensor shielded by aluminum foil against the thermal radiation from the hot surfaces.
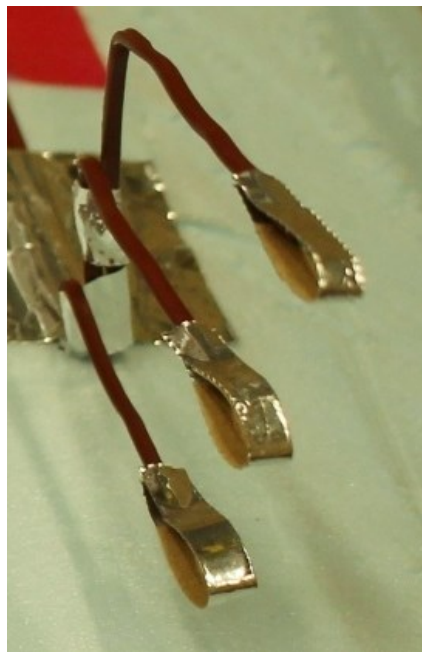
Figure A1.1. Photo of a group of thermocouples measuring air temperature at different heights in the second section of the two-inlet BIPV/T system

In the BIPV/T section measuring about 1 meter, there are five such thermocouple clusters along the length of the channel.

A2. Thermocouple reliability verification

The thermocouple measurements will be used to evaluate system performance and generate convective heat transfer coefficients. It is therefore essential to verify that the measured data fall in an acceptable error range.

The temperatures throughout the BIPV/T system were recorded for a whole night, with no solar radiation input, no human activity and air conditioning in the lab room. It was expected that the thermocouple measurements should eventually converge when the whole system reached a thermal steady state. As Figure A2.1 indicates, the measured data showed a narrow temperature band with the highest and lowest measurements differed by less than 0.4 ºC.
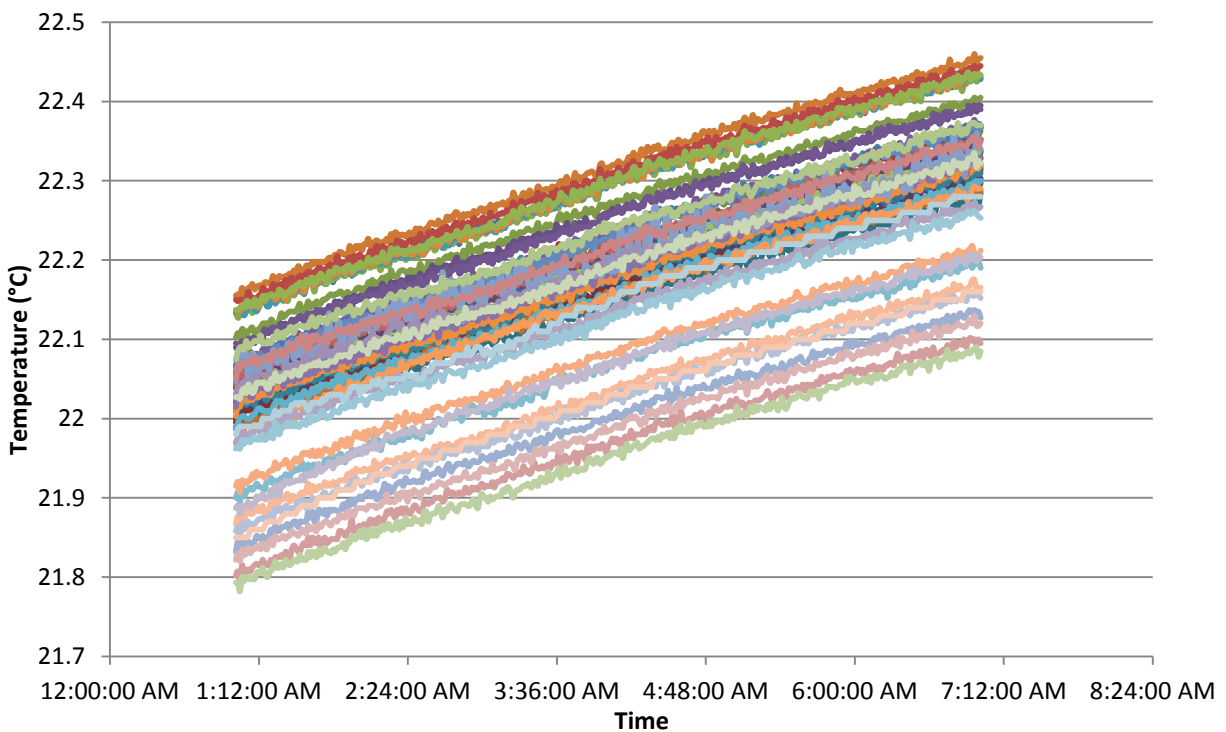
Figure A2.1. Thermocouple measurements when the system reaches a thermal steady state

In Figure 2A.1, a small gap divides the temperatures into upper and lower clusters. It was confirmed that the lower clusters reflect the insulation temperatures. The temperatures of the insulation inner surface were slightly lower because the insulation was inside the whole system and respond to the thermal gain at a lower rate.

A3. Uncertainty analysis

Area (A) is derived by multiplying length (L) and width (W). The measuring uncertainty of L and W are determined to be 0.0005 m (0.5 mm).

The uncertainty of A is calculated by

$$\delta A = A \sqrt{(\frac{\delta L}{L})^2 + (\frac{\delta W}{W})^2} = 0.0006$$

Radiative heat transfer rate is calculated by the following expression

$$Q_{rad} = \sigma F_{view} A \frac{(T_{pv}^4 - T_{ins}^4)}{\frac{1}{\varepsilon_{pv}} + \frac{1}{\varepsilon_{ins}} - 1}$$

For simplicity, an emissivity factor F_ε is assigned by

$$F_\varepsilon = \frac{1}{\frac{1}{\varepsilon_{pv}} + \frac{1}{\varepsilon_{ins}} - 1}$$

Thus the radiative heat transfer rate is rewritten as below

$$Q_{rad} = \sigma A F_\varepsilon (T_{pv}^4 - T_{ins}^4)$$

The uncertainty of Q_{rad} can be expressed by the uncertainties of A, F_ε, T_{pv} and T_{ins} as below

$$\delta Q_{rad} = \sqrt{(\frac{\partial Q_{rad}}{\partial A} \delta A)^2 + (\frac{\partial Q_{rad}}{\partial F_\varepsilon} \delta F_\varepsilon)^2 + (\frac{\partial Q_{rad}}{\partial T_{pv}} \delta T_{pv})^2 + (\frac{\partial Q_{rad}}{\partial T_{ins}} \delta T_{ins})^2}$$

The partial derivatives are:

$$\frac{\partial Q_{rad}}{\partial A} = \sigma F_\varepsilon (T_{pv}^4 - T_{ins}^4)$$

$$\frac{\partial Q_{rad}}{\partial F_\varepsilon} = \sigma A (T_{pv}^4 - T_{ins}^4)$$

$$\frac{\partial Q_{rad}}{\partial T_{pv}} = \sigma A F_\varepsilon \cdot 4 T_{pv}^3$$

$$\frac{\partial Q_{rad}}{\partial T_{ins}} = \sigma A F_\varepsilon \cdot 4 T_{ins}^3$$

Uncertainty in emissivity factor F_ε

$$\frac{\partial F_\varepsilon}{\partial \varepsilon_{pv}} = -\left(\frac{1}{\varepsilon_{pv}} + \frac{1}{\varepsilon_{ins}} - 1\right)^{-2} \cdot \left(-\varepsilon_{pv}^{-2}\right) = (\varepsilon_{pv} \cdot (\frac{1}{\varepsilon_{pv}} + \frac{1}{\varepsilon_{ins}} - 1))^{-2}$$

$$\frac{\partial F_\varepsilon}{\partial \varepsilon_{ins}} = -\left(\frac{1}{\varepsilon_{pv}} + \frac{1}{\varepsilon_{ins}} - 1\right)^{-2} \cdot \left(-\varepsilon_{ins}^{-2}\right) = (\varepsilon_{ins} \cdot (\frac{1}{\varepsilon_{pv}} + \frac{1}{\varepsilon_{ins}} - 1))^{-2}$$

Therefore the uncertainty in emissivity factor is

$$\delta F_\varepsilon = \sqrt{(\frac{\partial F_\varepsilon}{\partial \varepsilon_{pv}} \delta \varepsilon_{pv})^2 + (\frac{\partial F_\varepsilon}{\partial \varepsilon_{ins}} \delta \varepsilon_{ins})^2}$$

The uncertainty in measuring the emissivity values of PV and insulation is 1%, which results in

$$\delta \varepsilon_{pv} = \varepsilon_{pv} \times 1\%$$

$$\delta \varepsilon_{ins} = \varepsilon_{ins} \times 1\%$$

The uncertainty in temperature measurement is 0.2 °C, so that $\delta T_{pv} = \delta T_{ins} = 0.2$.

The convective heat transfer rate to air is given by

$$Q_{con} = \dot{m}c_p(T_{out} - T_{in})$$

Therefore the uncertainty in Q_{con} is calculated by

$$\delta Q_{con} = \sqrt{(\frac{\partial Q_{con}}{\partial m}\delta m)^2 + (\frac{\partial Q_{con}}{\partial T_{out}}\delta T_{out})^2 + (\frac{\partial Q_{con}}{\partial T_{in}}\delta T_{in})^2}$$

The partial derivatives are

$$\frac{\partial Q_{con}}{\partial m} = c_p(T_{out} - T_{in})$$

$$\frac{\partial Q_{con}}{\partial T_{out}} = \dot{m}c_p$$

$$\frac{\partial Q_{con}}{\partial T_{in}} = \dot{m}c_p$$

The relative uncertainty of the mass flow rate is 2%. The uncertainty related to temperature measurement is 0.2 °C.

The convective heat transfer coefficient is given by

$$h = \frac{Q_{con} - Q_{rad}}{A(T_{pv} - T_{in})}$$

Therefore the uncertainty in calculating h is given by

$$\delta h = h \cdot \sqrt{(\frac{\delta(Q_{con} - Q_{rad})}{Q_{con} - Q_{rad}})^2 + (\frac{\delta(A(T_{out} - T_{in}))}{A(T_{pv} - \overline{T}_{air})})^2}$$

where

$$\delta(Q_{con} - Q_{rad}) = \sqrt{\delta Q_{con}{}^2 + \delta Q_{rad}{}^2}$$

$$\delta\left(A(T_{pv} - \overline{T}_{air})\right) = \sqrt{((T_{pv} - \overline{T}_{air})\delta A)^2 + (A\delta T_{pv})^2 + (A\delta\overline{T}_{air})^2}$$

$$\overline{T}_{air} = \frac{1}{2}(T_{in} + T_{out})$$

$$\delta\overline{T}_{air} = \frac{1}{2}\sqrt{(\delta T_{in})^2 + (\delta T_{out})^2}$$

The Nusselt number is calculated by

$$Nu = \frac{hD_h}{k}$$

The uncertainty of Nusselt number is therefore expressed by

$$\delta Nu = Nu \cdot \sqrt{(\frac{\delta h}{h})^2 + (\frac{\delta D_h}{D_h})^2 + (\frac{\delta k}{k})^2}$$

D_h is the hydraulic diameter of the BIPV/T channel. It is determined by the width and height of

the air cavity by

$$D_h = \frac{4WH}{2(W + H)} = \frac{2WH}{W + H}$$

The partial derivatives are

$$\frac{\partial D_h}{\partial W} = 2H(W + H)^{-1} + 2WH \cdot (-1) \cdot (W + H)^{-2}$$

$$\frac{\partial D_h}{\partial H} = 2W(W + H)^{-1} + 2WH \cdot (-1) \cdot (W + H)^{-2}$$

Therefore the uncertainty of D_h is calculated by

$$\delta D_h = \sqrt{(\frac{\partial D_h}{\partial W}\delta W)^2 + (\frac{\partial D_h}{\partial H}\delta H)^2}$$

The Reynolds number is calculated by

$$Re = \frac{\rho u D_h}{\mu} = \frac{\dot{m}D_h}{A\mu}$$

The uncertainty in Reynolds number is expressed by the following formula

$$\delta Re = Re \cdot \sqrt{(\frac{\delta \dot{m}}{\dot{m}})^2 + (\frac{\delta D_h}{D_h})^2 + (\frac{\delta A}{A})^2 + (\frac{\delta \mu}{\mu})^2}$$